Manganese oxide structure and transformation during oxidation of phenolic contaminants

By

Sarah Jane Balgooyen

A dissertation submitted in partial fulfillment of

the requirements for the degree of

Doctor of Philosophy

(Environmental Chemistry and Technology)

at the

UNIVERSITY OF WISCONSIN-MADISON

2019

Date of final oral examination: 05/13/2019

The dissertation is approved by the following members of the Final Oral Committee:
Matthew Ginder-Vogel, Assistant Professor, Civil and Environmental Engineering
Christina K. Remucal, Associate Professor, Civil and Environmental Engineering
James P. Hurley, Professor, Civil and Environmental Engineering
Joel A. Pedersen, Professor, Civil and Environmental Engineering
Gregory W. Harrington, Professor, Civil and Environmental Engineering

Abstract

Manganese oxide structure and transformation during
oxidation of phenolic contaminants

by

Sarah Jane Balgooyen

Doctor of Philosophy – Environmental Chemistry and Technology Program

University of Wisconsin – Madison

Assistant Professor Matthew Ginder-Vogel

Associate Professor Christina K. Remucal

Manganese(III/IV) oxides are strong oxidants found in a wide range of natural environments. These oxides are formed through microbial activity and control the environmental fate of many harmful contaminants. Manganese oxides are able to oxidize a wide variety of inorganic and organic species, including phenols. Phenolic contamination is an issue driven by anthropogenic inputs. For example, bisphenol A (BPA) is an industrial environmental contaminant found at concentrations that are considered harmful for aquatic life. The focus of previous research is the initial kinetics of model phenol oxidation. In this dissertation, we investigate the oxidation of environmental contaminants and the concurrent changes to the manganese oxide substrate. Since the rate of phenol oxidation decreases as the reaction proceeds, analysis of extensive reactions is an important part of this study.

During twelve sequential additions of BPA to the same batch of δ-MnO$_2$, BPA oxidation rate decreases by three orders of magnitude. Additionally, the production of its predominant oxidation product, 4-hydroxycumyl alcohol (HCA) decreases from 40% to 3%. This is attributed to the accumulation of interlayer Mn(II/III) produced during the reaction. This use of multiple

additions simulates the continuous introduction of BPA in near-surface environments or water treatment systems.

In stirred flow reactors containing δ-MnO$_2$, higher influent BPA concentration (i.e., introduction rate) does not lead to higher production of polymeric products formed by radical coupling, including HCA. However, more extensive transformation of δ-MnO$_2$ is observed at lower introduction rates. This is attributed to the longer reaction times required to normalize the total amount of BPA reacting with δ-MnO$_2$ solids. Higher production of aqueous Mn(II) during longer reactions is due to the increased opportunity for disproportionation and comproportionation to occur.

The oxidation of four target phenolic contaminants (i.e., BPA, triclosan, estrone, and *p*-cresol) show that interlayer cation species in birnessite (MnO$_2$) determine its reactivity toward phenols. Synthetic birnessites that are pre-exchanged with Na$^+$, K$^+$, Mg^{2+}, and Ca^{2+} react at different rates with the phenols. All four phenols follow the same trend where birnessite with Na$^+$-interlayer reacts the fastest, then K$^+$-interlayer, then Mg^{2+}-interlayer, and finally Ca^{2+}-interlayer. This is attributed to cations changing the overall oxidation state and altering the electron transfer rate.

Table of Contents

List of Figures

List of Tables

Acknowledgements

This dissertation would not be possible if it weren't for the help of my mentors, family, friends, and peers who supported me throughout this degree. I would like to acknowledge this community for their guidance and encouragement over the last five years.

To my advisor Matt Ginder-Vogel, thank you for your endless support. With your mentoring and advice, you have helped me become the scientist that I am today. You are always willing to sit down and talk, whether it is about science or otherwise. I am so grateful that I have been able to work with you over the past five years. You know you are lucky when you have an advisor who reminds you not to worry so much and that you don't have to follow the "rules" in life.

To my co-advisor Christy Remucal, you have been an incredible scientific mentor to me. Thank you for all your advice in scientific approach and writing. You are the queen of badass women scientists that get work done and you have been an inspiration to me. I admire your dedication to your professional and personal endeavors (your career, your family, your students) as well as your unbelievable efficiency and thoroughness.

I would also like to thank the other three members of my Final Oral Committee, Jim Hurley, Joel Pedersen, and Greg Harrington. I appreciate your time and energy in reviewing this dissertation and your feedback over the last five years.

To the members of WSEL, the 152 crew, you are all so encouraging, so thoughtful, and so hilarious. You truly make coming to work fun. I am so fortunate to have worked in a place with such amazing community. Thank you for your energy, your spirit, and your collective wisdom. A huge thank you to both Chris Worley and James Lazarcik for enduring the barrage of requests placed by myself and others in order to keep WSEL running.

Chapter 1

Introduction

1.1 Motivation

In this dissertation, we examine the oxidation of four target phenolic contaminants by manganese oxide. These phenolic contaminants (bisphenol A, *p*-cresol, triclosan, and estrone) were selected based on their presence in the environment, their toxicity, and their chemical structure. Manganese oxides are ubiquitous in the environment and can oxidize phenolic contaminants. The knowledge of the oxidation mechanism of simple model phenols has been widely studied,[1–6] but the understanding of more complex contaminant transformation is poorly understood. Furthermore, the effect of manganese oxide mineral characteristics has not been assessed. For example, the rate of phenol decreases with time as the mineral transforms, but these changes have generally been neglect as most studies focus on the initial reaction kinetics. This dissertation applies novel techniques to couple the oxidation of phenols with concurrent changes to the mineral.

1.2 Manganese in the Environment

Manganese is the fifth most abundant metal in earth's crust (Figure **1.1**), existing primarily as manganese oxides or manganese carbonate.[7] Manganese(III/IV) oxides are widely distributed in the environment and occur in a wide variety of environments, such as soils and sediments, ocean floors, and freshwater bodies.[8–12] Most manganese oxides are formed via microbially mediated pathways where various biota catalytically oxidize Mn(II) to Mn(III/IV)-oxides.[13–18] Abiotic oxidation of Mn(II) by atmospheric O_2 is kinetically limited below pH 8 and

does not greatly contribute to oxide formation.[19] Since manganese oxides are redox active minerals and have a high sorptive capacity for metal ions, they often regulate the mobility and bioavailability of environmental contaminants.[10] They are considered to be the strongest naturally occurring oxidants in the near surface and are capable of oxidizing many inorganic[20–23] and organic contaminants.[1,2,24,25]
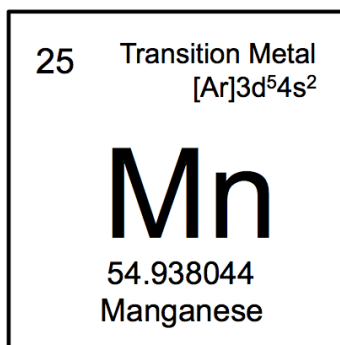
Figure 1.1. Elemental information about manganese.

1.3 Structure of Manganese Oxides

The building block of manganese oxides is the MnO_6 octahedron. These octahedra can connect via edge sharing and corner sharing (Figure **1.2**) to yield different structures.
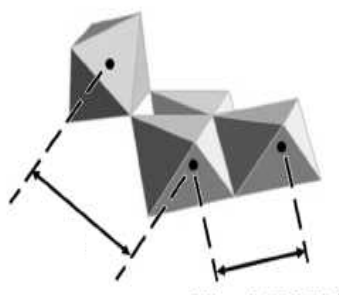
Figure 1.2. Schematic of corner-sharing (left) and edge-sharing (right) Mn octahedra in phyllomanganates. Adapted from Webb 2005.[26]

Manganese oxide structures can be divided into two categories that consist of tectomanganates (chain and tunnel structures) and phyllomanganates (layered structures). Phyllomanganates consist of planar sheets of edge-sharing octahedra that are stacked along the c-axis.[10,26] The layers often have Mn vacancies, where up to one out of every six MnO_6 octahedra is vacant. Interlayer water molecules and cations compensate for charge created by defects in the layers.[27,28] Manganese oxides studied as part of this dissertation are Mn(IV) phyllomanganates (Figure **1.3**) with some amount of Mn(III). These oxides are considered birnessite-like materials, defined by their structure and presence of Na^+ as an interlayer cation. Synthetic manganese oxides may be pure Mn(IV)-oxides, but most naturally occurring birnessites contain a significant amount of Mn(III) in the octahedral layers.[17,26,29–33]
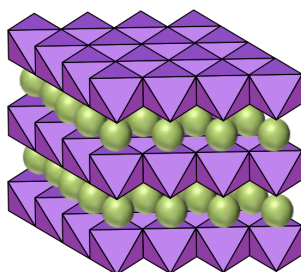
Figure 1.3. A representative phyllomanganate. Layers of MnO_6 octahedra (purple polygons) are offset by hydrated interlayer cations (green spheres).

1.4 Reactivity of Manganese Oxides

Manganese oxide minerals generally have high surface areas, which is conducive for both sorption and electron transfer reactions. As manganese oxide crystallinity increases, surface area decreases. Studies have found that certain heavy metals are often associated with manganese in soils and sediments.[34–37] Additionally, manganese oxides can oxidize inorganic metals such as

As(III) and Cr(III)[20,21,23,38,39] and organic contaminants such as anilines and phenols.[1,2,24,25] Previous research has examined the oxidation of model phenols[1,2,5,40–44] and anilines[45–47] to determine the reaction mechanism. Here, oxidation of phenolic contaminants is studied. The aim is to apply these fundamental mechanisms to more complex systems, working toward understanding how environmental factors impact oxidation.

1.5 Oxidation of Phenols

Phenolic compound oxidation by MnO_2 begins with diffusion to the mineral surface, followed by formation of a surface complex.[1,2,45,48] The phenolate anion (ArO$^-$) is then oxidized through a one-electron transfer via the surface complex.[1,6,45,49] The phenoxy radical (ArO·) formed in this process either diffuses away from the surface and reacts with other radicals to form polymeric products[1,24,45] or undergoes a second one-electron transfer to form a phenoxenium ion (ArO$^+$).[1,24,42,45,48] The phenoxenium ion then diffuses away from the mineral surface and undergoes hydrolysis to form a benzoquinone.[24,49] For some phenolic contaminants, this process triggers its degradation, resulting in the production of potentially less harmful compounds.

1.6 Phenolic Contamination

Anthropogenic phenols can be harmful to both humans and ecosystems. These compounds enter the environmental through municipal and industrial wastewater.[50–57] Many phenolic contaminants come from pharmaceuticals and industrial chemicals. Fortunately, phenols are susceptible to oxidation by manganese oxides via the mechanism presented above. Contaminants that are susceptible to oxidation by manganese oxide include antibacterial

agents,[48,58–69] polyaminocarboxylate ligands,[70] endocrine disruptors,[69,71–75] brominated flame retardants,[76] rubber additives,[77] pain relievers,[78,79] and anti-epileptic pharmaceuticals.[80] The four target phenols presented in this dissertation are bisphenol A, *p*-cresol, triclosan, and estrone (Figure **1.4**).

Bisphenol A   **p-Cresol**   **Triclosan**   **Estrone**
(BPA)   **(E1)**
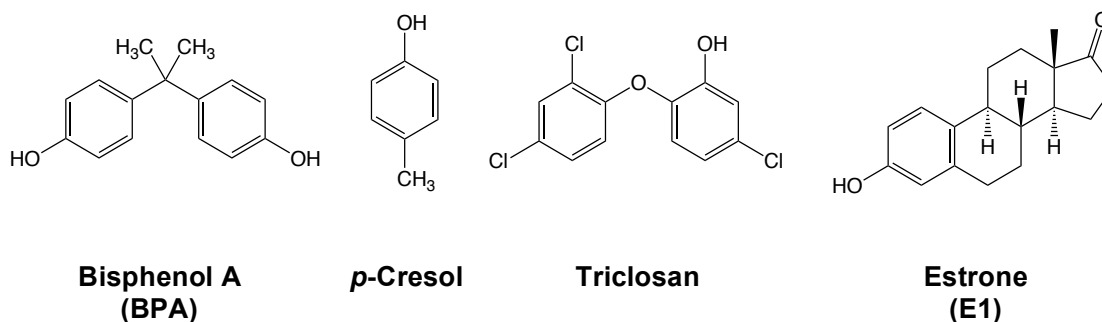
Figure 1.4. Four phenols used in this dissertation as target contaminants.

1.6.1 Bisphenol A

Bisphenol A, or BPA, is the primary phenolic contaminant used in this study. It is a complex compound that is used in numerous studies and is a contaminant of public concern. BPA is a phenol that is used in industry for the manufacture of polycarbonate plastics and epoxy resins. Releases of BPA to the environment exceed 1 million pounds per year.[81] BPA has been reported to be a reproductive, developmental, and systemic toxicant and weakly estrogenic.[82] It is found in drinking containers, toys, the lining in metal cans, water pipes, eyeglass lenses, sports safety equipment, dental monomers, medical equipment and tubing, and consumer electronics.[83] Most human exposure is due to ingestion of food that has been stored in a BPA-containing material.[84] In addition to the potential human health risks that BPA poses, it also threatens a severe disturbance to the environment. BPA is ubiquitous in the environment, appearing in

groundwater, soil, natural waters,[85,86] and even in the muscle, brain, and liver of wild fish.[87] BPA concentrations in the freshwater bodies in North America range from 0.45 to 8000 ng/L.[88]

1.6.2 Triclosan

Triclosan (5-chloro-2-(2,4-dichlorophenoxy)phenol) is an antibacterial agent used in personal care and consumer products. It is one of the most frequently detected contaminants of emerging concern in surface streams at a median concentration of 0.14 µg/L.[89] Its methyl derivative is found in wastewater,[90–92] surface water,[92,93] sediments,[93] and fish.[93] The Food and Drug Administration banned the use of triclosan in liquid antibacterial hand soaps in 2016, citing risks of bacterial resistance and hormonal effects.[94] The presence of antibacterial residues in the environment has the potential to promote growth of antibiotic resistant bacteria and may pose adverse health effects to humans.[95] The FDA also reports that there is not enough science to show that antibacterial soaps are more effective at preventing illness than other soaps.[96] Triclosan is still used in personal care products such as deodorant, toothpaste, and shaving gel.

1.6.3 p-Cresol

Cresols are a group of natural and manufactured phenolic compounds. They are found in low levels in ambient air from car exhaust, power plants, and oil refineries.[97] Acute inhalation or ingestion exposure by humans causes effects on the respiratory system, blood, liver, kidney, and central nervous system.[98,99] The isomer used in this dissertation, p-cresol, is primarily used for antioxidant formulation in fragrances and dyes.[97] This compound was chosen for the project to add a contaminant that is a simple substituted phenol to otherwise complex contaminants.

1.6.4 Estrone

Estrone, or E1, is a natural steroid estrogen produced by humans and other animals. Elevated levels of estrogens are found in the environment due to the production of both natural and synthetic steroidal estrogens by human activity.[100] This arises from birth control and other pharmaceuticals as well as a large amount from livestock.[101] Estrogens enter the environment through discharge of wastewater effluent and direct application of manure onto agricultural land.[102] Although these hormones are essential for human biology and physiology, adverse hormonal effects are seen in humans in even slightly elevated concentrations.[103] At high levels, they are causally linked to breast cancer in females[104] and prostate cancer in men.[105] Additionally, elevated estrogen levels in natural waters feminize male fish and vice versa.[106–110] Estrogens also influence growth rates in plants, although both growth inhibition and stimulation has been observed.[100]

1.7 Potential for Water Treatment

This research has the potential to be used in engineered systems to improve water quality in a variety of settings (Figure **1.5**). Phenolic contaminants are frequently detected in wastewater effluent and stormwater runoff.[53–57,111–113] Manganese oxides have been proposed for passive water treatment for contaminants in urban stormwater runoff, landfill leachate, green infrastructure, or water from other contaminated sources.[1,2,14,40,46,51–53,111,113–116] In order to implement such a treatment system, knowledge of the fundamental chemistry of this reaction is required. Important factors would include the lifetime of a MnO_2 filter, organic products formed, including those formed after repeated exposure, and production of aqueous Mn(II). The details

provided in the results of this research study greatly contribute to the knowledge base required for the development of such a product.
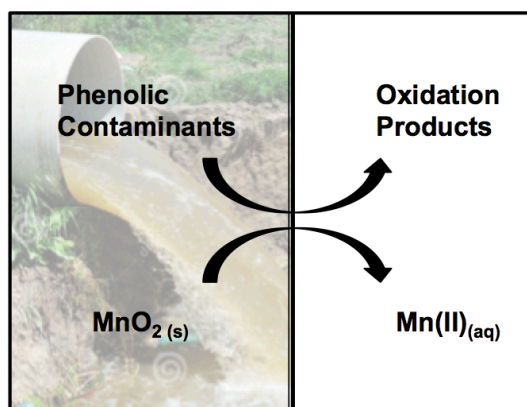
Figure 1.5. Solid MnO$_2$ oxidizes phenolic compounds, forming oxidation products and aqueous Mn(II).

1.8 Identified Research Needs

Initial studies of the oxidation of organic compounds in the presence of manganese oxides focus on reductive dissolution of the solids in the presence of high initial organic compound concentrations.[1,2,48,58] More recent studies focus on the loss rates of the organic compounds, rather than dissolution of the mineral. These studies report changes in reaction rates while varying pH,[48,59,73,115] in the presence of cations,[71,117–120] and/or dissolved organic matter.[118–120] Previous research provides extensive information describing the oxidation mechanism of model compounds. However, a missing component is the connection between oxidation kinetics and the mineral structure. One way that the structure could affect reactivity is via transformation during the reaction itself. As manganese oxide is reduced by an organic contaminant, it undergoes changes at the mineral surface. The effects of these changes have not been reported. Additionally, cations present in solution inhibit the reaction, but the effect of

interlayer cations on reactivity has not been assessed. Interlayer cations can affect the micromorphology of phyllomanganates[121] and therefore have the potential to affect reactivity.

1.9 Research Objectives

The focus of previous studies on phenolic compounds and MnO_2 is limited by the short exposure of MnO_2 to the organic. Since the rate of phenol oxidation decreases as the reaction proceeds, analysis of extensive reactions is an important part of this study. Repeated or continuous exposure of MnO_2 to an organic simulates redox-active MnO_2 in the environment and allows for the characterization of mineral changes and their effect on reactivity. This dissertation aims to fill in knowledge gaps of this reaction by determining 1) the cause of changes in kinetics and thoroughly examining mineralogical transformations by conducting multi-addition reactions; 2) if single-addition batch reactors used in previous studies are suitable surrogates for environmental reactions by comparing them to extended stirred-flow reactions; and 3) if the reported effects of cation cosolutes are representative of cations in solution or if they are integrating into the mineral as interlayer cations.

In Chapter 2, we quantify bisphenol A (BPA) oxidation rates and the formation of its predominant product, 4-hydroxycumyl alcohol (HCA), in tandem with transformation of Mn(III)-rich δ-MnO_2. We show how changes in the mineral, such as the production of reduced manganese on the surface, affect the oxidation kinetics of BPA. Since there is minimal information on phenol oxidation by manganese oxides over longer reactions, we perform multi-addition batch reactions by adding BPA 12 times to the same batch of MnO_2. We show that over the 12 additions, BPA oxidation rate decreases by three orders of magnitude and production of HCA decreases from 40% to 3%. The use of multiple additions simulates the continuous

introduction of BPA in near-surface environments or water treatment systems. By characterizing both the solution and solid phases, we provide a comprehensive conceptual model of this complex redox reaction.

In Chapter 3, we use δ-MnO$_2$ in stirred flow reactors to determine if higher influent BPA concentrations, or introduction rates, lead to increased polymer production. HCA, which is formed through radical coupling, is used as one metric for polymer production. Calculated HCA yield and aqueous Mn(II) detection shows that influent BPA concentration does not affect polymeric production, but it does affect BPA oxidation rate and manganese reduction. Further research on Mn(II) production and sorption in stirred flow reactors show that disproportionation and comproportionation influence changes in manganese reduction, rather than increased single electron transfer reactions (i.e., polymeric production). Radicals formed via single electron transfer are of concern as they can couple with dissolved organic matter or other compounds in the environment, forming unknown high molecular weight products.[122–124] By performing these reactions in a stirred flow reactor we are able to draw novel insights into the effects of contaminant loading over long time periods, which is more representative of contaminants in a flow-through treatment system.[51,111]

In Chapter 4, we investigate the effects of cations on the reactivity of birnessite towards four target phenols. Synthetic birnessites are pre-exchanged with interlayer cations (Na$^+$, K$^+$, Mg^{2+}, and Ca^{2+}) and are used to explore the effects mineral structure and reactivity. The four target phenols (i.e., BPA, triclosan, estrone, and p-cresol), react with birnessite at different rates, but all follow the same trend where Na$^+$-interlayer birnessite reacts the fastest, then K$^+$-interlayer, then Mg^{2+}-interlayer, and finally Ca^{2+}-interlayer. This change in reactivity is driven by the interlayer cations and is attributed to lower electron transfer rate as cations reduce the overall

oxidation state. These results indicate why there may be a large difference in the reaction rate measured in a laboratory setting compared to an environmental or engineered setting.

1.10 References:

(1)   Stone, A. T. Reductive dissolution of manganese(III/IV) oxides by substituted phenols. *Environ. Sci. Technol.* **1987**, *21* (10), 979–988.

(2)   Stone, A. T.; Morgan, J. J. Reduction and dissolution of manganese(III) and manganese(IV) oxides by organics. 1. Reaction with hydroquinone. *Environ. Sci. Technol.* **1984**, *18* (6), 450–456.

(3)   McBride, M. B. Adsorption and oxidation of phenolic compounds by iron and manganese oxides. *Env. Toxicol. Chem* **1987**, *51* (6), 1466–1472.

(4)   McBride, M. B. Oxidation of 1, 2-and 1, 4-dihydroxybenzene by birnessite in acidic aqueous suspension. *Clays Clay Min.* **1989**, *37*, 479–486.

(5)   Ukrainczyk, L.; McBride, M. B. Oxidation and dechlorination of chlorophenols in dilute aqueous suspensions of manganese oxides: Reaction products. *Environ. Toxicol. Chem.* **1993**, *12* (11), 2015–2022.

(6)   Ukrainczyk, L.; McBride, M. B. Oxidation of phenol in acidic aqueous suspensions of manganese oxides. *Clays Clay Min.* **1992**, *40* (2), 157–166.

(7)   Emsley, J. *Nature's Building Blocks: An A-Z Guide to the Elements*, 2nd ed.; Oxford University Press, 2011.

(8)   Dick, G. J.; Lee, Y. E.; Tebo, B. M. Manganese(II)-oxidizing *bacillus* spores in Guaymas Basin hydrothermal sediments and plumes. *Appl. Environ. Microbiol.* **2006**, *72* (5), 3184–3190.

(9)   Negra, C.; Ross, D. S.; Lanzirotti, A. Oxidizing behavior of soil manganese. *Soil Sci. Soc. Am. J.* **2005**, *69* (1), 87–95.

(10)   Post, J. E. Manganese oxide minerals: Crystal structures and economic and environmental significance. *Proc. Natl. Acad. Sci.* **1999**, *96* (7), 3447–3454.

(11)   Tani, Y.; Miyata, N.; Iwahori, K.; Soma, M.; Tokuda, S.; Seyama, H.; Theng, B. K. G. Biogeochemistry of manganese oxide coatings on pebble surfaces in the Kikukawa River System, Shizuoka, Japan. *Appl. Geochem.* **2003**, *18* (10), 1541–1554.

(12)   Wehrli, B.; Friedl, G.; Manceau, A. Reaction rates and products of manganese oxidation at the sediment-water interface. In *Aquatic Chemistry*; Huang, C. P., O'Melia, C. R., Morgan, J. J., Eds.; American Chemical Society: Washington, DC, 1995; Vol. 244, pp 111–134.

(13)   Tebo, B. M. Manganese(II) oxidation in the suboxic zone of the Black Sea. *Deep Sea Res. Part Oceanogr. Res. Pap.* **1991**, *38*, S883–S905.

(14)   Tebo, B. M.; Bargar, J. R.; Clement, B. G.; Dick, G. J.; Murray, K. J.; Parker, D.; Verity, R.; Webb, S. M. Biogenic manganese oxides: Properties and mechanisms of formation. *Annu. Rev. Earth Planet. Sci.* **2004**, *32* (1), 287–328.

(15)   Hastings, D.; Emerson, S. Oxidation of manganese by spores of a marine *bacillus*: Kinetic and thermodynamic considerations. *Geochim. Cosmochim. Acta* **1986**, *50* (8), 1819–1824.

(16)   Adams, L. F.; Ghiorse, W. C. Oxidation state of Mn in the Mn oxide produced by *Leptothrix discophora* SS-1. *Geochim. Cosmochim. Acta* **1988**, *52* (8), 2073–2076.

(17)   Villalobos, M.; Toner, B.; Bargar, J.; Sposito, G. Characterization of the manganese oxide produced by *Pseudomonas Putida* strain MnB1. *Geochim. Cosmochim. Acta* **2003**, *67* (14), 2649–2662.

(18) Miyata, N.; Tani, Y.; Maruo, K.; Tsuno, H.; Sakata, M.; Iwahori, K. Manganese(IV) oxide production by *Acremonium* sp. strain KR21-2 and extracellular Mn(II) oxidase activity. *Appl. Environ. Microbiol.* **2006**, *72* (10), 6467–6473.

(19) von Langen, P. J.; Johnson, K. S.; Coale, K. H.; Elrod, V. A. Oxidation kinetics of manganese (II) in seawater at nanomolar concentrations. *Geochim. Cosmochim. Acta* **1997**, *61* (23), 4945–4954.

(20) Eary, L. E.; Rai, D. Kinetics of chromium(III) oxidation to chromium(VI) by reaction with manganese dioxide. *Environ. Sci. Technol.* **1987**, *21* (12), 1187–1193.

(21) Lafferty, B. J.; Ginder-Vogel, M.; Sparks, D. L. Arsenite oxidation by a poorly-crystalline manganese oxide. 3. Arsenic and manganese desorption. *Environ. Sci. Technol.* **2011**, *45* (21), 9218–9223.

(22) Landrot, G.; Ginder-Vogel, M.; Livi, K.; Fitts, J. P.; Sparks, D. L. Chromium(III) oxidation by three poorly crystalline manganese(IV) oxides. 2. Solid phase analyses. *Environ. Sci. Technol.* **2012**, *46* (21), 11601–11609.

(23) Tournassat, C.; Charlet, L.; Bosbach, D.; Manceau, A. Arsenic(III) oxidation by birnessite and precipitation of manganese(II) arsenate. *Environ. Sci. Technol.* **2002**, *36* (3), 493–500.

(24) Remucal, C. K.; Ginder-Vogel, M. A critical review of the reactivity of manganese oxides with organic contaminants. *Environ. Sci. Process. Impacts* **2014**, *16* (6), 1247–1266.

(25) Xyla, A. G.; Sulzberger, B.; Luther III, G. W.; Hering, J. G.; Van Cappellen, P.; Stumm, W. Reductive dissolution of manganese(III,IV) (hydr)oxides by oxalate: The effect of pH and light. *Langmuir* **1992**, *8* (1), 95–103.

(26) Webb, S. M.; Tebo, B. M.; Bargar, J. R. Structural characterization of biogenic Mn oxides produced in seawater by the marine *bacillus* sp. strain SG-1. *Am. Mineral.* **2005**, *90* (8–9), 1342–1357.

(27) Lanson, B.; Drits, V. A.; Silvester, E.; Manceau, A. Structure of H-exchanged hexagonal birnessite and its mechanism of formation from Na-rich monoclinic buserite at low pH. *Am. Mineral.* **2000**, *85* (5–6), 826–838.

(28) Silvester, E.; Manceau, M.; Drits, V. A. Structure of synthetic monoclinic Na-rich birnessite and hexagonal birnessite: II. Results from chemical studies and EXAFS spectroscopy. *Am. Mineral.* **1997**, *82*, 962–978.

(29) Buatier, M. D.; Guillaume, D.; Wheat, C. G.; Herve, L.; Adatte, T. Mineralogical characterization and genesis of hydrothermal Mn oxides from the flank of the Juan the Fuca Ridge. *Am. Mineral.* **2004**, *89* (11–12), 1807–1815.

(30) McKeown, D. A.; Post, J. E. Characterization of manganese oxide mineralogy in rock varnish and dendrites using X-ray absorption spectroscopy. *Am. Mineral.* **2001**, *86* (5–6), 701–713.

(31) Bargar, J. R.; Fuller, C. C.; Marcus, M. A.; Brearley, A. J.; Perez De la Rosa, M.; Webb, S. M.; Caldwell, W. A. Structural characterization of terrestrial microbial Mn oxides from Pinal Creek, AZ. *Geochim. Cosmochim. Acta* **2009**, *73* (4), 889–910.

(32) Jurgensen, A.; Widmeyer, J. R.; Gordon, R. A.; Bendell-Young, L. I.; Moore, M. M.; Crozier, E. D. The structure of the manganese oxide on the sheath of the bacterium *Leptothrix discophora*: An XAFS study. *Am. Mineral.* **2004**, *89* (7), 1110–1118.

(33) Saratovsky, I.; Wightman, P. G.; Pastén, P. A.; Gaillard, J.-F.; Poeppelmeier, K. R. Manganese oxides: Parallels between abiotic and biotic structures. *J. Am. Chem. Soc.* **2006**, *128* (34), 11188–11198.

(34) Whitney, P. R. Relationship of manganese-iron oxides and associated heavy metals to grain size in stream sediments. *J. Geochem. Explor.* **1975**, *4* (2), 251–263.

(35) Gadde, R. Rao.; Laitinen, H. A. Heavy metal adsorption by hydrous iron and manganese oxides. *Anal. Chem.* **1974**, *46* (13), 2022–2026.

(36) Jenne, E. A. Controls on Mn, Fe, Co, Ni, Cu, and Zn concentrations in soils and water: The significant role of hydrous Mn and Fe oxides. In *Trace Inorganics in Water*; Advances in Chemistry; American Chemical Society, 1968; Vol. 73, pp 337–387.

(37) Krauskopf, K. B. Factors controlling the concentrations of thirteen rare metals in sea-water. *Geochim. Cosmochim. Acta* **1956**, *9* (1–2), 1–32.

(38) Landrot, G.; Ginder-Vogel, M.; Sparks, D. L. Kinetics of chromium(III) oxidation by manganese(IV) oxides using quick scanning X-ray absorption fine structure spectroscopy (Q-XAFS). *Environ. Sci. Technol.* **2010**, *44* (1), 143–149.

(39) Tang, Y.; Webb, S. M.; Estes, E. R.; Hansel, C. M. Chromium(III) oxidation by biogenic manganese oxides with varying structural ripening. *Env. Sci Process. Impacts* **2014**, *16* (9), 2127–2136.

(40) Ulrich, H. J.; Stone, A. T. The oxidation of chlorophenols adsorbed to manganese oxide surfaces. *Environ. Sci. Technol.* **1989**, *23* (4), 421–428.

(41) Nico, P. S.; Zasoski, R. J. Mn(III) center availability as a rate controlling factor in the oxidation of phenol and sulfide on δ-MnO_2. *Environ. Sci. Technol.* **2001**, *35* (16), 3338–3343.

(42) Stone, A. T.; Morgan, J. J. Reduction and dissolution of manganese(III) and manganese(IV) oxides by organics: 2. Survey of the reactivity of organics. *Environ. Sci. Technol.* **1984**, *18* (8), 617–624.

(43) Bertino, D. J.; Zepp, R. G. Effects of solar radiation on manganese oxide reactions with selected organic compounds. *Environ. Sci. Technol.* **1991**, *25* (7), 1267–1273.

(44) Zhao, L.; Yu, Z.; Peng, P.; Huang, W.; Dong, Y. Oxidative transformation of tetrachlorophenols and trichlorophenols by manganese dioxide. *Env. Toxicol Chem* **2009**, *28* (6), 1120–1129.

(45) Laha, S.; Luthy, R. G. Oxidation of aniline and other primary aromatic amines by manganese dioxide. *Environ. Sci. Technol.* **1990**, *24* (3), 363–373.

(46) Pizzigallo, M. D.; Ruggiero, P.; Crecchio, C.; Mascolo, G. Oxidation of chloroanilines at metal oxide surfaces. *J. Agric. Food Chem.* **1998**, *46* (5), 2049–2054.

(47) Li, H.; Lee, L. S.; Schulze, D. G.; Guest, C. A. Role of soil manganese in the oxidation of aromatic amines. *Environ. Sci. Technol.* **2003**, *37* (12), 2686–2693.

(48) Zhang, H.; Huang, C.-H. Oxidative transformation of triclosan and chlorophene by manganese oxides. *Environ. Sci. Technol.* **2003**, *37* (11), 2421–2430.

(49) Jiang, J.; Gao, Y.; Pang, S.-Y.; Lu, X.-T.; Zhou, Y.; Ma, J.; Wang, Q. Understanding the role of manganese dioxide in the oxidation of phenolic compounds by aqueous permanganate. *Environ. Sci. Technol.* **2015**, *49* (1), 520–528.

(50) Fan, Z.; Hu, J.; An, W.; Yang, M. Detection and occurrence of chlorinated byproducts of bisphenol A, nonylphenol, and estrogens in drinking water of China: Comparison to the parent compounds. *Environ. Sci. Technol.* **2013**, *47* (19), 10841–10850.

(51) Charbonnet, J. A.; Duan, Y.; van Genuchten, C. M.; Sedlak, D. L. Chemical regeneration of manganese oxide-coated sand for oxidation of organic stormwater contaminants. *Environ. Sci. Technol.* **2018**, *52* (18), 10728–10736.

(52) Grebel, J. E.; Mohanty, S. K.; Torkelson, A. A.; Boehm, A. B.; Higgins, C. P.; Maxwell, R. M.; Nelson, K. I.; Sedlak, D. L. Engineered infiltration systems for urban stormwater reclamation. *Env. Eng Sci* **2013**, *30* (8), 437–454.

(53) Luthy, R. G.; Sedlak, D. L. *Enhanced removal of nutrients and trace organic contaminants in pilot-scale stormwater treatment systems*; Annual Report; U. S. EPA: Water Research Foundation, 2017.

(54) Bina, B.; Mohammadi, F.; Amin, M. M.; Pourzamani, H. R.; Yavari, Z. Determination of 4-nonylphenol and 4-*tert*-octylphenol compounds in various types of wastewater and their removal rates in different treatment processes in nine wastewater treatment plants of Iran. *Chin. J. Chem. Eng.* **2018**, *26* (1), 183–190.

(55) Bulloch, D. N.; Nelson, E. D.; Carr, S. A.; Wissman, C. R.; Armstrong, J. L.; Schlenk, D.; Larive, C. K. Occurrence of halogenated transformation products of selected pharmaceuticals and personal care products in secondary and tertiary treated wastewaters from southern California. *Environ. Sci. Technol.* **2015**, *49* (4), 2044–2051.

(56) Lin, K.; Liu, W.; Gan, J. Reaction of tetrabromobisphenol A (TBBPA) with manganese dioxide: Kinetics, products, and pathways. *Environ. Sci. Technol.* **2009**, *43* (12), 4480–4486.

(57) Montes-Grajales, D.; Fennix-Agudelo, M.; Miranda-Castro, W. Occurrence of personal care products as emerging chemicals of concern in water resources: A review. *Sci. Total Environ.* **2017**, *595*, 601–614.

(58) Zhang, H.; Chen, W.-R.; Huang, C.-H. Kinetic modeling of oxidation of antibacterial agents by manganese oxide. *Environ. Sci. Technol.* **2008**, *42* (15), 5548–5554.

(59) Rubert, Kennedy F.; Pedersen, J. A. Kinetics of oxytetracycline reaction with a hydrous manganese oxide. *Environ. Sci. Technol.* **2006**, *40* (23), 7216–7221.

(60) Chen, W.-R.; Ding, Y.; Johnston, C. T.; Teppen, B. J.; Boyd, S. A.; Li, H. Reaction of lincosamide antibiotics with manganese oxide in aqueous solution. *Environ. Sci. Technol.* **2010**, *44* (12), 4486–4492.

(61) Chen, W.-R.; Huang, C.-H. Transformation of tetracyclines mediated by Mn(II) and Cu(II) ions in the presence of oxygen. *Environ. Sci. Technol.* **2009**, *43* (2), 401–407.

(62) Dong, J.; Li, Y.; Zhang, L.; Liu, C.; Zhuang, L.; Sun, L.; Zhou, J. The oxidative degradation of sulfadiazine at the interface of α-MnO$_2$ and water: Degradation of antibiotics by manganese dioxides. *J. Chem. Technol. Biotechnol.* **2009**, *84* (12), 1848–1853.

(63) Feitosa-Felizzola, J.; Hanna, K.; Chiron, S. Adsorption and transformation of selected human-used macrolide antibacterial agents with iron(III) and manganese(IV) oxides. *Environ. Pollut.* **2009**, *157* (4), 1317–1322.

(64) Liu, C.; Zhang, L.; Li, F.; Wang, Y.; Gao, Y.; Li, X.; Cao, W.; Feng, C.; Dong, J.; Sun, L. Dependence of sulfadiazine oxidative degradation on physicochemical properties of manganese dioxides. *Ind. Eng. Chem. Res.* **2009**, *48* (23), 10408–10413.

(65) Chen, W.-R.; Huang, C.-H. Transformation kinetics and pathways of tetracycline antibiotics with manganese oxide. *Environ. Pollut.* **2011**, *159* (5), 1092–1100.

(66) Chen, G.; Zhao, L.; Dong, Y. Oxidative degradation kinetics and products of chlortetracycline by manganese dioxide. *J. Hazard. Mater.* **2011**, *193*, 128–138.

(67) Gao, J.; Hedman, C.; Liu, C.; Guo, T.; Pedersen, J. A. Transformation of sulfamethazine by manganese oxide in aqueous solution. *Environ. Sci. Technol.* **2012**, *46* (5), 2642–2651.

(68) Xiao, X.; Sun, S.-P.; McBride, M. B.; Lemley, A. T. Degradation of ciprofloxacin by cryptomelane-type manganese(III/IV) oxides. *Environ. Sci. Pollut. Res.* **2013**, *20* (1), 10–21.

(69) Shaikh, N.; Taujale, S.; Zhang, H.; Artyushkova, K.; Ali, A.-M. S.; Cerrato, J. M. Spectroscopic investigation of interfacial interaction of manganese oxide with triclosan, aniline, and phenol. *Environ. Sci. Technol.* **2016**, *50* (20), 10978–10987.

(70) McArdell, C. S.; Stone, A. T.; Tian, J. Reaction of EDTA and related aminocarboxylate chelating agents with $Co^{III}OOH$ (heterogenite) and $Mn^{III}OOH$ (manganite). *Environ. Sci. Technol.* **1998**, *32* (19), 2923–2930.

(71) Lu, Z.; Lin, K.; Gan, J. Oxidation of bisphenol F (BPF) by manganese dioxide. *Environ. Pollut.* **2011**, *159* (10), 2546–2551.

(72) Jiang, L.; Huang, C.; Chen, J.; Chen, X. Oxidative transformation of 17β-estradiol by MnO_2 in aqueous solution. *Arch. Environ. Contam. Toxicol.* **2009**, *57* (2), 221–229.

(73) Xu, L.; Xu, C.; Zhao, M.; Qiu, Y.; Sheng, G. Oxidative removal of aqueous steroid estrogens by manganese oxides. *Water Res.* **2008**, *42* (20), 5038–5044.

(74) Rudder, J. de; Wiele, T. V. de; Dhooge, W.; Comhaire, F.; Verstraete, W. Advanced water treatment with manganese oxide for the removal of 17α-ethynylestradiol (EE2). *Water Res.* **2004**, *38* (1), 184–192.

(75) Kim, D.-G.; Jiang, S.; Jeong, K.; Ko, S.-O. Removal of 17α-ethinylestradiol by biogenic manganese oxides produced by the *Pseudomonas putida* strain MnB1. *Water. Air. Soil Pollut.* **2012**, *223* (2), 837–846.

(76) Lin, K.; Liu, W.; Gan, J. Reaction of tetrabromobisphenol A (TBBPA) with manganese dioxide: Kinetics, products, and pathways. *Environ. Sci. Technol.* **2009**, *43* (12), 4480–4486.

(77) Dong, J.; Zhang, L.; Liu, H.; Liu, C.; Gao, Y.; Sun, L. The oxidative degradation of 2-mercaptobenzothialzole by different manganese dioxides. *Fresenius Environ. Bull.* **2010**, *19*, 1615–1622.

(78) Zhang, Y.; Yang, Y.; Zhang, Y.; Zhang, T.; Ye, M. Heterogeneous oxidation of naproxen in the presence of α-MnO_2 nanostructures with different morphologies. *Appl. Catal. B Environ.* **2012**, *127*, 182–189.

(79) Xiao, H.; Song, H.; Xie, H.; Huang, W.; Tan, J.; Wu, J. Transformation of acetaminophen using manganese dioxide − mediated oxidative processes: Reaction rates and pathways. *J. Hazard. Mater.* **2013**, *250–251*, 138–146.

(80) He, Y.; Xu, J.; Zhang, Y.; Guo, C.; Li, L.; Wang, Y. Oxidative transformation of carbamazepine by manganese oxides. *Environ. Sci. Pollut. Res.* **2012**, *19* (9), 4206–4213.

(81) Bisphenol A Action Plan. U.S. EPA March 2010.

(82) Takeuchi, T.; Tsutsumi, O.; Ikezuki, Y.; Takai, Y.; Taketani, Y. Positive relationship between androgen and the endocrine disruptor, bisphenol A, in normal women and women with ovarian dysfunction. *Endocr. J.* **2004**, *51* (2), 165–169.

(83) The Polycarbonate/BPA Global Group https://plastics.americanchemistry.com (accessed Apr 16, 2019).

(84) Calafat, A. M.; Ye, X.; Wong, L.-Y.; Reidy, J. A.; Needham, L. L. Exposure of the U.S. population to bisphenol A and 4-tertiary-octylphenol: 2003-2004. *Environ. Health Perspect.* **2008**, *116* (1), 39–44.

(85) Baldwin, A. K.; Corsi, S. R.; De Cicco, L. A.; Lenaker, P. L.; Lutz, M. A.; Sullivan, D. J.; Richards, K. D. Organic contaminants in Great Lakes tributaries: Prevalence and potential aquatic toxicity. *Sci. Total Environ.* **2016**, *554–555*, 42–52.

(86) Belfroid, A.; van Velzen, M.; van der Horst, B.; Vethaak, D. Occurrence of bisphenol A in surface water and uptake in fish: Evaluation of field measurements. *Chemosphere* **2002**, *49* (1), 97–103.

(87) Renz, L.; Volz, C.; Michanowicz, D.; Ferrar, K.; Christian, C.; Lenzner, D.; El-Hefnawy, T. A study of parabens and bisphenol A in surface water and fish brain tissue from the Greater Pittsburgh Area. *Ecotoxicology* **2013**, *22* (4), 632–641.

(88) Staples, C. A.; Dorn, P. B.; Klecka, G. M.; O'Block, S. T.; Branson, D. R.; Harris, L. R. Bisphenol A concentrations in receiving waters near US manufacturing and processing facilities. *Chemosphere* **2000**, *40* (5), 521–525.

(89) Kolpin, D. W.; Furlong, E. T.; Meyer, M. T.; Thurman, E. M.; Zaugg, S. D.; Barber, L. B.; Buxton, H. T. Pharmaceuticals, hormones, and other organic wastewater contaminants in U.S. streams, 1999−2000: A national reconnaissance. *Environ. Sci. Technol.* **2002**, *36* (6), 1202–1211.

(90) Paxeus, N. Organic pollutants in the effluents of large wastewater treatment plants in Sweden. *Water Res.* **1996**, *30* (5), 1115–1122.

(91) McAvoy, D. C.; Schatowitz, B.; Jacob, M.; Hauk, A.; Eckhoff, W. S. Measurement of triclosan in wastewater treatment systems. *Environ. Toxicol. Chem.* **2002**, *21* (7), 1323–1329.

(92) Lindström, A.; Buerge, I. J.; Poiger, T.; Bergqvist, P.-A.; Müller, M. D.; Buser, H.-R. Occurrence and environmental behavior of the bactericide triclosan and its methyl derivative in surface waters and in wastewater. *Environ. Sci. Technol.* **2002**, *36* (11), 2322–2329.

(93) Okumura, T.; Nishikawa, Y. Gas chromatography-mass spectrometry determination of triclosans in water, sediment and fish samples via methylation with diazomethane. *Anal. Chim. Acta* **1996**, *325* (3), 175–184.

(94) Food and Drug Administration. *Safety and effectiveness of consumer antiseptics; topical antimicrobial drug products for over-the-counter human use*; Rules and Regulations 21 CFR Part 310; Federal Register, 2016; p Vol. 81, No. 172.

(95) Levy, S. B.; Marshall, B. Antibacterial resistance worldwide: Causes, challenges and responses. *Nat. Med.* **2004**, *10* (12s), S122–S129.

(96) U.S. Food & Drug Administration. Antibacterial soap? You can skip it, use plain soap and water www.fda.gov (accessed Apr 22, 2019).

(97) Agency for Toxic Substances and Disease Registry. *Toxicological Profile for Cresols*; U.S. Department of Health and Human Services: Atlanta, GA, 1990.

(98) U.S. Environmental Protection Agency. *Cresol/Cresylic Acid*; Fact Sheet; 2000.

(99) De Smet, R.; Van Kaer, J.; Van Vlem, B.; De Cubber, A.; Brunet, P.; Lameire, N.; Vanholder, R. Toxicity of free *p*-cresol: A prospective and cross-sectional analysis. *Clin. Chem.* **2003**, *49* (3), 470–478.

(100) Adeel, M.; Song, X.; Wang, Y.; Francis, D.; Yang, Y. Environmental impact of estrogens on human, animal and plant life: A critical review. *Environ. Int.* **2017**, *99*, 107–119.

(101) Shrestha, S. L.; Casey, F. X. M.; Hakk, H.; Smith, D. J.; Padmanabhan, G. Fate and transformation of an estrogen conjugate and its metabolites in agricultural soils. *Environ. Sci. Technol.* **2012**, *46* (20), 11047–11053.

(102) Biswas, S.; Shapiro, C. A.; Kranz, W. L.; Mader, T. L.; Shelton, D. P.; Snow, D. D.; Bartelt-Hunt, S. L.; Tarkalson, D. D.; van Donk, S. J.; Zhang, T. C.; et al. Current knowledge on the environmental fate, potential impact, and management of growth-promoting steroids used in the US beef cattle industry. *J. Soil Water Conserv.* **2013**, *68* (4), 325–336.

(103) Plotan, M.; Elliott, C. T.; Frizzell, C.; Connolly, L. Estrogenic endocrine disruptors present in sports supplements. A risk assessment for human health. *Food Chem.* **2014**, *159*, 157–165.

(104) Moore, S. C.; Matthews, C. E.; Ou Shu, X.; Yu, K.; Gail, M. H.; Xu, X.; Ji, B.-T.; Chow, W.-H.; Cai, Q.; Li, H.; Yang, G.; Ruggieri, D.; Boyd-Morin, J.; Rothman, N.; Hoover, R. N.; Gao, Y.-T.; Zheng, W.; Ziegler, R. G. Endogenous estrogens, estrogen metabolites, and breast cancer risk in postmenopausal Chinese women. *J. Natl. Cancer Inst.* **2016**, *108* (10).

(105) Nelles, J. L.; Hu, W.-Y.; Prins, G. S. Estrogen action and prostate cancer. *Expert Rev. Endocrinol. Metab.* **2011**, *6* (3), 437–451.

(106) Arnold, K. E.; Brown, A. R.; Ankley, G. T.; Sumpter, J. P. Medicating the environment: Assessing risks of pharmaceuticals to wildlife and ecosystems. *Philos. Trans. R. Soc. B Biol. Sci.* **2014**, *369* (1656), 20130569–20130569.

(107) Tetreault, G. R.; Bennett, C. J.; Shires, K.; Knight, B.; Servos, M. R.; McMaster, M. E. Intersex and reproductive impairment of wild fish exposed to multiple municipal wastewater discharges. *Aquat. Toxicol.* **2011**, *104* (3–4), 278–290.

(108) Rose, E.; Paczolt, K. A.; Jones, A. G. The effects of synthetic estrogen exposure on premating and postmating episodes of selection in sex-role-reversed Gulf pipefish. *Evol. Appl.* **2013**, *6* (8), 1160–1170.

(109) Kidd, K. A.; Blanchfield, P. J.; Mills, K. H.; Palace, V. P.; Evans, R. E.; Lazorchak, J. M.; Flick, R. W. Collapse of a fish population after exposure to a synthetic estrogen. *Proc. Natl. Acad. Sci.* **2007**, *104* (21), 8897–8901.

(110) Van Donk, E.; Peacor, S.; Grosser, K.; Domis, L. N. D. S.; Lurling, M. Pharmaceuticals may disrupt natural chemical information flows and species interactions in aquatic systems: Ideas and perspectives on a hidden global change. In *Reviews of Environmental Contamination and Toxicology*; Springer, 2016; Vol. 238, pp 91–105.

(111) Grebel, J. E.; Charbonnet, J. A.; Sedlak, D. L. Oxidation of organic contaminants by manganese oxide geomedia for passive urban stormwater treatment systems. *Water Res.* **2016**, *88*, 481–491.

(112) Yang, Y.; Ok, Y. S.; Kim, K.-H.; Kwon, E. E.; Tsang, Y. F. Occurrences and removal of pharmaceuticals and personal care products (PPCPs) in drinking water and water/sewage treatment plants: A review. *Sci. Total Environ.* **2017**, *596–597*, 303–320.

(113) Huang, J.; Zhong, S.; Dai, Y.; Liu, C.-C.; Zhang, H. Effect of MnO_2 Phase structure on the oxidative reactivity toward bisphenol A degradation. *Environ. Sci. Technol.* **2018**, *52* (19), 11309–11318.

(114) Balgooyen, S.; Alaimo, P. J.; Remucal, C. K.; Ginder-Vogel, M. Structural transformation of MnO_2 during the oxidation of bisphenol A. *Environ. Sci. Technol.* **2017**, *51* (11), 6053–6062.

(115) Klausen, J.; Haderlein, S. B.; Schwarzenbach, R. P. Oxidation of substituted anilines by aqueous MnO_2: Effect of co-solutes on initial and quasi-steady-state kinetics. *Environ. Sci. Technol.* **1997**, *31* (9), 2642–2649.

(116) Shaikh, N.; Taujale, S.; Zhang, H.; Artyushkova, K.; Ali, A.-M. S.; Cerrato, J. M. Spectroscopic investigation of interfacial interaction of manganese oxide with triclosan, aniline, and phenol. *Environ. Sci. Technol.* **2016**, *50* (20), 10978–10987.

(117) Gao, N.; Hong, J.; Yu, Z.; Peng, P.; Huang, W. Transformation of bisphenol A in the presence of manganese dioxide. *Soil Sci.* **2011**, *176* (6), 265–272.

(118) Lin, K.; Liu, W.; Gan, J. Oxidative Removal of bisphenol A by manganese dioxide: Efficacy, products, and pathways. *Environ. Sci. Technol.* **2009**, *43* (10), 3860–3864.

(119) Lin, K.; Peng, Y.; Huang, X.; Ding, J. Transformation of bisphenol A by manganese oxide-coated sand. *Environ. Sci. Pollut. Res.* **2013**, *20* (3), 1461–1467.

(120) Zhang, T.; Zhang, X.; Yan, X.; Ng, J.; Wang, Y.; Sun, D. D. Removal of bisphenol A via a hybrid process combining oxidation on β-MnO₂ nanowires with microfiltration. *Colloids Surf. Physicochem. Eng. Asp.* **2011**, *392* (1), 198–204.

(121) Zhang, T.; Liu, L.; Tan, W.; Suib, S. L.; Qiu, G.; Liu, F. Photochemical formation and transformation of birnessite: Effects of cations on micromorphology and crystal structure. *Environ. Sci. Technol.* **2018**, *52* (12), 6864–6871.

(122) Tong, F.; Gu, X.; Gu, C.; Xie, J.; Xie, X.; Jiang, B.; Wang, Y.; Ertunc, T.; Schäffer, A.; Ji, R. Stimulation of tetrabromobisphenol A binding to soil humic substances by birnessite and the chemical structure of the bound residues. *Environ. Sci. Technol.* **2016**, *50* (12), 6257–6266.

(123) Kang, K.-H.; Dec, J.; Park, H.; Bollag, J.-M. Effect of phenolic mediators and humic acid on cyprodinil transformation in presence of birnessite. *Water Res.* **2004**, *38* (11), 2737–2745.

(124) Li, C.; Zhang, B.; Ertunc, T.; Schaeffer, A.; Ji, R. Birnessite-induced binding of phenolic monomers to soil humic substances and nature of the bound residues. *Environ. Sci. Technol.* **2012**, *46* (16), 8843–8850.

Chapter 2

Structural transformation of MnO$_2$ during the oxidation of bisphenol A[1]
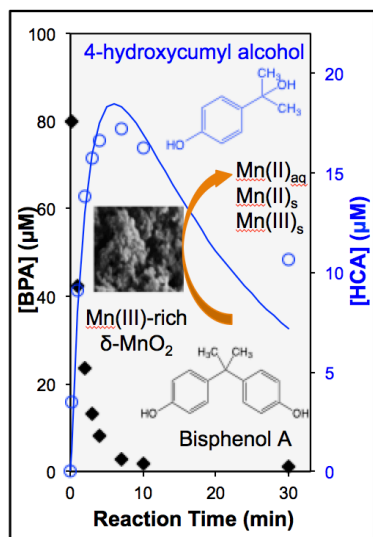
2.1 Abstract

Bisphenol A (BPA) is an endocrine-disrupting compound widely used in the plastic industry and found in natural waters at concentrations considered harmful for aquatic life. BPA is susceptible to oxidation by Mn(III/IV) oxides, which are commonly found in near-surface environments. Here, we quantify BPA oxidation rates and the formation of its predominant product, 4-hydroxycumyl alcohol (HCA), in tandem with transformation of a synthetic, Mn(III)-rich δ-MnO$_2$. To investigate the effect of Mn oxide structural changes on BPA oxidation rate, twelve sequential additions of 80 μM BPA are performed at pH 7. During the additions, BPA oxidation rate decreases by three orders of magnitude and HCA yield decreases from 40% to 3%. This is attributed to accumulation of interlayer Mn(II/III) produced during the reaction, as

---

observed using X-ray absorption spectroscopy as well as additional spectroscopic and wet chemical techniques. HCA is oxidized at a rate that is 12.6 times slower than BPA and accumulates in solution. These results demonstrate that BPA degradation by environmentally-relevant Mn(III/IV) oxides is inhibited by build-up of solid-phase Mn(II/III), specifically in interlayer sites. Nevertheless, Mn oxides may limit BPA migration in near-surface environments and have potential for use in drinking and wastewater treatment.

2.2 Introduction

Manganese (III/IV) oxides (MnO_x) are considered to be one of the strongest naturally-occurring oxidants in near surface environments, and are capable of oxidizing several classes of inorganic[1–4] and organic contaminants.[5–8] They are found in a wide range of geologic settings, including ocean floors, soils and sediments, and marine and freshwater bodies.[9–13] MnO_x oxidize many phenolic compounds, including bisphenol A (BPA).[14–16] BPA is a monomer used in the manufacture of polymeric products, such as epoxy and polycarbonate plastics.[17] It is an endocrine disruptor and, at high concentrations, has deleterious effects on the human reproductive system and child development.[18] It is also leads to teratogenic, endocrine, and pleiotropic effects in aquatic species.[19] Due to its widespread use and incomplete removal during conventional wastewater treatment,[20] BPA is commonly detected in both wastewater[21,22] and surface water.[23,24]

The general transformation mechanism of phenolic compounds by manganese oxides is well understood. Oxidation of phenolic compounds by MnO_x begins with diffusion of the organic compound to the mineral surface, followed by formation of a surface complex.[6,7,25,26] The phenolate anion is then oxidized through a one-electron transfer via the surface complex.[6,25,27,28] The phenoxy radical formed in this process either diffuses away from the

surface and reacts with other radicals to form polymeric products[5,6,25] or undergoes a second one-electron transfer to form a phenoxenium ion.[5,6,25,26,29] The phenoxenium ion can then diffuse away from the mineral surface and undergo hydrolysis to form a benzoquinone.[5,27] Up to 64% of BPA oxidized by MnO_x reacts to form 4-hydroxycumyl alcohol (HCA; Figure **A1**) through radical coupling.[15,30]

Mn(IV) undergoes reduction to Mn(III) and Mn(II) during its reaction with phenolic compounds, leading to changes in the overall reactivity of the oxide. The role of Mn(III) in organic compound oxidation is unclear. Mn(III) may act as a potent oxidant of organic compounds because it has a faster rate of ligand exchange[31] and a higher redox potential compared to Mn(IV).[8,28] However, the presence of Mn(III) decreases MnO_x oxidizing capacity, metal sorption capacity, and photochemical activity under some conditions.[32–38] In contrast, Mn(II) does not oxidize organic compounds. Once formed, Mn(II) initially remains sorbed on the solid and later undergoes desorption once the mineral surface reaches saturation with respect to Mn(II).[6,7,39]

The study of organic chemical oxidation by manganese oxides has evolved from examining reductive dissolution of the mineral to quantifying organic contaminant transformation. Initial studies of the oxidation of organic compounds in the presence of manganese oxides quantify reductive dissolution of the solids in the presence of high initial organic compound concentrations, and suggest that the rate-limiting steps of the reaction are either the formation of the surface complex or the first electron transfer.[6,7,26,40] Later studies determine the loss rates of the organic compounds and the organic compound transformation mechanism, rather than dissolution of the mineral. In general, the degradation rate of organic compounds follows pseudo-first-order kinetics during the initial phase, but later deviates from

this regime.[15,26,41–43] Additionally, these studies examine changes in reaction rates while varying pH,[26,41–43] in the presence of cations,[14–16,44,45] or dissolved organic matter.[15,16,45] While there has been little effort to comprehensively connect changes in the mineral surface with organic contaminant transformation, one previous study quantifies the decrease in Mn oxidation state after reaction with high initial concentrations of phenol, aniline, and triclosan (i.e., 1 mM) at pH 5.[46] However, the experimental conditions limit the environmental relevance of the study and the change in oxidation state is not compared with the reaction kinetics or organic product evolution.

Here, we examine how changes to the mineral, such as the production of reduced manganese and change in structure, affect the oxidation kinetics of BPA by Mn(III)-rich δ-MnO$_2$, a mineral similar to biogenic birnessite.[47–50] Experiments with single additions of BPA or HCA are used to characterize the aqueous-phase kinetics and probe the reactivity of the manganese oxide. Experiments with multiple, sequential additions of environmentally relevant concentrations of BPA at neutral pH are used to induce transformations in the solid phase from repeated exposure. Though this is a simplified system, the use of multiple BPA additions simulates the continuous introduction of BPA in near-surface environments or water treatment systems. By characterizing both the solution and solid phases using a suite of complementary techniques, we provide a comprehensive conceptual model of this complex redox reaction.

2.3 Materials and Methods

2.3.1 Materials

Commercially available chemicals were used as received. HCA was synthesized by modifying a previous method.[51] Ultrapure water was supplied by a Milli-Q water purification

system maintained at 18.2 MΩ·cm. Further details on the materials used and the HCA synthesis are provided in Supporting Information (Section **A1**).

2.3.2 Preparation and Characterization of Mn(III)-rich δ-MnO$_2$

The mineral used in this study was prepared by rapidly adding 100 mL of 11.29 g Mn(NO$_3$)$_2$·4H$_2$O to a 100 mL solution containing 2.4 g NaOH and 4.74 g KMnO$_4$ and stirring for at least twelve hours. The resulting slurry was centrifuged and washed five times in Milli-Q water. The solids were then suspended in Milli-Q water, stored at 4°C, and used within 10 days. The slurry concentration was determined by gravimetric analysis. The starting material was characterized by X-ray diffraction (XRD; Rigaku Rapid II, Mo Kα source; λ = 0.7093 Å), X-ray absorption near edge structure (XANES) spectroscopy, X-ray photoelectron spectroscopy (XPS), oxalate titration,[52–54] and Brunauer-Emmett-Teller (BET) surface area measurements (Quantachrome Autosorb-1, Nitrogen Adsorbate). XRD showed that δ-MnO$_2$ was the only crystalline phase. BET measurements revealed a specific surface area of 113 ± 14 m^2/g. XANES data showed that the valence state of the starting material is 3.55 valence units (v.u.), with percentages of Mn(IV), Mn(III), and Mn(II) at 62%, 31%, and 7%, respectively. These values were corroborated by XPS, which reported 65% Mn(IV), 32% Mn(III), and 3% Mn(II). Oxalate titration resulted in a valence state of 3.66 v.u.. Due to its low average valence state, the starting material is considered a Mn(III)-rich δ-MnO$_2$, rather than a pure Mn(IV) mineral. The presence of Mn(III) in the starting material is due to incomplete comproportionation of Mn(II) and Mn(VII) during synthesis and yields a mineral similar to environmental solids.

2.3.3 Solution Preparation

All reactions were performed in a pH 7 solution buffered with 10 mM piperazine-*N,N'*-bis(2-ethanesulfonic acid) (PIPES) and adjusted to an ionic strength of 20 mM using NaCl. PIPES was selected as a buffer because it does not form complexes with Mn(II) or Mn(III)[55,56] and does not sorb to the manganese oxide surface.[57] BPA (107 mM) and HCA (10 mM) stock solutions were prepared in methanol and stored at 4ºC.

2.3.4 Kinetics of BPA and HCA Oxidation During Single-Addition and Triple-Addition Experiments

The initial reactivity of Mn(III)-rich δ-MnO_2 was determined using single addition batch reactions with either BPA or HCA. BPA or HCA (80 µM) was added to a 200 mL slurry of 0.33 g/L Mn(III)-rich δ-MnO_2 in the buffered solution. The reactors were stirred at room temperature for the duration of the reaction (30 minutes for BPA and 90 minutes for HCA). Two reaction slurry aliquots (1 mL each) were taken at pre-determined time points to quantify the concentration of BPA and HCA. One aliquot from each time point was quenched with excess ascorbic acid (40 µL of a 280 mM stock in Milli-Q stored at 4ºC) to reduce all Mn(III/IV) solids to dissolved Mn(II), while the other aliquot was filtered through a 0.2 µm polytetrafluoroethylene filter. The samples were analyzed by high performance liquid chromatography (HPLC; Section **A2**). Single-addition batch experiments were conducted in triplicate and the resulting data averaged. Loss rates were determined by fitting the data by assuming pseudo-first-order kinetics (Section **A3**). Error was calculated using the standard deviation of loss rates determined at various time points. HCA was confirmed as a product in

BPA reactors using HPLC retention time and UV spectroscopy (Section **A4**; Figures **A6** and **A7**).

HCA production rate and yield were calculated according to:

$$[\text{HCA}] = k_1 \cdot F_{\text{HCA}} \cdot \frac{[\text{BPA}]_0}{k_2 - k_1} \cdot (e^{-k_1 t} - e^{-k_2 t}) \qquad \textbf{(2.1)}$$

where k_1 is the rate constant of BPA oxidation, F_{HCA} is the fraction of BPA converted to HCA, $[\text{BPA}]_0$ is the initial BPA concentration (80 μM), k_2 is the oxidation rate constant of HCA, and t is time after BPA addition. k_1 was determined by fitting the BPA loss data by assuming pseudo-first-order kinetics (Section **A3**). F_{HCA} was calculated by least-squares minimization (Section **A4**).

Organic sorption was determined by comparing concentrations in quenched and filtered aliquots over three sequential additions of 80 μM BPA to the same batch of MnO_2. Quenched samples contained total BPA and HCA (aqueous and sorbed), whereas filtered samples contained only aqueous BPA and HCA. Sorbed BPA or HCA was calculated by $[\text{BPA}]_{\text{total}} - [\text{BPA}]_{\text{aqueous}}$ or $[\text{HCA}]_{\text{total}} - [\text{HCA}]_{\text{aqueous}}$, respectively.

2.3.5 Aqueous Chemistry During Twelve-Addition Experiments

Twelve-addition experiments were conducted to observe changes in BPA oxidation kinetics with repeated exposure. Mn(III)-rich δ-MnO_2 was reacted with BPA in duplicate 6 L batch reactors containing 0.33 g/L MnO_2 in pH 7 buffered solution. BPA (80 μM) was introduced into the reactor at each of the twelve additions. Concentrations and addition intervals were dictated by the number of electrons estimated to induce structural changes.[2] Reaction durations were determined by preliminary work. The first two reactions lasted 1 hour, the third was 1.5 hours, the fourth was 3 hours, the fifth was 6 hours, and reactions 6-12 were each twelve

hours in duration. The volume of BPA stock added was <0.8% of the reactor volume per addition. No variation in pH was observed over the course of the experiments. Aliquots were removed at pre-determined time points and quenched with excess ascorbic acid, as described above, and used to quantify total BPA and HCA concentrations using HPLC (Section **A2**). Additionally, dissolved Mn was quantified in filtered aliquots (0.2 μm polytetrafluoroethylene filters) by inductively coupled plasma-optical emission spectroscopy (ICP-OES; Section **A2**) at the end of each reaction period.

2.3.6 Characterization of Solid-Phase from the Twelve-Addition Experiments

Mn oxide solids obtained after each of the twelve additions of BPA were analyzed to determine mineralogical transformations. At the end of each reaction period, solids were collected by vacuum-filtration (0.7 μm borosilicate glass fiber filters) of 150 mL of slurry from each duplicate reactor. The solids were then rinsed with methanol to desorb organic reaction products and quench the reaction. The solids from both reactors were dried at room temperature, combined, ground, and used for solid phase characterization. Solids were characterized using XRD, calcium exchange, and spectroscopic analysis, as described below.

XPS was performed using a Thermo Scientific K-Alpha XPS system with an Al Kα X-ray source. Spectra from the Mn*3p* orbital were collected and analyzed to quantify the oxidation state of the multivalent manganese oxides. Briefly, data was processed in CasaXPS (2016 Casa Software Ltd.) using Shirley background subtraction and fit using a packet of correlated component peaks representing each possible oxidation state.[58] The binding energies, intensities, and peak widths were allowed to vary. At these energies, XPS is expected to interrogate only the

top 10-50 Å of aggregated particles (not crystalline domains), therefore results are reported as a percentage of surface Mn(IV), Mn(III), and Mn(II).

Extended X-ray absorption fine structure (EXAFS) and XANES data was collected at beamline 13-BM-D at the Advanced Photon Source at Argonne National Laboratory. This beamline has a bending magnet source equipped with a Si(111) double crystal monochromator, which was detuned by 40%. Samples were prepared by diluting 18 mg of solid MnO_2 in 72 mg of boron nitride and ground until homogenous. Data was collected at room temperature in both transmission and fluorescence (Canberra 16-element Ge detector). Successive XANES scans were identical, indicating no change in Mn oxidation state during data collection. XANES and EXAFS data were processed using SIXPack.[59] XANES data were fit using the multi-standard Combo method[60] by fitting the first derivative of the XANES spectra with restriction to a non-negative fit. XANES and EXAFS spectroscopies interrogate the average environment of all Mn nuclei in the sample and are therefore reported as the bulk valence state and percentages of bulk Mn(II), Mn(III), and Mn(IV). EXAFS fitting was done using a full, multiple scattering model of layered Mn-oxides.[2,61] Phase and amplitude files were created using FEFF 7.2.[62] SIXPack's FEFF EXAFS fitting uses IFEFFIT as its primary fitting algorithm and fits were optimized by minimizing X^2.[63] The EXAFS model accounted for splitting of Mn-O and Mn-Mn distances in the MnO_6 octahedral layer due to Jahn-Teller distortion, out-of-plane bending of the octahedral layer, vacancies in the Mn octahedral layer, and interlayer cations. Production of reduced manganese within the layer is detected by a change in the fractional occupancy of manganese centers within the layer as they fill in the vacancies in a Mn(IV) phyllomanganate structure.[35,48,64] Reduced manganese sorbed onto the layer is detected by Mn at a slightly longer interatomic distance than the other Mn centers. This is because sorbed Mn generally forms a

corner-sharing complex with an interatomic distance of 3.45 Å, while Mn centers within the layer have an interatomic distance of 2.85-2.95 Å.[61]

Calcium exchange experiments were performed to quantify Mn(II) sorbed on the surface of the solid phase. Weighed samples were suspended in 10 mM PIPES (pH 7) with 25 mM $CaCl_2$ and placed on a shaker table for 48 hours. After 48 hours, aqueous Mn(II) that was displaced by Ca^{2+} was quantified by ICP-OES.

2.4 Results

2.4.1 Kinetics of BPA and HCA Oxidation During Single-Addition and Triple-Addition Experiments

When BPA is exposed to Mn(III)-rich δ-MnO_2, rapid oxidation of BPA occurs (Figure **A8**). The loss of BPA initially follows pseudo-first-order kinetics, with a loss rate of 0.585 min^{-1} over the first four minutes of the reaction. However, the reaction rate of BPA oxidation deviates from pseudo-first-order kinetics if the first 10 minutes of the reaction are considered (Figure **A4**). HCA appears in solution immediately after BPA addition; however, it is also oxidized by MnO_2 and does not accumulate in solution during single-addition experiments (Figure **A8**). The molar yield (moles of HCA produced/moles of BPA consumed) of HCA production from BPA oxidation is 32% for the 30-minute reaction.

Additional experiments are conducted with HCA as the target organic compound to quantify its oxidation rate due to reaction with Mn(III)-rich δ-MnO_2. The oxidation rate of HCA by MnO_2 is 0.0465 min^{-1} over the first 10 minutes of reaction, which is 12.6 times slower than that of BPA under the same conditions (Figures **A4** and **A5**). The slower oxidation of HCA by MnO_2 relative to BPA is similar to a previous report, which found HCA to react 5 times

slower.[30] As observed for BPA, the loss rate of HCA deviates from pseudo-first-order kinetics over longer reaction periods (e.g., 60 minutes; Figure **A5**).

The amount of sorbed BPA and HCA is determined by quenching the reaction using two different methods (i.e., ascorbic acid addition or filtration). Over three additions of BPA to a batch of MnO_2, BPA sorbs to the surface during the first addition ($14.3 \pm 7.4\%$ of total BPA), but not during the second and third additions (Table **A2**). The amount of HCA generated as a product of BPA oxidation and then subsequently sorbed on the surface is negligible during the first addition, but increases with each addition of BPA up to $1.0 \pm 0.9\%$ in the third addition.

2.4.2 Aqueous Chemistry During Twelve-Addition Experiments

Twelve sequential additions of BPA are used to induce structural changes and to probe how the reactivity of the Mn oxide changes during the reaction. This approach allows the observation of the effects of repeated exposure of an environmentally-relevant amount of BPA to Mn(III)-rich δ-MnO_2.

Over sequential additions of BPA to the same batch of MnO_2, both the BPA oxidation rate and the yield of HCA decrease with each addition. The first-order rate constant after one addition of BPA is 0.56 min^{-1} ($t_{1/2} = 1.24$ min), while the rate constant after twelve additions of BPA is 2.38×10^{-4} min^{-1} ($t_{1/2} = 2910$ min; Figure **2.1a**). After the fifth addition, BPA is not completely consumed within the allotted reaction time and begins to accumulate in the reactors (Figure **2.2a**). The main oxidation product, HCA, appears immediately in the reactors, but is quickly oxidized by the Mn(III)-rich δ-MnO_2. After three additions of BPA, HCA begins to accumulate in solution (Figure **2.2b**). Assuming that the ratio between BPA and HCA loss rates remains constant (i.e., 12.6:1), the mole percent of BPA converted to HCA decreases over the

sequential addition experiment. After the first addition of BPA, 39.7% of added BPA is recovered as HCA. After the twelfth addition, only 3.5% of added BPA is recovered as HCA (Figure **2.1b**; Table **A1**).

Aqueous manganese is not present above the detection limit after the first five reactions with BPA. After the sixth addition of BPA, aqueous manganese begins to accumulate in solution (Figure **2.1c**). By the end of the twelfth addition of BPA, 2.6% of the total Mn (158.7 µM) is in solution. Strong ligands (e.g., pyrophosphate, citrate, or ethylenediaminetetraacetic acid) are required to solubilize Mn(III).[65] Therefore, it is likely that the aqueous manganese detected is predominantly Mn(II).

2.4.3 Solid-Phase Changes During Twelve-Addition Experiments

The valence state at the surface of the mineral is measured using XPS, which probes only the top 10 – 50 Å of the aggregated particles at this energy. These aggregates are estimated to be hundreds of nanometers in diameter.[50] A sample of the fitted data is provided in Figure **A11**. Overall, the amount of surficial Mn(III) increases while Mn(IV) decreases during sequential additions of BPA (Figure **2.3a**). For example, surface Mn(III) increases from 32% (initial material) to 42% after the sixth addition, then decreases to 37% by the end of the twelfth addition. Conversely, surface Mn(IV) decreases from 65% (initial material) to 56% after the sixth addition, then increases slightly to 60% after the twelfth addition. A low percentage of solid Mn(II) is detected by XPS (3-10%), with no observable trends.

The speciation and average oxidation state of the bulk solid is measured by XANES spectroscopy, which probes the entire sample. An example of the fitted data is provided in Figure **A12**. Over twelve additions of BPA, bulk Mn(III) decreases from 31% to 25%. As bulk Mn(III)

decreases, the quantity of bulk Mn(IV) increases from 62% to 69% (Figure **2.3a**). A small amount of solid Mn(II) is detected in all samples (i.e., 3-5% in all analyzed samples), with no observable trends. The quantification limit for Mn(II) in this technique is 5% by mole Mn.[60] The bulk valence state for the starting material (3.55 v.u.) increases to 3.63 v.u. by the end of the twelfth addition (Figure **A13**). The accuracy of this method is 0.04 v.u..[60]

Analysis of the EXAFS data (Figure **A14**) using a full, multiple scattering model reveals that the fractional occupancy of Mn within the layer increases slightly upon reaction with BPA (Table **A4**), but does not follow a notable trend throughout the experiment (Figure **2.3b**). Solids from the first three additions of BPA have no detectable corner-sharing Mn centers. After the fourth reaction with BPA, corner-sharing Mn centers are detected, and its coordination number steadily increases until the end of the experiment (Figure **2.3b**).

Changes in surface area over the twelve additions of BPA were negligible, as observed by BET measurements (Table **A3**). XRD data (Figure **A15**) show that no new phases form over twelve additions of BPA. However, qualitative changes in the diffraction pattern are observed, such as the reduced tailing of the *hkl* diffraction band at 37° and the appearance of a dip at ~47° after twelve additions of BPA.

Calcium exchange experiments show that Ca^{2+}-extractable Mn(II) increases with increasing additions of BPA (Figure **A16**). After the first addition of BPA, 0.11 μg/mg is extracted from the solid, while after seven additions of BPA, 2.88 μg/mg is extracted. The amount of Ca^{2+}-extractable Mn(II) remains constant for the remainder of the experiment. Control experiments using only PIPES pH 7 buffer show that very little Mn is extracted in the absence of Ca^{2+} (i.e. 0-0.4 μg/mg).

2.5 Discussion

2.5.1 Deviation from Pseudo-First-Order Kinetics

The oxidation rate of model compounds[6,7,25,41,66–68] and BPA[14,15] follow pseudo-first-order kinetics during the initial phase of the reaction, but the rates of oxidation decrease as the reaction proceeds. Previous studies show that the oxidation rates deviate from pseudo-first-order kinetics, but generally only examine solution kinetics during the first phase of the reaction by using the initial rate approach.[14,15,41–46] A limited number of studies examine longer reactions by fitting data by empirical or semi-empirical equations[42,69] or by applying a kinetic model based on the observed organic compound loss rate and the number of reaction sites.[40] Here, this same kinetic deviation is observed in single addition batch experiments of BPA (Figure **A4**). Furthermore, the decrease in reactivity of the Mn oxide due to reaction with the phenolic contaminant is clearly observed in experiments with twelve sequential additions of BPA, with BPA oxidation rates slowing by three orders of magnitude over the course of the reaction (Figure **2.1a**).

The connection between changes in oxidation kinetics and the mineral surface has not been closely examined. Previous studies demonstrate that the addition of aqueous Mn(II), which is a product of the reductive dissolution of MnO_x, inhibits organic contaminant oxidation rates.[14,15,44,45] This indicates that the accumulation of Mn(II) can change the reactivity of the mineral surface, but does not provide direct mechanistic evidence. Another study observes changes in MnO_x oxidation state after a single exposure to triclosan, aniline, and phenol.[46] An increase in the amount of Mn(II) and Mn(III) on the surface of the Mn oxide was detected by XPS, but not linked to the target organic oxidation kinetics. In the present study, changes in oxidation kinetics and concurrent structural changes are explored using a wide range of analytical techniques to examine both solution and solid-phase chemistry. The results are used to

systematically evaluate potential factors that may lead to the widely observed decrease in manganese oxide reactivity after exposure to organic target compounds.

2.5.2 Changes in Surface Area

Since the reaction between Mn oxides and target organic compounds occurs on the surface of the mineral,[41] changes in MnO_x surface area can potentially affect the reactivity of MnO_x by decreasing the number of available reactive surface sites.[70] However, only minor changes in the surface area are observed over the course of twelve additions of BPA (Table **A3**). The lack of correlation between changes in surface area and the wide range of BPA oxidation rates observed in this study (Figure **2.1a**) indicates that the decrease in oxidation rate cannot be attributed solely to a decrease in overall number of reactive sites; however, this measurement does not account for changes in interlamellar spaces and micropores.

2.5.3 Changes in MnO_x Average Oxidation State

A decrease in average oxidation state could affect the reactivity of the solid by decreasing the rate of electron transfer.[40] Changes in average oxidation state have been reported under some conditions. For example, the oxidation state of a synthetic Mn(III/IV) oxide, determined with XPS, decreases from 3.7 v.u. to 3.3 v.u. after reaction with 1 mM triclosan for 24 hours at pH 5.[46] In this study, repeated reaction of MnO_2 with 80 μM BPA for variable experimental durations (i.e., 1-12 hours for twelve sequential additions) at pH 7 decreases the surface oxidation state by 0.09 v.u. (quantified by XPS) and increases the bulk oxidation state by 0.08 v.u. (quantified using XANES; Figure **A13**). At this energy, XPS only probes the top 10-50 Å of the aggregated particles. The increase in bulk oxidation state throughout the reaction is likely due

to the dissolution of Mn(II) during manganese reduction, lowering the fraction of reduced Mn centers present in the solid. The valence state at the mineral surface, as determined by XPS, differs from the bulk, decreasing slightly over the twelve additions of BPA (Figure **A13**). This small change may be one explanation for the decrease in oxidation rate, and the increasing disparity between the bulk and surface oxidation state may imply that electrons are not being conducted throughout the mineral assemblage and accumulate at the surface.

Differences in the change in average oxidation state between this study and prior reports of a large decrease in average oxidation state[46] may be attributable to the differences in the experimental conditions. While both studies use Mn(III)-rich δ-MnO$_2$ synthesized with similar methods, and examine the oxidation of phenols, major differences between the studies remain. First, while the initial organic compound concentrations in the two studies are quite different (i.e., 80 μM compared to 1 mM), the total amount of BPA added in this study over the course of twelve additions is similar (i.e., 0.96 mM). Second, the total experimental duration in this study is 96.5 hours, compared to 24 hours. Finally, the oxidation of organic compounds by Mn oxides is highly pH dependent and typically faster under acidic conditions;[26,41–43] although the initial rates of organic compound oxidation were not reported in the previous study, less than 30 μM of triclosan, phenol, and aniline remained in solution after only 5 minutes of reaction at pH 5. Additionally, the rate of Mn(III) disproportionation into Mn(II) and Mn(IV) increases in conjunction with pH,[65] which could result in additional Mn(IV) accumulation on the mineral surface with concomitant Mn(II) production and release into solution. Collectively, these differences suggest that a rapid reaction with a high initial organic concentration is needed to induce substantial changes in Mn oxidation state, whereas a more gradual reaction of the same total amount of organic results in very small changes in the Mn oxidation state.

2.5.4 Sorption of BPA and Organic Products

Sorption of the target organic compound (i.e., BPA) may enhance the overall reactivity of MnO_x by facilitating the formation of a surface complex, while the sorption of organic reaction products (e.g., HCA) can decrease reactivity by obscuring reactive sites on the surface.[25,26,40–42,66] Sorption of organic compounds depends on both the type of compound and the experimental conditions (e.g., pH). For example, sorption of sulfonamides,[71] lincosamides,[72] and carbamazepine[73] to Mn oxides is negligible. In contrast, sorption of triclosan to δ-MnO_2 can be extensive, primarily under acidic conditions (e.g., 55% sorbed at pH 5 and 10% sorbed at pH 8).[26] While the sorption of organic transformation products on Mn oxides has received little attention, one previous study observes increased carbon and chlorine on the mineral surface after reaction with triclosan at pH 5, indicating that there are organic species sorbed on the mineral.[46]

Here, over three additions of BPA, sorption of BPA occurs only during the initial addition of BPA into the reactor (i.e., 14.3 ± 7.4% sorbed; Table **A2**). The low steady-state concentration of sorbed BPA supports the supposition that the formation of the surface complex is the rate-limiting step in BPA degradation, rather than the first electron transfer,[2,6,7,40] and suggests that the starting material has a higher binding affinity to BPA than the reacted material. Sorption of produced HCA is very small over all three additions (i.e., <1.0 ± 0.9%). This relative trend between BPA and HCA sorption is in agreement with the reported octanol/water partitioning coefficient (K_{ow}) of HCA being much smaller than that of BPA (log K_{ow} of 0.76 and 2.76, respectively),[30] and the reported solubility of HCA being much higher than BPA (2.65 g/L and 0.31 g/L, respectively).[30]

The oxidation of BPA produces a suite of organic products[15] which may have different affinity for the mineral surface. For example, polymeric products produced by radical coupling

are more likely to sorb to the mineral surface due to their larger size and decreased polarity, and may prevent sorption of BPA during sequential exposures. However, no major product peaks with a longer retention times than BPA, indicative of polymeric products, are observed by HPLC with either UV or fluorescence detection (Figures **A9** and **A10**), while many peaks with shorter retention times are present in the chromatograms. Although identification of additional BPA oxidation products is beyond the scope of this study, the HPLC results indicate that many of the oxidation products are highly polar and that minimal polymeric products are produced in this reaction. While sorption of HCA does not appear to play a role in obscuring reaction sites because it sorbs less strongly than BPA, the relative sorption of other proposed organic products[15] warrants further investigation. Collectively, the relative sorption of BPA and HCA (Table **A2**), the absence of less polar products (Figures **A9** and **A10**), and the decreased sorption of phenols at circumneutral pH values[26] suggest that sorption of organics does not contribute to the decrease in BPA oxidation rate observed over twelve sequential additions.

2.5.5 Solid-Phase Accumulation of Reduced Manganese

The production of reduced manganese could decrease the organic compound reaction rate by obscuring reactive sites on the mineral surface or by competitively reacting with the mineral surface. This mechanism has been proposed as an explanation for the deviation from pseudo-first-order kinetics during the oxidation of several classes of antibacterial agents,[26,40,72] halogenated phenols,[68,74] and naproxen[75] by MnO_2. Furthermore, the addition of aqueous Mn(II) consistently results in inhibition of BPA oxidation by Mn oxides.[14,15,45]

Corner-sharing Mn is detected after the fourth addition of BPA, and its coordination number increases throughout twelve additions of the target compound (Figure **2.3b**). Corner-

sharing Mn is assumed to be Mn(III) or Mn(II) in interlayer positions. Surface-bound Mn(II) also increases after the fourth addition of BPA, as measured by Ca^{2+} exchange (Figure **A16**). In contrast, aqueous Mn(II) is not detected until after six additions of BPA (Figure **2.1c**). Stone and Ulrich demonstrate that the desorption of Mn(II) from the surface of the mineral is a slow reaction compared to the desorption of organic molecules.[76] This observation is confirmed in this study as Mn(II) is detected on the solid before it appears in solution (i.e., addition 4 compared to addition 6; Figures **A16** and **2.1c**). Our results show that accumulation of aqueous Mn(II) over sequential additions of BPA corresponds with the decrease in BPA oxidation rate (Figure **2.1**). Therefore, the production of Mn(II), which may arise from Mn(III) reduction or disproportionation, is a likely cause of decreasing MnO_2 reactivity with BPA. Additionally, while bulk measurements of the oxidation state remain relatively constant throughout twelve additions of BPA, XPS reveals that Mn(III) preferentially accumulates at the mineral surface (Figure **2.3a**). The increase of Mn(III) at the mineral surface likely contributes to the decreased transformation rate of BPA even in the absence of large changes in the bulk MnO_2 oxidation state. It is unlikely that the increase in Mn(III) is due to comproportionation of Mn(II) and Mn(IV), which would lead to the formation of orthogonal layered birnessite detectable by changes in the XRD pattern.[77]

2.5.6 Structural Changes

Changes to the mineral structure consist predominantly of the increase in interlayer Mn. Interlayer Mn could be Mn(II) or Mn(III), and exhibits corner-sharing geometry, as shown in the EXAFS model (Figure **2.3b**). The increase of interlayer Mn is corroborated by the analysis of the diffraction patterns (Figure **A15**), which show a decrease in the high-angle scattering tail of the

peak at 37° and the appearance of a characteristic dip at 47°, both of which indicate capping of vacancies by metal cations (i.e. Mn(II) or Mn(III)).[33,47,48,78,79] Previous studies have reported that these cation vacancy sites are of critical importance in adsorption and electron transfer processes that occur on the mineral surface.[50,80,81]

2.5.7 Changes in HCA Yield

Another example of the importance of quantifying changes in both aqueous- and solid-phase geochemistry is the 10-fold decrease in HCA yield over twelve sequential additions of BPA (Figure **2.1b**). The initial yield of HCA from BPA oxidation ranges from 32 – 39.7% in this study. In comparison, earlier work reports yields up to 64% under similar conditions (e.g., pH 7.4); however, the MnO_2 used in the previous study is synthesized under hydrothermal conditions[30] and is likely more crystalline than the solid used in the present study. During the twelfth addition of BPA, only 3.5% of oxidized BPA is converted to HCA. Therefore, the production or relative stability of other transformation products becomes more important as the MnO_2 solids undergo repeated reaction with BPA. Previous studies have identified 11 of the numerous products that form through radical coupling, fragmentation, substitution, and elimination, including HCA.[15,30] Regardless of the identity of the suite of oxidation products, the mechanism of BPA oxidation and importance of HCA as a major product clearly changes as repeated additions to MnO_x alter the reactivity of the Mn oxide. These results suggest that the products or yields identified in single-addition batch reactors may not be representative for more complex environments.

2.5.8 Conceptual Framework

By systematically quantifying changes in the mineral structure during BPA oxidation by MnO$_x$, it is possible to develop a conceptual model that provides direct evidence to explain why the reactivity of the mineral towards BPA decreases with time. The Mn(III)-rich δ-MnO$_2$ starting material contains no detectable interlayer Mn, indicating the Mn(III) is located within the octahedral sheets. After diffusion of the phenol to the mineral surface and formation of a surface complex, the organic compound is oxidized through a one-electron transfer and Mn(IV) is reduced to Mn(III).[6,25,27,28] The Mn(III) may then either remain in the interlayer, disproportionate to Mn(II) and Mn(IV), undergo a second one electron transfer with BPA or its degradation products to produce Mn(II), or migrate to a vacancy site in the octahedral sheet. Mn(III) does not appear to play a primary role in the transformation of BPA because BPA oxidation rates decline despite Mn(III) accumulation during the first five BPA additions. The data also suggests that, at a predominance above 40%, surficial Mn(III) is consumed by disproportionation to Mn(II) and Mn(IV), resulting in the decrease in surface Mn(III) and production of Mn(IV) and Mn(II) at the surface. Mn(III) does not appear to fill in vacancy sites as the fractional occupancy of the material does not notably increase over BPA additions (Figure **2.3b**). Mn(II) accumulates on the mineral surface (Figure **A16**) until it reaches saturation.[6,7,39] After this point, excess Mn(II) dissolves and is detected in solution (Figure **2.1c**). As a result, the overall oxidation state of the Mn oxide remains within 3.60 ± 0.07 valence units (Figure **A13**), despite extensive reaction with BPA. With increasing BPA additions, reduced Mn centers migrate to the interlayer, capping highly reactive vacancy sites (Figures **2.3b** and **A15**). By using BPA oxidation kinetics as a way to probe the reactivity of MnO$_2$ (Figure **2.1a**), it is clear that changes in reactivity due to accumulation of interlayer Mn and Mn(II) on the surface of the mineral happen prior to the

appearance of dissolved Mn(II), emphasizing the importance of these structural changes to the mineral. The accumulation of reduced manganese within the mineral, and ultimately in solution, is also correlated with the change in HCA yield (Figure **2.1b**), suggesting that mineral transformation alters the mechanism of BPA oxidation and its intermediate products. In contrast, the observed decrease in BPA oxidation rate is not associated with changes in surface area, sorption of organics, or a change in bulk MnO_x oxidation state.

2.6 Environmental Implications

BPA is an endocrine-disrupting compound[18] that is found in elevated concentrations in many aquatic environments.[23,82] It is especially damaging to fish and other aquatic species.[19] Manganese oxides are found in high concentrations in the environment as well, primarily in soils and sediments.[83] Oxidation by MnO_2 is a potential fate for BPA in the environment. The formation of HCA as an oxidation product of BPA could have effects on the environment because HCA is more mobile[30] and less susceptible to oxidation by MnO_2. It may also be more estrogenic than BPA; an in vitro estrogen receptor binding assay suggests that HCA has 100-fold higher binding affinity to the estrogen receptor than BPA.[51] Nevertheless, HCA is removed by Mn oxides, albeit at a slower rate.

The transformation of phenolic contaminants by Mn(III/IV) oxides could potentially be used in wastewater, urban stormwater, or landfill leachate treatment,[84] preventing BPA, HCA, and other phenolic compounds from entering natural waters and disrupting wildlife ecosystems. Manganese oxides are capable of transforming a range of organic compounds, including antibacterial agents,[26,40,42,46,69,72,85–91] polyaminocarboxylate ligands,[92] endocrine disruptors,[43,44,46,93–95] brominated flame retardants,[96] rubber additives,[97] pain relievers,[75,98] and

anti-epileptic pharmaceuticals.[73] The comprehensive approach used here provides details required for the implementation of Mn oxides for water treatment, such as mechanism, mineralogical changes, and changes in kinetics.

2.7 Acknowledgements

Figure 2.1. (a) BPA pseudo-first-order loss rate constants for duplicate reactors, (b) HCA production yield as a percent of oxidized BPA for reactor averages, and (c) aqueous manganese concentrations for duplicate reactors over twelve additions of 80 µM BPA with 0.33 g/L of Mn(III)-rich δ-MnO$_2$ in a PIPES buffer (pH 7). Error bars for aqueous manganese concentrations are smaller than data point size.
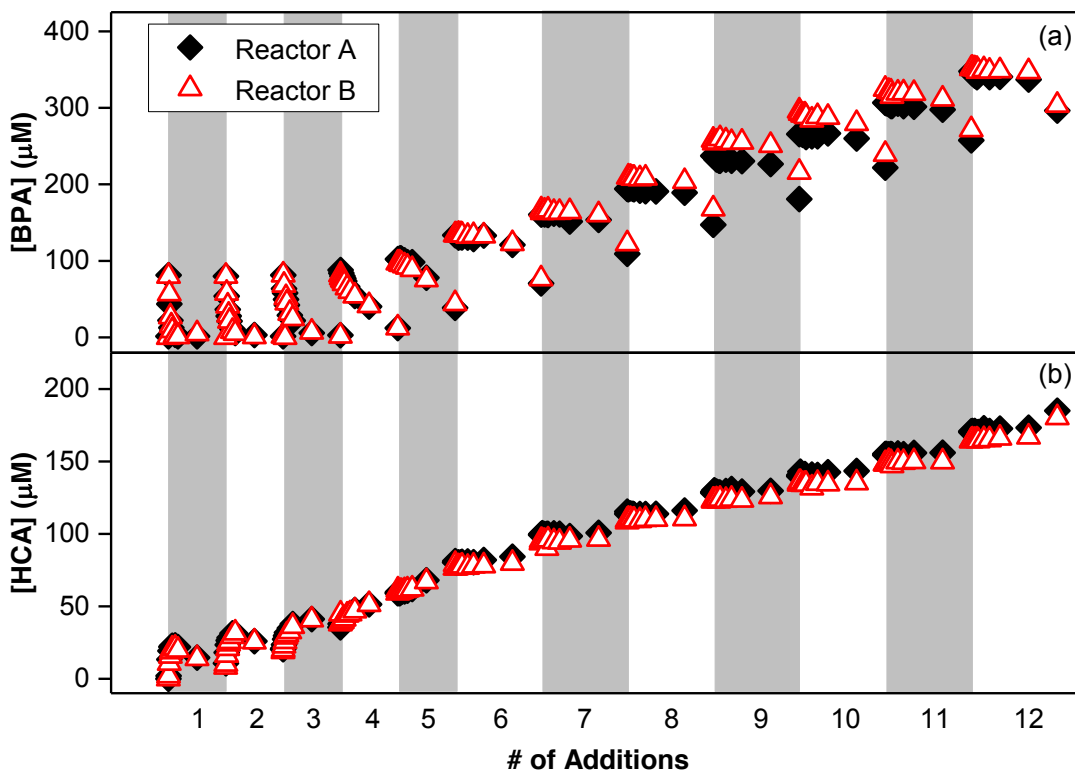
Figure 2.2. (a) BPA and (b) HCA concentrations over twelve additions of 80 µM BPA with 0.33 g/L of Mn(III)-rich δ-MnO$_2$ in a PIPES buffer (pH 7). Data sets are for duplicate 6 L reactors. Note that kinetic data is collected in the first hour of each addition, but the total lengths of additions are not the same. The first two additions were 1 hour, the third was 1.5 hours, the fourth was 3 hours, the fifth was 6 hours, and additions 6-12 were twelve hours.
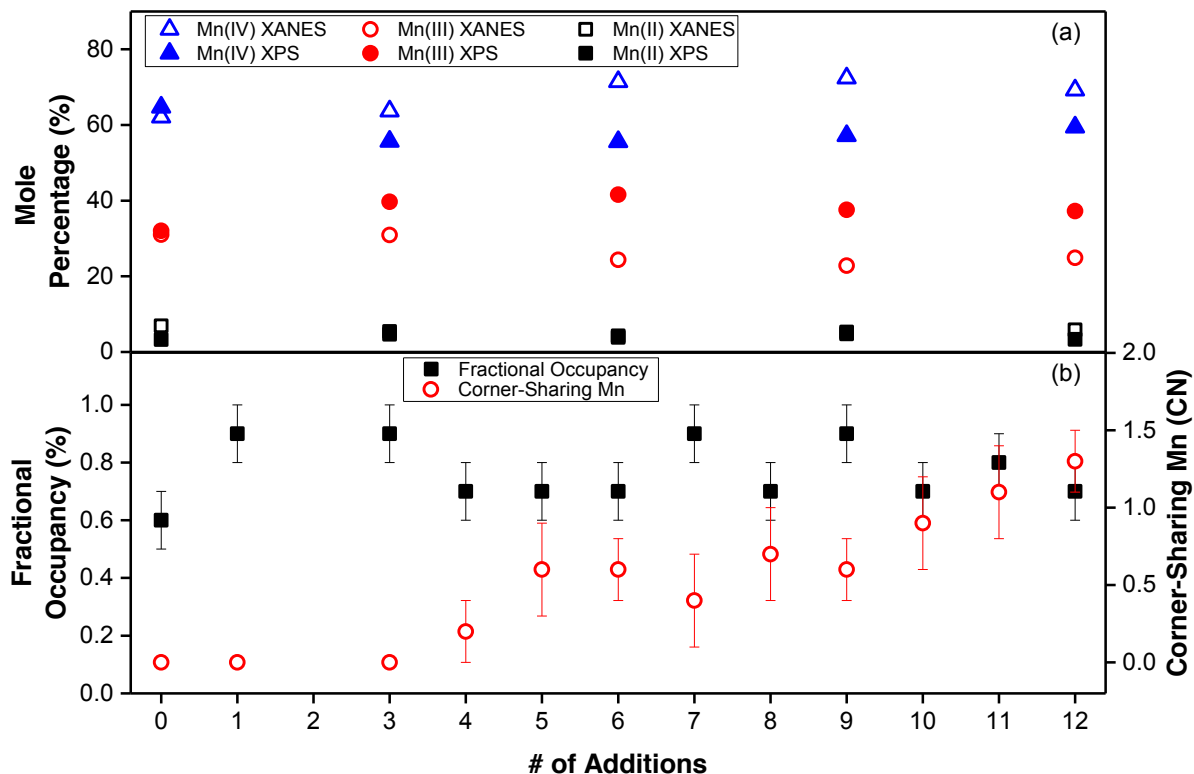
Figure 2.3. (a) Mole percentages of Mn(II), Mn(III), and Mn(IV) in a subset of solid samples determined by both XPS and XANES, and (b) variables obtained from the EXAFS spectra modeling of solids obtained over twelve additions of 80 µM BPA with 0.33 g/L of Mn(III)-rich δ-MnO$_2$ in a PIPES pH 7 buffer. Corner-sharing Mn is reported as coordination number (CN). Error for fractional occupancy and corner-sharing Mn was calculated by SIXPack during the modeling process. Samples from both reactors were combined and then analyzed.

2.9 References

(1)   Eary, L. E.; Rai, D. Kinetics of chromium(III) oxidation to chromium(VI) by reaction with manganese dioxide. *Environ. Sci. Technol.* **1987**, *21* (12), 1187–1193.

(2)   Lafferty, B. J.; Ginder-Vogel, M.; Sparks, D. L. Arsenite oxidation by a poorly-crystalline manganese oxide. 3. Arsenic and manganese desorption. *Environ. Sci. Technol.* **2011**, *45* (21), 9218–9223.

(3)   Landrot, G.; Ginder-Vogel, M.; Livi, K.; Fitts, J. P.; Sparks, D. L. Chromium(III) oxidation by three poorly crystalline manganese(IV) oxides. 2. Solid phase analyses. *Environ. Sci. Technol.* **2012**, *46* (21), 11601–11609.

(4)   Tournassat, C.; Charlet, L.; Bosbach, D.; Manceau, A. Arsenic(III) oxidation by birnessite and precipitation of manganese(II) arsenate. *Environ. Sci. Technol.* **2002**, *36* (3), 493–500.

(5)   Remucal, C. K.; Ginder-Vogel, M. A critical review of the reactivity of manganese oxides with organic contaminants. *Environ. Sci. Process. Impacts* **2014**, *16* (6), 1247-1266.

(6)   Stone, A. T. Reductive dissolution of manganese(III/IV) oxides by substituted phenols. *Environ. Sci. Technol.* **1987**, *21* (10), 979–988.

(7)   Stone, A. T.; Morgan, J. J. Reduction and dissolution of manganese(III) and manganese(IV) oxides by organics. 1. Reaction with hydroquinone. *Environ. Sci. Technol.* **1984**, *18* (6), 450–456.

(8)   Xyla, A. G.; Sulzberger, B.; Luther III, G. W.; Hering, J. G.; Van Cappellen, P.; Stumm, W. Reductive dissolution of manganese(III,IV) (hydr)oxides by oxalate: The effect of pH and light. *Langmuir* **1992**, *8* (1), 95–103.

(9)   Dick, G. J.; Lee, Y. E.; Tebo, B. M. Manganese(II)-oxidizing *Bacillus* spores in Guaymas Basin hydrothermal sediments and plumes. *Appl. Environ. Microbiol.* **2006**, *72* (5), 3184–3190.

(10) Negra, C.; Ross, D. S.; Lanzirotti, A. Oxidizing behavior of soil manganese. *Soil Sci. Soc. Am. J.* **2005**, *69* (1), 87–95.

(11) Post, J. E. Manganese oxide minerals: Crystal structures and economic and environmental significance. *Proc. Natl. Acad. Sci.* **1999**, *96* (7), 3447–3454.

(12) Tani, Y.; Miyata, N.; Iwahori, K.; Soma, M.; Tokuda, S.; Seyama, H.; Theng, B. K. Biogeochemistry of manganese oxide coatings on pebble surfaces in the Kikukawa River System, Shizuoka, Japan. *Appl. Geochem.* **2003**, *18* (10), 1541–1554.

(13) Wehrli, B.; Friedl, G.; Manceau, A. Reaction rates and products of manganese oxidation at the sediment-water interface. In *Aquatic Chemistry*; American Chemical Society, 1995; Vol. 244, pp 111–134.

(14) Gao, N.; Hong, J.; Yu, Z.; Peng, P.; Huang, W. Transformation of bisphenol A in the presence of manganese dioxide. *Soil Sci.* **2011**, *176* (6), 265–272.

(15) Lin, K.; Liu, W.; Gan, J. Oxidative removal of bisphenol A by manganese dioxide: Efficacy, products, and pathways. *Environ. Sci. Technol.* **2009**, *43* (10), 3860–3864.

(16) Lin, K.; Peng, Y.; Huang, X.; Ding, J. Transformation of bisphenol A by manganese oxide-coated sand. *Environ. Sci. Pollut. Res.* **2013**, *20* (3), 1461–1467.

(17) Bisphenol A (BPA) Information & Resources http://www.bisphenol-a.org/ (accessed Sep 6, 2016).

(18) Vandenberg, L. N.; Hauser, R.; Marcus, M.; Olea, N.; Welshons, W. V. Human exposure to bisphenol A (BPA). *Reprod. Toxicol.* **2007**, *24* (2), 139–177.

(19) Canesi, L.; Fabbri, E. Environmental effects of BPA: Focus on aquatic species. *Dose-Response* **2015**, *13* (3).

(20) Tan, B. L. L.; Hawker, D. W.; Müller, J. F.; Leusch, F. D. L.; Tremblay, L. A.; Chapman, H. F. Modelling of the fate of selected endocrine disruptors in a municipal wastewater treatment plant in South East Queensland, Australia. *Chemosphere* **2007**, *69* (4), 644–654.

(21) Masoner, J. R.; Kolpin, D. W.; Furlong, E. T.; Cozzarelli, I. M.; Gray, J. L.; Schwab, E. A. Contaminants of emerging concern in fresh leachate from landfills in the conterminous United States. *Env. Sci Process. Impacts* **2014**, *16* (10), 2335–2354.

(22) Yu, X.; Xue, J.; Yao, H.; Wu, Q.; Venkatesan, A. K.; Halden, R. U.; Kannan, K. Occurrence and estrogenic potency of eight bisphenol analogs in sewage sludge from the U.S. EPA targeted national sewage sludge survey. *J. Hazard. Mater.* **2015**, *299*, 733–739.

(23) Baldwin, A. K.; Corsi, S. R.; De Cicco, L. A.; Lenaker, P. L.; Lutz, M. A.; Sullivan, D. J.; Richards, K. D. Organic contaminants in Great Lakes tributaries: Prevalence and potential aquatic toxicity. *Sci. Total Environ.* **2016**, *554–555*, 42–52.

(24) Belfroid, A.; van Velzen, M.; van der Horst, B.; Vethaak, D. Occurrence of bisphenol A in surface water and uptake in fish: Evaluation of field measurements. *Chemosphere* **2002**, *49* (1), 97–103.

(25) Laha, S.; Luthy, R. G. Oxidation of aniline and other primary aromatic amines by manganese dioxide. *Environ. Sci. Technol.* **1990**, *24* (3), 363–373.

(26) Zhang, H.; Huang, C.-H. Oxidative transformation of triclosan and chlorophene by manganese oxides. *Environ. Sci. Technol.* **2003**, *37* (11), 2421–2430.

(27) Jiang, J.; Gao, Y.; Pang, S.-Y.; Lu, X.-T.; Zhou, Y.; Ma, J.; Wang, Q. Understanding the role of manganese dioxide in the oxidation of phenolic compounds by aqueous permanganate. *Environ. Sci. Technol.* **2015**, *49* (1), 520–528.

(28) Ukrainczyk, L.; McBride, M. B. Oxidation of phenol in acidic aqueous suspensions of manganese oxides. *Clays Clay Min.* **1992**, *40* (2), 157–166.

(29) Stone, A. T.; Morgan, J. J. Reduction and dissolution of manganese(III) and manganese(IV) oxides by organics: 2. Survey of the reactivity of organics. *Environ. Sci. Technol.* **1984**, *18* (8), 617–624.

(30) Im, J.; Prevatte, C. W.; Campagna, S. R.; Löffler, F. E. Identification of 4-hydroxycumyl alcohol as the major MnO_2-mediated bisphenol A transformation product and evaluation of its environmental fate. *Environ. Sci. Technol.* **2015**, *49* (10), 6214–6221.

(31) Nico, P. S.; Zasoski, R. J. Mn(III) center availability as a rate controlling factor in the oxidation of phenol and sulfide on δ-MnO_2. *Environ. Sci. Technol.* **2001**, *35* (16), 3338–3343.

(32) Cui, H.; Liu, X.; Tan, W.; Feng, X.; Liu, F.; Daniel Ruan, H. Influence of Mn(III) availability on the phase transformation from layered buserite to tunnel-structured todorokite. *Clays Clay Miner.* **2008**, *56* (4), 397–403.

(33) Drits, V. A.; Lanson, B.; Gaillot, A.-C. Birnessite polytype systematics and identification by powder X-ray diffraction. *Am. Mineral.* **2007**, *92* (5–6), 771–788.

(34) Kwon, K. D.; Refson, K.; Sposito, G. Defect-induced photoconductivity in layered manganese oxides: A density functional theory study. *Phys. Rev. Lett.* **2008**, *100* (14), 146601.

(35) Lanson, B.; Drits, V. A.; Gaillot, A.-C.; Silvester, E.; Plançon, A.; Manceau, A. Structure of heavy-metal sorbed birnessite: Part 1. Results from X-ray diffraction. *Am. Mineral.* **2002**, *87* (11–12), 1631–1645.

(36) Manceau, A.; Drits, V. A.; Silvester, E.; Bartoli, C.; Lanson, B. Structural mechanism of Co^{2+} oxidation by the phyllomanganate buserite. *Am. Mineral.* **1997**, *82* (11–12), 1150–1175.

(37) Zhao, W.; Cui, H.; Liu, F.; Tan, W.; Feng, X. Relationship between Pb^{2+} adsorption and average Mn oxidation state in synthetic birnessites. *Clays Clay Miner.* **2009**, *57* (5), 513–520.

(38) Zhu, M.; Ginder-Vogel, M.; Parikh, S. J.; Feng, X.-H.; Sparks, D. L. Cation effects on the layer structure of biogenic Mn-oxides. *Environ. Sci. Technol.* **2010**, *44* (12), 4465–4471.

(39) McBride, M. B. Adsorption and oxidation of phenolic compounds by iron and manganese oxides. *Env. Toxicol Chem* **1987**, *51* (6), 1466–1472.

(40) Zhang, H.; Chen, W.-R.; Huang, C.-H. Kinetic modeling of oxidation of antibacterial agents by manganese oxide. *Environ. Sci. Technol.* **2008**, *42* (15), 5548–5554.

(41) Klausen, J.; Haderlein, S. B.; Schwarzenbach, R. P. Oxidation of substituted anilines by aqueous MnO_2: Effect of co-solutes on initial and quasi-steady-state kinetics. *Environ. Sci. Technol.* **1997**, *31* (9), 2642–2649.

(42) Rubert; Pedersen, J. A. Kinetics of oxytetracycline reaction with a hydrous manganese oxide. *Environ. Sci. Technol.* **2006**, *40* (23), 7216–7221.

(43) Xu, L.; Xu, C.; Zhao, M.; Qiu, Y.; Sheng, G. Oxidative removal of aqueous steroid estrogens by manganese oxides. *Water Res.* **2008**, *42* (20), 5038–5044.

(44) Lu, Z.; Lin, K.; Gan, J. Oxidation of bisphenol F (BPF) by manganese dioxide. *Environ. Pollut.* **2011**, *159* (10), 2546–2551.

(45) Zhang, T.; Zhang, X.; Yan, X.; Ng, J.; Wang, Y.; Sun, D. D. Removal of bisphenol A via a hybrid process combining oxidation on β-MnO_2 nanowires with microfiltration. *Colloids Surf. Physicochem. Eng. Asp.* **2011**, *392* (1), 198–204.

(46) Shaikh, N.; Taujale, S.; Zhang, H.; Artyushkova, K.; Ali, A.-M. S.; Cerrato, J. M. Spectroscopic investigation of interfacial interaction of manganese oxide with triclosan, aniline, and phenol. *Environ. Sci. Technol.* **2016**, *50* (20), 10978–10987.

(47) Drits, V. A.; Silvester, E.; Gorshkov, A. I.; Manceau, A. Structure of synthetic monoclinic Na-rich birnessite and hexagonal birnessite: I. Results from X-ray diffraction and selected-area electron diffraction. *Am. Mineral.* **1997**, *82* (9), 946–961.

(48) Silvester, E.; Manceau, M.; Drits, V. A. Structure of synthetic monoclinic Na-rich birnessite and hexagonal birnessite: II. Results from chemical studies and EXAFS spectroscopy. *Am. Mineral.* **1997**, *82*, 962–978.

(49) Tan, W.; Lu, S.; Liu, F.; Feng, X.; He, J.; Koopal, L. K. Determination of the point-of-zero charge of manganese oxides with different methods including an improved salt titration method. *Soil Sci.* **2008**, *173* (4), 277–286.

(50) Lafferty, B. J.; Ginder-Vogel, M.; Zhu, M.; Livi, K. J. T.; Sparks, D. L. Arsenite oxidation by a poorly crystalline manganese-oxide. 2. Results from X-ray absorption spectroscopy and X-ray diffraction. *Environ. Sci. Technol.* **2010**, *44* (22), 8467–8472.

(51) Nakamura, S.; Tezuka, Y.; Ushiyama, A.; Kawashima, C.; Kitagawara, Y.; Takahashi, K.; Ohta, S.; Mashino, T. Ipso substitution of bisphenol A catalyzed by microsomal cytochrome P450 and enhancement of estrogenic activity. *Toxicol. Lett.* **2011**, *203* (1), 92–95.

(52) Piper, D. Z.; Basler, J. R.; Bischoff, J. L. Oxidation state of marine manganese nodules. *Geochim. Cosmochim. Acta* **1984**, *48* (11), 2347–2355.

(53) Murray, J. W.; Balistrieri, L. S.; Paul, B. The oxidation state of manganese in marine sediments and ferromanganese nodules. *Geochim. Cosmochim. Acta* **1984**, *48* (6), 1237–1247.

(54) Freeman, D. S.; Chapman, W. G. An improved oxalate method for the determination of active oxygen in manganese dioxide. *Analyst* **1971**, *96* (1149), 865–869.

(55) Good, N. E.; Winget, G. D.; Winter, W.; Connolly, T. N.; Izawa, S.; Singh, R. M. Hydrogen ion buffers for biological research. *Biochemistry (Mosc.)* **1966**, *5* (2), 467–477.

(56) Ferreira, C. M. H.; Pinto, I. S. S.; Soares, E. V.; Soares, H. M. V. M. (Un)suitability of the use of pH buffers in biological, biochemical and environmental studies and their interaction with metal ions – a review. *RSC Adv* **2015**, *5* (39), 30989–31003.

(57) Ying, S. C.; Kocar, B. D.; Fendorf, S. Oxidation and competitive retention of arsenic between iron- and manganese oxides. *Geochim. Cosmochim. Acta* **2012**, *96*, 294–303.

(58) Ilton, E. S.; Post, J. E.; Heaney, P. J.; Ling, F. T.; Kerisit, S. N. XPS determination of Mn oxidation states in Mn (hydr)oxides. *Appl. Surf. Sci.* **2016**, *366*, 475–485.

(59) Webb, S. M. SIXpack: A graphical user interface for XAS analysis using IFEFFIT. *Phys. Scr.* **2005**, *2005* (T115), 1011.

(60) Manceau, A.; Marcus, M. A.; Grangeon, S. Determination of Mn valence states in mixed-valent manganates by XANES spectroscopy. *Am. Mineral.* **2012**, *97* (5–6), 816–827.

(61) Webb, S. M. Structural characterization of biogenic Mn oxides produced in seawater by the marine *Bacillus* sp. strain SG-1. *Am. Mineral.* **2005**, *90* (8–9), 1342–1357.

(62) Rehr, J. J.; Albers, R. C.; Zabinsky, S. I. High-order multiple-scattering calculations of X-ray-absorption fine structure. *Phys. Rev. Lett.* **1992**, *69* (23), 3397.

(63) Newville, M. IFEFFIT: Interactive XAFS analysis and FEFF fitting. *J. Synchrotron Radiat.* **2001**, *8* (2), 322–324.

(64) Lanson, B.; Drits, V. A.; Silvester, E.; Manceau, A. Structure of H-exchanged hexagonal birnessite and its mechanism of formation from Na-rich monoclinic buserite at low pH. *Am. Mineral.* **2000**, *85* (5–6), 826–838.

(65) Klewicki, J. K.; Morgan, J. J. Kinetic behavior of Mn(III) complexes of pyrophosphate, EDTA, and citrate. *Environ. Sci. Technol.* **1998**, *32* (19), 2916–2922.

(66) Pizzigallo, M. D.; Ruggiero, P.; Crecchio, C.; Mascolo, G. Oxidation of chloroanilines at metal oxide surfaces. *J. Agric. Food Chem.* **1998**, *46* (5), 2049–2054.

(67) Ulrich, H. J.; Stone, A. T. The oxidation of chlorophenols adsorbed to manganese oxide surfaces. *Environ. Sci. Technol.* **1989**, *23* (4), 421–428.

(68) Lin, K.; Yan, C.; Gan, J. Production of hydroxylated polybrominated diphenyl ethers (OH-PBDEs) from bromophenols by manganese dioxide. *Environ. Sci. Technol.* **2014**, *48* (1), 263–271.

(69) Xiao, X.; Sun, S.-P.; McBride, M. B.; Lemley, A. T. Degradation of ciprofloxacin by cryptomelane-type manganese(III/IV) oxides. *Environ. Sci. Pollut. Res.* **2013**, *20* (1), 10–21.

(70) Liu, C. S.; Zhang, L. J.; Feng, C. H.; Wu, C. A.; Li, F. B.; Li, X. Z. Relationship between oxidative degradation of 2-mercaptobenzothiazole and physicochemical properties of manganese (hydro)oxides. *Environ. Chem.* **2009**, *6* (1), 83.

(71) Bialk, H. M.; Simpson, A. J.; Pedersen, J. A. Cross-coupling of sulfonamide antimicrobial agents with model humic constituents. *Environ. Sci. Technol.* **2005**, *39* (12), 4463–4473.

(72) Chen, W.-R.; Ding, Y.; Johnston, C. T.; Teppen, B. J.; Boyd, S. A.; Li, H. Reaction of lincosamide antibiotics with manganese oxide in aqueous solution. *Environ. Sci. Technol.* **2010**, *44* (12), 4486–4492.

(73) He, Y.; Xu, J.; Zhang, Y.; Guo, C.; Li, L.; Wang, Y. Oxidative transformation of carbamazepine by manganese oxides. *Environ. Sci. Pollut. Res.* **2012**, *19* (9), 4206–4213.

(74) Petrie, R. A.; Grossl, P. R.; Sims, R. C. Oxidation of pentachlorophenol in manganese oxide suspensions under controlled E_h and pH environments. *Environ. Sci. Technol.* **2002**, *36* (17), 3744–3748.

(75) Zhang, Y.; Yang, Y.; Zhang, Y.; Zhang, T.; Ye, M. Heterogeneous oxidation of naproxen in the presence of α-MnO_2 nanostructures with different morphologies. *Appl. Catal. B Environ.* **2012**, *127*, 182–189.

(76) Stone, A. T.; Ulrich, H. J. Kinetics and reaction stoichiometry in reductive dissolution of manganese(IV) dioxide and Co(III) oxide by hydroquinone. *J. Colloid Interface Sci.* **1989**, *132* (2), 509–522.

(77) Feng, X. H.; Zhu, M.; Ginder-Vogel, M.; Ni, C.; Parikh, S. J.; Sparks, D. L. Formation of nano-crystalline todorokite from biogenic Mn oxides. *Geochim. Cosmochim. Acta* **2010**, *74* (11), 3232–3245.

(78) Villalobos, M.; Toner, B.; Bargar, J.; Sposito, G. Characterization of the manganese oxide produced by *Pseudomonas putida* strain MnB1. *Geochim. Cosmochim. Acta* **2003**, *67* (14), 2649–2662.

(79) Villalobos, M.; Lanson, B.; Manceau, A.; Toner, B.; Sposito, G. Structural model for the biogenic Mn oxide produced by *Pseudomonas putida*. *Am. Mineral.* **2006**, *91* (4), 489–502.

(80) Grangeon, S.; Manceau, A.; Guilhermet, J.; Gaillot, A.-C.; Lanson, M.; Lanson, B. Zn sorption modifies dynamically the layer and interlayer structure of vernadite. *Geochim. Cosmochim. Acta* **2012**, *85*, 302–313.

(81) Grangeon, S.; Lanson, B.; Lanson, M.; Manceau, A. Crystal structure of Ni-sorbed synthetic vernadite: A powder X-ray diffraction study. *Mineral. Mag.* **2008**, *72* (6), 1279–1291.

(82) Kolpin, D. W.; Furlong, E. T.; Meyer, M. T.; Thurman, E. M.; Zaugg, S. D.; Barber, L. B.; Buxton, H. T. Pharmaceuticals, hormones, and other organic wastewater contaminants in U.S. streams, 1999−2000: A national reconnaissance. *Environ. Sci. Technol.* **2002**, *36* (6), 1202–1211.

(83) Smith, R. A.; Alexander, R. B.; Wolman, G. M. Water-quality trends in the nation's rivers. *Science* **1987**, *235* (4796), 1607–1615.

(84) Grebel, J. E.; Charbonnet, J. A.; Sedlak, D. L. Oxidation of organic contaminants by manganese oxide geomedia for passive urban stormwater treatment systems. *Water Res.* **2016**, *88*, 481–491.

(85) Chen, W.-R.; Huang, C.-H. Transformation of tetracyclines mediated by Mn(II) and Cu(II) ions in the presence of oxygen. *Environ. Sci. Technol.* **2009**, *43* (2), 401–407.

(86) Dong, J.; Li, Y.; Zhang, L.; Liu, C.; Zhuang, L.; Sun, L.; Zhou, J. The oxidative degradation of sulfadiazine at the interface of α-MnO_2 and water: Degradation of antibiotics by manganese dioxides. *J. Chem. Technol. Biotechnol.* **2009**, *84* (12), 1848–1853.

(87)   Feitosa-Felizzola, J.; Hanna, K.; Chiron, S. Adsorption and transformation of selected human-used macrolide antibacterial agents with iron(III) and manganese(IV) oxides. *Environ. Pollut.* **2009**, *157* (4), 1317–1322.

(88)   Liu, C.; Zhang, L.; Li, F.; Wang, Y.; Gao, Y.; Li, X.; Cao, W.; Feng, C.; Dong, J.; Sun, L. Dependence of sulfadiazine oxidative degradation on physicochemical properties of manganese dioxides. *Ind. Eng. Chem. Res.* **2009**, *48* (23), 10408–10413.

(89)   Chen, W.-R.; Huang, C.-H. Transformation kinetics and pathways of tetracycline antibiotics with manganese oxide. *Environ. Pollut.* **2011**, *159* (5), 1092–1100.

(90)   Chen, G.; Zhao, L.; Dong, Y. Oxidative degradation kinetics and products of chlortetracycline by manganese dioxide. *J. Hazard. Mater.* **2011**, *193*, 128–138.

(91)   Gao, J.; Hedman, C.; Liu, C.; Guo, T.; Pedersen, J. A. Transformation of sulfamethazine by manganese oxide in aqueous solution. *Environ. Sci. Technol.* **2012**, *46* (5), 2642–2651.

(92)   McArdell, C. S.; Stone, A. T.; Tian, J. Reaction of EDTA and related aminocarboxylate chelating agents with $Co^{III}OOH$ (heterogenite) and $Mn^{III}OOH$ (manganite). *Environ. Sci. Technol.* **1998**, *32* (19), 2923–2930.

(93)   Jiang, L.; Huang, C.; Chen, J.; Chen, X. Oxidative transformation of 17β-estradiol by MnO_2 in aqueous solution. *Arch. Environ. Contam. Toxicol.* **2009**, *57* (2), 221–229.

(94)   Rudder, J. d.; Wiele, T. V. de; Dhooge, W.; Comhaire, F.; Verstraete, W. Advanced water treatment with manganese oxide for the removal of 17α-ethynylestradiol (EE2). *Water Res.* **2004**, *38* (1), 184–192.

(95)   Kim, D.-G.; Jiang, S.; Jeong, K.; Ko, S.-O. Removal of 17α-ethinylestradiol by biogenic manganese oxides produced by the *Pseudomonas putida* strain MnB1. *Water. Air. Soil Pollut.* **2012**, *223* (2), 837–846.

(96)   Lin, K.; Liu, W.; Gan, J. Reaction of tetrabromobisphenol A (TBBPA) with manganese dioxide: Kinetics, products, and pathways. *Environ. Sci. Technol.* **2009**, *43* (12), 4480–4486.

(97)   Dong, J.; Zhang, L.; Liu, H.; Liu, C.; Gao, Y.; Sun, L. The oxidative degradation of 2-mercaptobenzothialzole by different manganese dioxides. *Fresenius Environ. Bull.* **2010**, *19*, 1615–1622.

(98)   Xiao, H.; Song, H.; Xie, H.; Huang, W.; Tan, J.; Wu, J. Transformation of acetaminophen using manganese dioxide − mediated oxidative processes: Reaction rates and pathways. *J. Hazard. Mater.* **2013**, *250–251*, 138–146.

Chapter 3

Impact of bisphenol A influent concentration and reaction time on MnO$_2$ transformation in a stirred flow reactor[2]
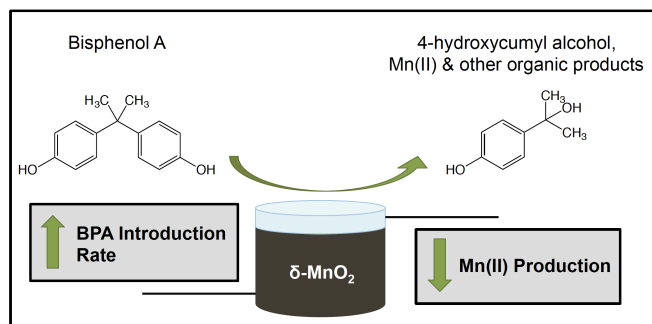
3.1 Abstract

Bisphenol A (BPA) is an endocrine disrupting compound commonly found in natural waters at concentrations that are considered harmful for aquatic life. Manganese(III/IV) oxides are strong oxidants capable of oxidizing organic and inorganic contaminants, including BPA. Here we use δ-MnO$_2$ in stirred flow reactors to determine if higher influent BPA concentrations, or introduction rates, lead to increased polymer production. A major BPA oxidation product, 4-hydroxycumyl alcohol (HCA), is formed through radical coupling, and was therefore used as one metric for polymer production in this study. The influent BPA concentration in stirred flow reactors did not affect HCA yield, suggesting that polymeric production is not strongly dependent on influent concentrations. However, changes in influent BPA concentration affected BPA oxidation rates and the rate of δ-MnO$_2$ reduction. Lower aqueous Mn(II) production was observed in reactors at higher BPA introduction rates, suggesting that single-electron transfer

---

and polymer production are favored under these conditions. However, an examination of Mn(II) sorption during these reactions indicated that the length of the reaction, rather than BPA introduction rate, caused enhanced aqueous Mn(II) production in reactors with low introduction rates and longer reaction times due to increased opportunity for disproportionation and comproportionation. This study demonstrates the importance of investigating both the organic and inorganic reactants in the aqueous and solid phases in this complex reaction.

3.2 Introduction

Manganese oxides (MnO_x) are one of the strongest naturally-occurring oxidants and can oxidize a wide range of organic contaminants, including phenols.[1–4] Previous studies have demonstrated oxidation of phenols by manganese oxides using model organic compounds[2,3,5–10] and complex pollutants.[11–19] Bisphenol A (BPA) is an industrial plasticizer[20] that is commonly found in wastewater,[21] landfill leachate,[22] and surface water.[23,24] In the environment, BPA leads to teratogenic, endocrine, and pleiotropic effects in fish and other aquatic species.[25]

BPA is susceptible to oxidation by manganese oxides.[12,18,26,27] Similar to other phenols, BPA undergoes a one-electron transfer with manganese oxides to form a radical species that can form polymeric products through radical coupling or undergo further oxidation through a second one-electron transfer.[1–3,10,11,28,29] BPA oxidation is affected by MnO_2 concentration, pH, and metal cosolutes, and 11 transformation products have been identified, including 10 phenols and 4 polymers.[12] 4-Hydroxycumyl alcohol (HCA) is a major product of BPA oxidation and is generated at yields up to 64% HCA per mole of BPA.[30] Note that this yield is based on direct measurement of HCA and does not consider oxidation of HCA by manganese oxide.[30] Since

HCA is formed through radical coupling, its production can potentially be used to probe the relative amount of polymeric coupling.

Oxidation rates of organic compounds by manganese oxide are highly dependent on mineral properties. The reaction follows pseudo-first-order kinetics during the initial phase, but the rate of oxidation decreases as the reaction proceeds.[11,12,14,31,32] Previous investigations of manganese oxide transformation during organic compound oxidation are limited, but they provide unique insights into changes to the mineral surface. For example, decreased rates of phenol, aniline, and triclosan oxidation by MnO_x are associated with decreasing oxidation state and accumulation of reduced manganese species and organic species on the mineral surface.[19] Similarly, δ-MnO_2 can transform to other phases after accumulating Mn(III) in the presence of high concentrations of fulvic acid.[33] Our previous study using Mn(III)-rich MnO_2 and BPA shows that changes at the mineral surface are enough to decrease the oxidation rate even without changes in the bulk mineral oxidation state.[18]

Previous studies typically use batch reactors to characterize the reactivity of manganese oxides.[1] These closed systems are experimentally simple and results can be readily compared to previous data. However, stirred flow reactors can provide further benefits, allowing for slow and constant addition of an influent media that can be easily altered. Additionally, batch reactors retain both organic and inorganic reaction products, which can affect the reaction. For example, the addition of Mn(II) can considerably decrease phenol oxidation rate by manganese oxides.[12,13,26,27,34] In the environment and in stirred flow reactors, these products are constantly removed. A few studies use stirred flow reactors[32,35] or column reactors[36,37] to examine manganese oxide reactivity, but none have investigated both the changes in the aqueous and solid phases.

Here calculated HCA yield, aqueous Mn(II) production, and solid phase characterization are used to detect differences in BPA oxidation mechanism by δ-MnO$_2$ in stirred flow reactors as a function of influent BPA concentration. This method is used to test the hypothesis that higher influent BPA concentrations lead to greater polymer production and therefore less overall electron transfer. Radicals formed via single electron transfer are of concern as they can couple with dissolved organic matter or other compounds in the environment, forming unknown high molecular weight products.[38–40] HCA is used as an indicator of conditions that favor single-electron transfer (i.e., polymer production), rather than two sequential electron transfers (i.e., benzoquinone production). Aqueous Mn(II) is produced by reductive dissolution and is used to quantitatively compare electron transfer across different solution conditions. We use this data, along with measurements from solid phase characterization using X-ray absorption near edge structure (XANES) spectroscopy and X-ray diffraction (XRD), to make inferences about the mechanism of the redox reaction and how the δ-MnO$_2$ structure changes throughout the reaction. By performing these reactions in a stirred flow reactor, this study provides novel insights into the effects of contaminant loading over long time periods, which is more representative of contaminants in a flow-through treatment system.[36,41]

3.3 Materials and Methods

3.3.1 Materials

Commercially available chemicals were used as received (Section **B1**). HCA was synthesized as described previously.[18] Ultrapure water was supplied by a Milli-Q water purification system maintained at 18.2 MΩ·cm. BPA and HCA stock solutions were prepared in methanol and stored at 4ºC. Information on preparation and characterization of δ-MnO$_2$ is

provided in Section **B1**. This synthesis yielded a mineral with an average valence state of $3.94 \pm$ 0.11 v.u. determined by oxalate titration,[42] indicating that the mineral is predominantly Mn(IV).

3.3.2 HCA Characterization

The acid dissociation constant (pK_a) of HCA was determined spectrophotometrically at 240 nm by titration of 0.1 HCl into a solution of 100 µM HCA following a previously published method.[43]

3.3.3 Solution Conditions

All stirred flow reactions and batch reactors used to determine initial rates of BPA and HCA oxidation were performed at pH 5 in 10 mM sodium acetate to avoid experimental artifacts. Acetate did not affect δ-MnO$_2$ reactivity with BPA over time at pH 5 (Figure **B1**), whereas many common circumneutral pH buffers can form complexes with Mn(II) or reduce manganese oxides.[44–47] For example, preliminary experiments with 10 mM piperazine-*N,N'*-bis(2-ethanesulfonic acid) (PIPES) at pH 7 demonstrated that the buffer decreases MnO$_2$ reactivity (Figure **B1**). Klausen et al. reported that PIPES sorbs to the manganese oxide surface, decreasing the number of reactive sites on the surface.[32]

3.3.4 Batch Reactors

Batch reactors were used to determine initial rates of BPA and HCA oxidation by δ-MnO$_2$. Prepared δ-MnO$_2$ slurry (stock concentrations: 30-50 g/L) was equilibrated in a pH 5 acetate buffered solution for 30 minutes before the addition of BPA or HCA (initial concentration: 40 or 80 µM). BPA and HCA concentrations were determined by high-

performance liquid chromatography (HPLC; Agilent 1260) in samples that were quenched in excess ascorbic acid (10.8 mM) in order to completely dissolve the δ-MnO$_2$. Aqueous manganese was quantified by inductively coupled plasma-optical emission spectroscopy (ICP-OES; PerkinElmer Optima 4300 DV) analysis of filtered samples (0.2 μm polytetrafluoroethylene) diluted in 2% nitric acid. Batch reactor experiments were conducted in triplicate.

3.3.5 Stirred Flow Reactors

Each 12.7 mL stirred flow reactor contained 1.58 g/L δ-MnO$_2$ slurry and a stir bar (Figure **B2**). A filter (0.1 μm VCWP, Millipore) and filter holder prevented δ-MnO$_2$ from leaving the reactor. The solution was continuously stirred, with BPA in acetate buffer constantly being introduced at a rate of 1 mL/min (hydraulic retention time = 12.7 minutes). Each reactor was equilibrated with 10 mM acetate for 30 minutes before introducing BPA. The tubing used for the reactors was Pt-cured Si (2.06 mm I.D. Cole Parmer) and exhibited < 7% sorption of BPA and phenol in control experiments (Figure **B3**).

Stirred flow reactor effluent was analyzed by HPLC and ICP-OES to quantify BPA, HCA, and aqueous manganese. These samples were not filtered or quenched using excess ascorbic acid since the reaction stops upon exiting the δ-MnO$_2$ reactor. Media with varying BPA concentrations (20 – 160 μM, corresponding to a BPA introduction rate of 20 – 160 nmol/min) were used in stirred flow experiments to determine mechanistic differences due to influent BPA concentrations. The length of the experiment was adjusted so that 20 – 25 μmol BPA was added to each reactor in total.

Solids were recovered at the end of the reaction. This material was washed in methanol to remove organics, dried at room temperature, and ground before analysis. Average manganese oxidation number (AMON) was determined using XANES spectra collected at beamline 10-BM at the Advanced Photon Source at Argonne National Laboratory (Section **B4**). Samples were prepared by diluting 3 mg of manganese oxide into 8 mg of polyvinylpyrrolidone, grinding until homogenous, and pressing into a 7 mm pellet. XANES data was analyzed for AMON using the Combo method.[48] XRD patterns were collected (Rigaku Rapid II, Mo Kα source; λ = 0.7093 Å) to determine changes in the order and crystallinity of the mineral.

3.3.6 HCA Yield Calculation

HCA is a phenolic product of BPA oxidation by manganese oxide that is also susceptible to oxidation by the mineral.[18,30] In batch reactors, HCA yield was calculated as described previously:[18]

$$[\text{HCA}] = k_1 \cdot F_{\text{HCA}} \cdot \frac{[\text{BPA}]_0}{k_2 - k_1} \cdot (e^{-k_1 t} - e^{-k_2 t}) \tag{3.1}$$

where k_1 is the BPA oxidation rate constant, F_{HCA} is the fraction of BPA converted to HCA, $[\text{BPA}]_0$ is the initial BPA concentration, k_2 is the HCA oxidation rate constant, and t is time after BPA addition. F_{HCA} was calculated by least-squares minimization.

In stirred flow reactors, a steady-state assumption was used to estimate the HCA yield once the reactions reach a plateau in BPA and HCA concentrations using the following equation:

$$F_{HCA} = \frac{Q[HCA]}{k_1[BPA]_0 V - k_2[BPA]_0 V} \tag{3.2}$$

where Q is the flow rate of the reactor, V is the volume of the reactor, and k_1 is calculated according to:

$$k_1 = \frac{Q[BPA]_0 - Q[BPA]}{[BPA]_0 V}$$ **(3.3)**

k_2 is calculated using an initial rates ratio determined experimentally at each condition. Derivation of equations **3.2** and **3.3** is provided in Section **B5**.

3.4 Results and Discussion

3.4.1 HCA Production and Characterization

Upon exposure to δ-MnO$_2$, BPA concentration quickly decreases via oxidation, producing HCA as a major oxidation product (Figure **3.1**). The production of HCA during BPA oxidation is consistent with its identification and characterization in two previous studies.[18,30] BPA oxidation by MnO$_x$ produces a multitude of products,[12] but at up to 64% yield,[30] HCA is the only product detectable by HPLC analysis (Figure **B4**). HCA only accounts for 60% of the carbon atoms present in BPA and it is likely that the C$_6$ moiety formed during HCA production is susceptible to rapid degradation.[30] The pK_a of HCA is determined to be 10.24 ± 0.05 in this study (Figure **B5**), whereas the pK_a values for BPA are 9.6 and 10.2.[49] This is an important measurement for HCA since pK_a values strongly affect sorption capacity of phenols.

HCA is also susceptible to oxidation by δ-MnO$_2$, albeit at a slower rate than BPA, which is consistent with previous literature.[18,30] For example, the pseudo-first-order oxidation rate constants of BPA and HCA at pH 5 are 0.228 min^{-1} and 0.029 min^{-1}, respectively (Figure **B6**; Table **B1**). As shown in Figure **3.1**, HCA concentration increases with time in BPA oxidation reactions, but then reaches a maximum and slowly decreases. Using relative BPA and HCA initial oxidation rate constants determined in separate batch reactors, theoretical HCA yields can be calculated for BPA oxidation reactions in both batch reactors and stirred flow reactors using

equations **3.1** and **3.2**. For example, the HCA yield in a batch reactor with 0.33 g/L δ-MnO$_2$ and 80 μM BPA at pH 5 is 44% (least-squares fit line in Figure **3.1**).

3.4.2 Characteristics of Stirred Flow Reactors

In these reactions, the BPA solution is introduced into the reactor while the effluent is collected and analyzed. An example data set is presented in Figure **3.2**. Initially, BPA is completely oxidized by δ-MnO$_2$ and is not detected in the reactor effluent. Similarly, the HCA concentration in the effluent is initially below detection because all HCA produced through BPA oxidation is also completely oxidized by δ-MnO$_2$. As the reaction rate decreases due to changes in the mineral during oxidation of BPA and its phenolic transformation products, BPA and HCA concentrations increase in the reactor effluent. After about 40 hours, or 200 μmol BPA introduced, δ-MnO$_2$ is no longer capable of oxidizing BPA during the 12.7-minute hydraulic retention time. As the manganese oxide becomes less reactive, HCA concentrations increase and eventually reach a maximum before returning to zero as BPA ceases reacting with δ-MnO$_2$ and therefore no longer produces HCA.

Aqueous Mn(II) is a product of Mn(III/IV) reduction by phenols and is commonly used to quantify reductive dissolution.[12–14,19,26,31,32,34] Here, Mn(II) appears in the reactor effluent after the first hour (Figure **3.2**), showing that reductive dissolution of the mineral is occurring.[2,3,50] After six hours, dissolved Mn(II) reaches a maximum and returns to below detection limit as δ-MnO$_2$ stops reacting with BPA and its transformation products. The BPA concentration experiments described below focus on the early stages of this reaction, where 70 – 100% of BPA is oxidized by δ-MnO$_2$ during the retention time, similar to previous studies investigating As(III)[35,51] and aniline[32] oxidation by MnO$_2$.

3.4.3 Effect of BPA Influent Concentration

Four stirred flow reactors with varying concentrations of influent BPA are used to determine the effect of BPA introduction rate on reaction kinetics, aqueous products, and mineral transformation. Influent BPA concentrations range from 20 – 160 μM, which correspond to BPA introduction rates of 20 – 160 nmol/min. All reactors have the same flow rate and retention time but vary in length of reaction time so that each reactor is exposed to the same amount of BPA (20 – 25 μmol). Due to this difference in time (150 – 1200 min), data is normalized by plotting as a function of BPA introduced to the reactor (Figure **3.3**). Data is presented as a function of time in Figure **B7 – B8**.

The BPA oxidation rate decreases with exposure of δ-MnO$_2$ to BPA throughout the shorter time-scale of these experiments, as was observed in the 140-hour experiment (Figure **3.2**). The BPA concentration in the effluent reaches an apparent plateau in which 5 – 30% of the BPA is oxidized, depending on the concentration of the influent solution (Figure **3.3a**). At the lowest BPA introduction rate (20 nmol/min), BPA appears in the effluent after 11 μmol of BPA are introduced and reaches a plateau almost immediately (i.e., after 13 μmol of BPA are introduced). This trend is also followed for the 40 and 80 nmol/min reactors. The plateau that is reached is modeled using a steady-state approximation to calculate BPA oxidation rate constants and HCA yields. At the highest BPA introduction rate (160 nmol/min), BPA also appears in the effluent after 11 μmol of BPA are introduced but no plateau is observed during the reaction period (25 μmol of BPA introduced).

HCA concentration in the effluent varies with influent BPA concentration, with higher concentrations of BPA leading to higher concentrations of HCA in the effluent and vice versa (Figure **3.3b**). HCA is found in the effluent earlier in the reaction with lower BPA introduction

rates (e.g., after 8 µmol of BPA introduced for 20 nmol/min reactor and after 13 µmol of BPA for 160 nmol/min reactor). Furthermore, a plateau of HCA concentration is reached sooner in reactors with lower BPA introduction rate (i.e., after 11 µmol of BPA for 20 nmol/min reactor and after 25 µmol of BPA for 160 nmol/min reactor). However, when plotted as a fraction of BPA consumed in the reactor (Figure **3.3c**), all reactors produce the same ratio of moles of HCA in effluent per moles of BPA consumed within 3.1% (30.0 – 33.1%) by the end of the reaction, excluding the 160 nmol/min reactor, which does not fully reach a plateau.

The steady-state approximation (Section **B5**) and relative initial rates of BPA and HCA oxidation in batch reactors (Table **B1**; Figure **B6**) are used to calculate BPA oxidation rate constants and HCA yields in stirred flow reactors when the reaction reaches a plateau (e.g., after 12 µmol of BPA introduced for the 20 nmol/min reactor). Although the system is not truly at steady-state because δ-MnO_2 reactivity changes gradually over extended reaction times (Figure **3.2**), the steady-state approximation is valid because the BPA and HCA concentrations are not changing from one time point to the next within this shorter timeframe. However, it is not possible to calculate HCA yield with the 160 nmol/min introduction rate because this reactor does not reach a distinct plateau by the end of the reaction time. Calculated BPA oxidation rate constants steadily increase with BPA introduction rate in reactors with 20, 40, and 60 nmol/min introduction rates (Figure **3.4**). This observation is in agreement with previous batch reactor studies that show an increase in oxidation rate with increases in either phenol concentration or MnO_2 concentration.[5,12]

HCA yields provide insight into changes in BPA reaction mechanism as a function of BPA concentration. Reactors with 20, 40, and 80 nmol/min BPA introduction rates have nearly identical HCA yields between 38 – 40% at the reaction plateau (Figure **3.4**). As a major

oxidation product formed through radical coupling,[30] the fraction of HCA production is theoretically proportional to the fraction of one-electron transfer reactions in this system. Since these polymeric products are more likely to form when there are high concentrations of BPA, we hypothesized that HCA yield would be higher when δ-MnO$_2$ is exposed at a higher BPA introduction rate. However, the data indicates that there is no difference in HCA yield within this BPA concentration range.

Additional experiments were conducted at different BPA influent concentrations to further test whether HCA yields change under different conditions. First, influent BPA concentrations below 20 μM were preliminarily examined but were inconclusive. For example, a trial using 5 nmol/min BPA, which corresponds to an initial concentration of 5 μM BPA for 83 hours, shows that BPA is entirely consumed in the reaction (Figure **B9**). Therefore, HCA yields could not be determined at lower BPA influent concentrations due to complete BPA oxidation. Second, a separate experiment using longer reaction times compares HCA yields of 20 nmol/min and 160 nmol/min introduction rates after they have both reached a plateau (Figure **B10**). The observed yields of 44% and 40% respectively indicate that the higher introduction rate does not yield more HCA than lower introduction rate, further disproving our hypothesis that more polymeric products are produced at higher influent BPA concentrations.

Although the organic data does not indicate a shift in BPA oxidation mechanism, the inorganic data shows a strong trend among the reactors. Aqueous manganese concentrations in stirred flow reactor effluent show that there is a relationship between influent BPA concentration and Mn(II) production (Figure **3.3d**). At lower BPA introduction rates, Mn(II) is produced earlier in the reaction and in larger quantities than at higher BPA introduction rates. For example, the 20 nmol/min introduction rate results in 19.8 μmol total Mn(II) beginning after 11.4 μmol BPA

introduced, while the 160 nmol/min introduction rate results in 6.3 µmol total beginning after 18.7 µmol BPA introduced. Despite the difference in Mn(II) produced, minimal bulk mineralogical changes are observed in the XRD patterns or XANES data. Figure **3.5a** shows that commonly observed changes, such as reduced tailing of the *hkl* diffraction band at 37° and the appearance of a dip at ~47°, only noticeably appear in the 20 nmol/min reactor. Analysis of XANES data using the Combo method fits the raw data and provides a calculated AMON for the sample. The AMON of the starting material is 3.85 v.u. (90% Mn(IV), 5% Mn(III), 5% Mn(II)). In samples recovered from stirred flow reactors, the AMON decreased due to reduction, but was the same value of 3.67 ± 0.01 v.u. for all BPA introduction rates (Figure **3.5b**; Table **B2**). Unsurprisingly, no mineral phase changes occurred due to the low pH and relatively low accumulation of reduced Mn. This is consistent with previous work that shows changes in Mn(III)-rich δ-MnO$_2$ reactivity can occur due to mineral transformation at the surface, such as increased interlayer Mn(II/III), and not necessarily changes to the bulk structure.[18]

The differences in Mn(II) production, despite lack of changes in the bulk average manganese oxidation number, indicate that there are more overall electron transfer reactions occurring at lower BPA introduction rates, resulting in increased reductive dissolution of δ-MnO$_2$. This is further shown by the estimated net electron transfer from organic compounds to δ-MnO$_2$ calculated for each reactor (Table **B3**), where electron transfer in 20, 40, 80, and 160 nmol/min reactors are estimated to be 79.7, 72.0, 64.9, and 50.7 µmol, respectively. There are several potential explanations for this observation. First, it is possible that two sequential single-electron transfers are favored in reactors with lower BPA introduction rates, forming more Mn(II) through a second single-electron transfer, rather than just one single-electron transfer reaction to produce Mn(III). However, if HCA is used to determine the relative amount of

polymeric products formed, the absence of a trend in HCA yield over the 20 – 80 nmol/min reactors indicates that the proportion of single-electron transfer reactions, and therefore polymer production, is consistent over the range of BPA introduction rates. A second explanation is that the differences in reaction lengths allow for more redox reaction to take place, including oxidation of BPA oxidation products (e.g., HCA) and transfer of electrons within the manganese oxide mineral (i.e., disproportionation and comproportionation). This is supported by both data sets, but does not follow the generally accepted concept that more radical coupling and polymeric production will occur at higher concentrations of the target organic compound.[52] A third possibility is that HCA does not accurately quantify polymeric production since other polymers can be formed by BPA oxidation.[12]

One way to narrow down these possibilities is to determine how accurately Mn(II) production quantifies the total number of electrons transferred to δ-MnO$_2$. When Mn(II), Mn(III), and Mn(IV) are present in the same system, the mineral is susceptible to disproportionation and comproportionation (equation **3.4**).[53–56] A Mn(II) center and Mn(IV) center can exchange electrons, or comproportionate, to form two Mn(III) centers. Conversely, two Mn(III) centers can disproportionate to form Mn(II) and Mn(IV) centers. Due to these reactions, the fraction of reduced Mn(II) species formed in a reaction is not necessarily the same as the reduced species measured in the aqueous phase.

$$Mn(II) + Mn(IV) \rightleftharpoons 2Mn(III) \tag{3.4}$$
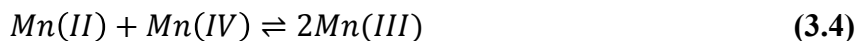
3.4.4 Desorption Experiments

To determine if disproportionation and comproportionation reactions are occurring, Ca^{2+} is used as a desorption agent to quantify solid-bound Mn(II) concentrations at various points in

the reaction. These experiments use stirred flow reactors to introduce buffered BPA, buffer only, and Ca^{2+} solutions into a δ-MnO_2 slurry. Disproportionation and comproportionation reactions can readily occur in mixed-valent manganese oxides,[53–57] affecting the distribution of Mn(II), Mn(III), and Mn(IV) over time. These reactions make it difficult to characterize small changes in the mineral structure because they can be attributed to either the reaction of interest (i.e., reaction with BPA) or disproportionation and/or comproportionation. Here, Ca^{2+} is added to desorb Mn(II) from the δ-MnO_2 solid after the oxide reacts with BPA. If aqueous Mn(II) is continually produced after all solid-associated Mn(II) and BPA has been removed, this would indicate that Mn(III) is undergoing disproportionation to form Mn(II) since there is no other reductant present. Preliminary experiments show that BPA and HCA undergo minimal sorption to δ-MnO_2 (Section **B7**; Table **B1**), meaning negligible amounts of Mn(II) should be produced by continued reaction in this system.

The desorption experiments indicate that Mn(III) disproportionation occurs under our experimental conditions. In Reactor A, exposure of δ-MnO_2 to 20 µM BPA (buffered to pH 5 in 10 mM acetate) for 20 hours produces a total of 6.75 µmol aqueous Mn(II). The addition of 25 mM Ca^{2+} for three hours desorbs an additional 1.54 µmol of Mn(II) that was generated during BPA oxidation (Figure **3.6a**). We then added 10 mM acetate with no BPA for 7 hours, which does not react with δ-MnO_2 (Figure **B1**), but allows time for disproportionation of Mn(III) to occur; minimal Mn(II) is produced during this time (i.e., a total of 0.06 µmol). A second introduction of 25 mM Ca^{2+} for two hours yielded 0.37 µmol additional Mn(II), indicating that Mn(II) is produced via disproportionation during the time between Ca^{2+} introductions.

In Reactor B, δ-MnO_2 is exposed to a 20 µM BPA solution (buffered to pH 5 in 10 mM acetate) for 20 hours, 10 mM acetate buffer for 9 hours, and a final 25 mM Ca^{2+} solution for two

hours. Mn(II) is produced during BPA oxidation as described above, but does not desorb during exposure to 10 mM acetate (Figure **3.6b**). When the Ca^{2+} solution is introduced, Mn(II) desorbs from the mineral and is found in the effluent. Reactor A produces 1.54 µmol Mn(II), while Reactor B produces a total of 0.3 µmol Mn(II). Since both reactors were exposed to the same amount of reductant (i.e., 24 µmol BPA), this indicates that the Mn(II) produced during BPA oxidation is able to undergo comproportionation with Mn(IV) to form Mn(III) if it is not desorbed from the mineral in a timely fashion.

Three conclusions can be drawn from the desorption experiments. First, Mn(II) does not continue to desorb from the mineral after oxidation with BPA, indicating that desorption of Mn(II) occurs after the mineral reaches saturation either by Mn(II) or organics and is driven by exposure to organics and further production of Mn(II). Second, disproportionation, which is highly dependent on pH, occurs in the system within the timescale of the reaction (i.e., on the order of 7 hours at pH 5). Finally, the amount of Mn(II) desorbed by the first exposure to 25 mM Ca^{2+} in each reactor (i.e., 1.54 µmol in Reactor A with immediate exposure to Ca^{2+}, and 0.3 µmol in Reactor B with delayed exposure) indicates that comproportionation is occurring in Reactor B. Overall, these desorption experiments show that both disproportionation and comproportionation are possible within the reaction times of our stirred flow experiments. This indicates that the differences in aqueous Mn(II) production (Figure **3.3d**) are due to the differences in reaction time rather than the BPA introduction rate, as increasing reaction time will lead to a proportional amount of electron transfer between manganese centers.

3.5 Conclusions

This study demonstrates the importance of including both organic and inorganic analysis when examining oxidation of organic contaminants by an inorganic substrate. Although there are many studies on the degradation of BPA and other phenols by manganese oxides, most look only at the disappearance of the organic[11,12,14,31,32] or the complete reductive dissolution of the mineral.[2,11,50,58] Here, we see differences in aqueous Mn(II) production proportional to the introduction rate of BPA into stirred flow reactors. On its own, this information suggests that the introduction rate of BPA determines the redox mechanism, with higher introduction rates leading to more polymeric production via a single-electron transfer, as predicted. However, in tandem with the information from the HCA yield calculations that show no difference in HCA yield with varying introduction rates and the desorption experiments that show that both disproportionation and comproportionation occur in these reactions, we conclude that BPA introduction rate has minimal effect on BPA oxidation mechanism. The difference in aqueous Mn(II) production is likely due to the longer reaction times, which allow for more disproportionation of Mn(III) to occur in reactors with lower BPA introduction rates. This also explains why a plateau is not reached for BPA and HCA concentrations in the shorter 160 nmol/min reactor since not as much Mn(II) has formed via disproportionation, which would hinder the reaction. These findings indicate that Mn(III) is prevalent in reacted δ-MnO$_2$, but undergoes disproportionation or further redox reactions over time in extended reactions.

3.6 Acknowledgements

Figure 3.1. Measured BPA concentrations and measured and theoretical HCA concentrations over time in a batch reactor containing 80 µM BPA and 0.33 g/L δ-MnO$_2$ in a pH 5 acetate buffer.
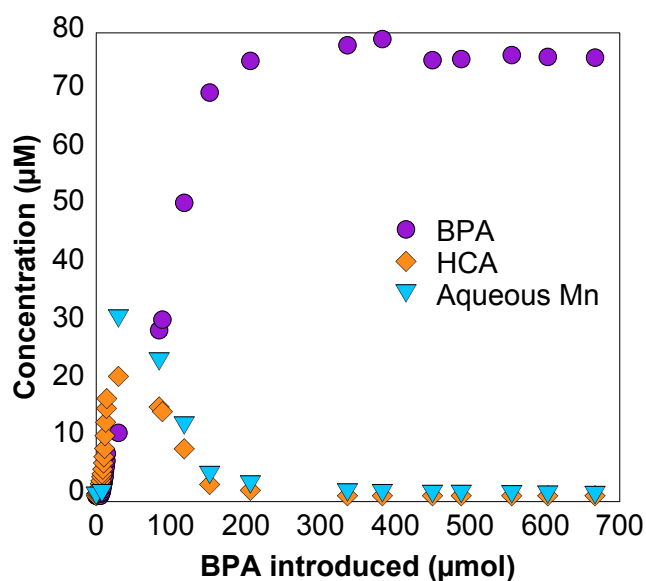
Figure 3.2. Concentrations of BPA, HCA, and aqueous Mn in the effluent of a stirred flow reactor containing 1.58 g/L δ-MnO$_2$, 10 mM acetate buffer (pH 5), and 80 µM BPA over an extended reaction time of 140 hours.
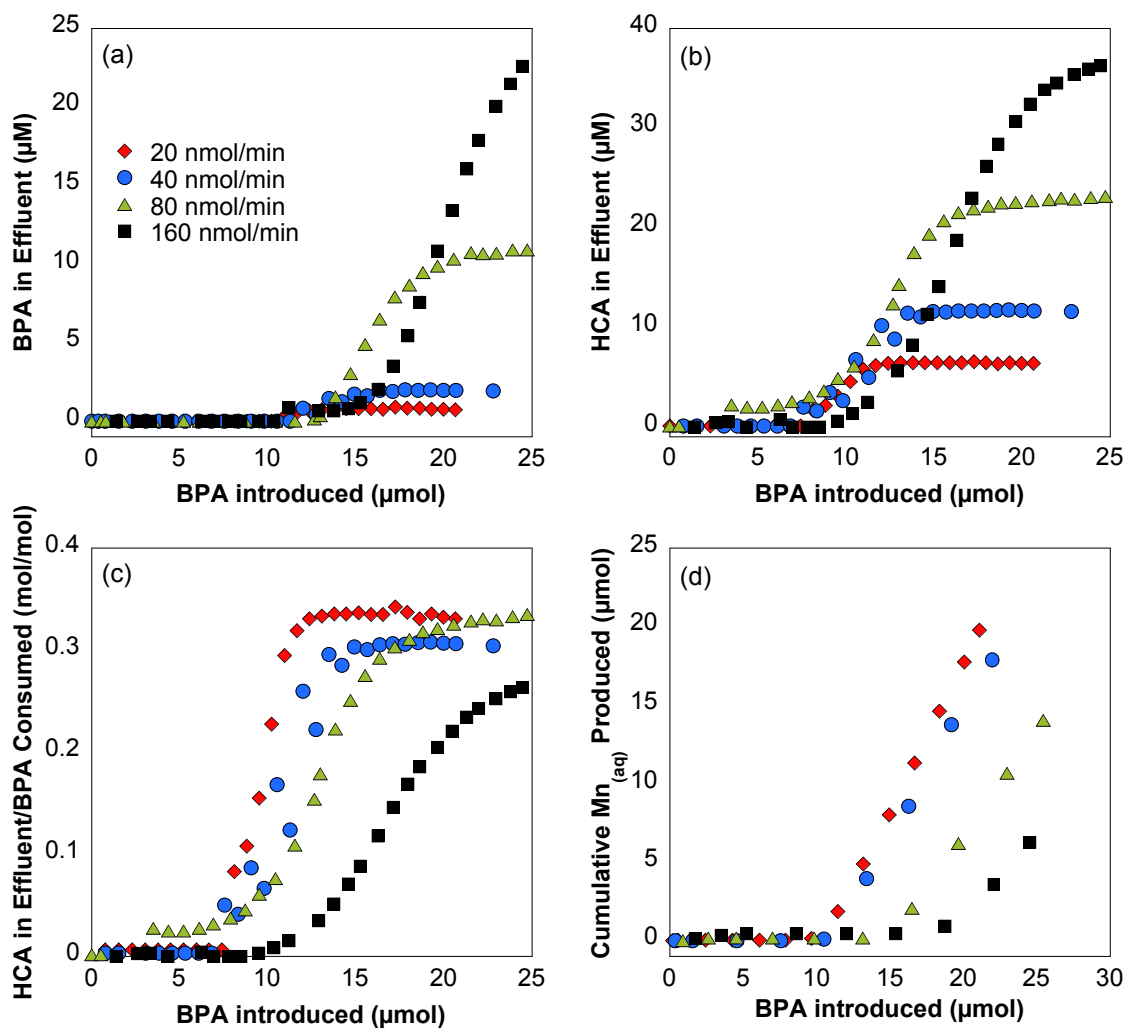
Figure 3.3. (a) BPA and (b) HCA present in the effluent, as well as (c) the ratio of HCA produced to BPA consumed, and (d) aqueous Mn(II) produced in stirred flow reactors containing 1.58 g/L δ-MnO$_2$ in 10 mM acetate buffer (pH 5). Reaction times range from 2.5 – 20 hours.
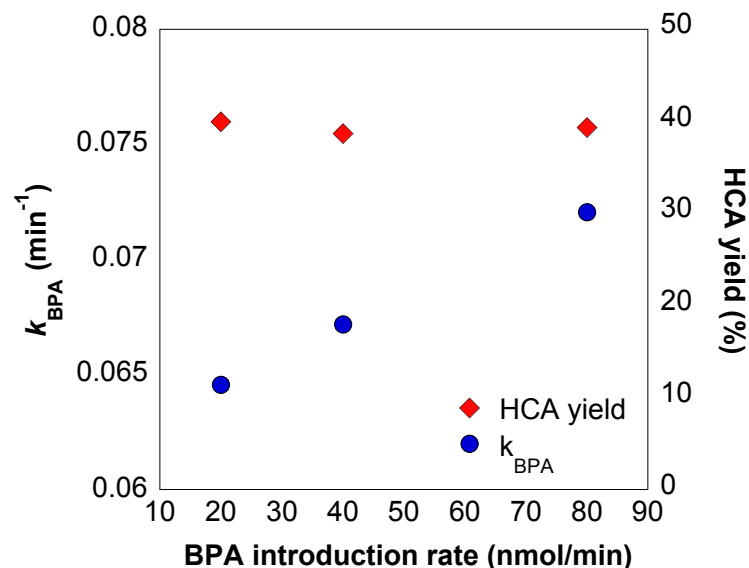
Figure 3.4. Concentrations of BPA, HCA, and aqueous Mn in the effluent of a stirred flow reactor containing 1.58 g/L δ-MnO$_2$ in 10 mM acetate buffer (pH 5) containing 80 µM BPA over an extended reaction time of 140 hours.
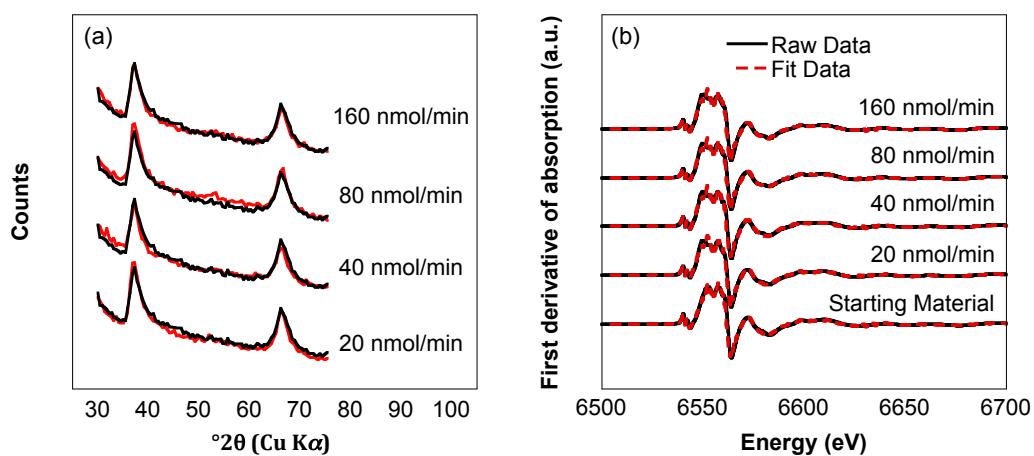
Figure 3.5. (a) XRD patterns of solids from each reactor in red overlaid by the starting material in black and (b) fitted XANES data of solids recovered from each reactor and the starting material. XANES data was analyzed using the Combo method.[48]
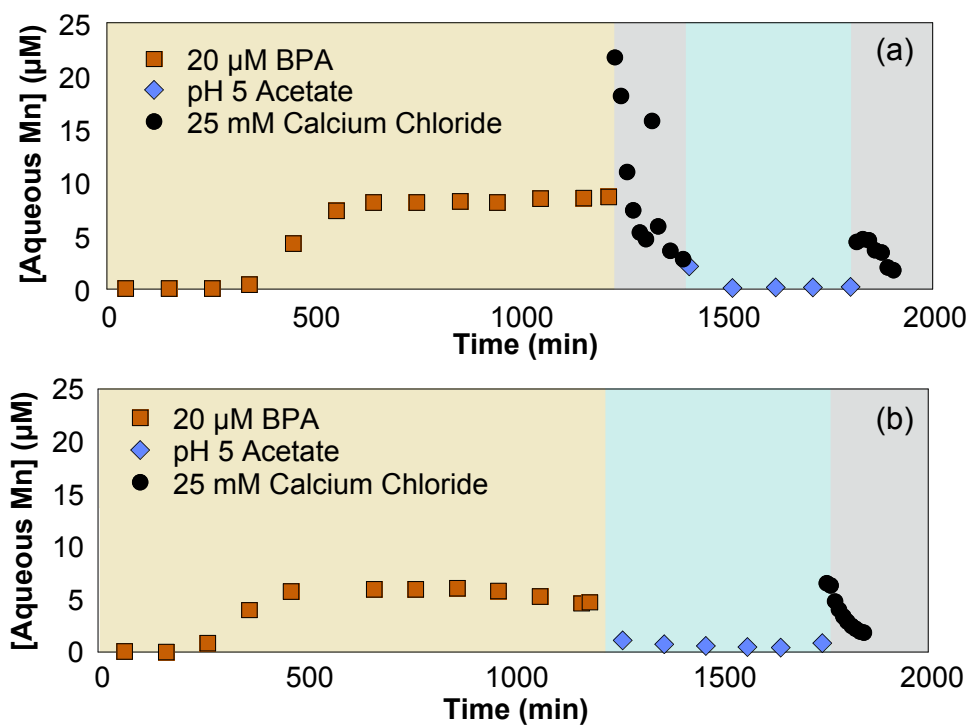
Figure 3.6. Stirred flow reactors with 1.58 g/L δ-MnO$_2$ exposed to (a) 20 µM BPA from 0-1215 min, 25 mM Ca^{2+} from 1215-1395 min, 10 mM acetate at pH 5 from 1395-1800 min, and 25 mM Ca^{2+} from 1800-1905 min (Reactor A), and (b) 20 µM BPA from 0-1185 min, 10 mM acetate at pH 5 from 1185-1745 min, and 25 mM Ca^{2+} from 1745-1845 min (Reactor B).

3.8 References

(1) Remucal, C. K.; Ginder-Vogel, M. A critical review of the reactivity of manganese oxides with organic contaminants. *Environ. Sci. Process. Impacts* **2014**, *16* (6), 1247–1266.

(2) Stone, A. T. Reductive dissolution of manganese(III/IV) oxides by substituted phenols. *Environ. Sci. Technol.* **1987**, *21* (10), 979–988.

(3) Stone, A. T.; Morgan, J. J. Reduction and dissolution of manganese(III) and manganese(IV) oxides by organics: 2. Survey of the reactivity of organics. *Environ. Sci. Technol.* **1984**, *18* (8), 617–624.

(4) Xyla, A. G.; Sulzberger, B.; Luther III, G. W.; Hering, J. G.; Van Cappellen, P.; Stumm, W. Reductive dissolution of manganese(III,IV) (hydr)oxides by oxalate: The effect of pH and light. *Langmuir* **1992**, *8* (1), 95–103.

(5) Ulrich, H. J.; Stone, A. T. The oxidation of chlorophenols adsorbed to manganese oxide surfaces. *Environ. Sci. Technol.* **1989**, *23* (4), 421–428.

(6) Nico, P. S.; Zasoski, R. J. Mn(III) center availability as a rate controlling factor in the oxidation of phenol and sulfide on δ-MnO$_2$. *Environ. Sci. Technol.* **2001**, *35* (16), 3338–3343.

(7) Ukrainczyk, L.; McBride, M. B. Oxidation and dechlorination of chlorophenols in dilute aqueous suspensions of manganese oxides: Reaction products. *Environ. Toxicol. Chem.* **1993**, *12* (11), 2015–2022.

(8) Bertino, D. J.; Zepp, R. G. Effects of solar radiation on manganese oxide reactions with selected organic compounds. *Environ. Sci. Technol.* **1991**, *25* (7), 1267–1273.

(9) Zhao, L.; Yu, Z.; Peng, P.; Huang, W.; Dong, Y. Oxidative transformation of tetrachlorophenols and trichlorophenols by manganese dioxide. *Env. Toxicol Chem* **2009**, *28* (6), 1120–1129.

(10) Ukrainczyk, L.; McBride, M. B. Oxidation of phenol in acidic aqueous suspensions of manganese oxides. *Clays Clay Min.* **1992**, *40* (2), 157–166.

(11) Zhang, H.; Huang, C.-H. Oxidative transformation of triclosan and chlorophene by manganese oxides. *Environ. Sci. Technol.* **2003**, *37* (11), 2421–2430.

(12) Lin, K.; Liu, W.; Gan, J. Oxidative removal of bisphenol A by manganese dioxide: Efficacy, products, and pathways. *Environ. Sci. Technol.* **2009**, *43* (10), 3860–3864.

(13) Lu, Z.; Lin, K.; Gan, J. Oxidation of bisphenol F (BPF) by manganese dioxide. *Environ. Pollut.* **2011**, *159* (10), 2546–2551.

(14) Xu, L.; Xu, C.; Zhao, M.; Qiu, Y.; Sheng, G. Oxidative removal of aqueous steroid estrogens by manganese oxides. *Water Res.* **2008**, *42* (20), 5038–5044.

(15) Xiao, H.; Song, H.; Xie, H.; Huang, W.; Tan, J.; Wu, J. Transformation of acetaminophen using manganese dioxide − mediated oxidative processes: Reaction rates and pathways. *J. Hazard. Mater.* **2013**, *250–251*, 138–146.

(16) Lin, K.; Liu, W.; Gan, J. Reaction of tetrabromobisphenol A (TBBPA) with manganese dioxide: Kinetics, products, and pathways. *Environ. Sci. Technol.* **2009**, *43* (12), 4480–4486.

(17) Lu, Z.; Gan, J. Oxidation of nonylphenol and octylphenol by manganese dioxide: Kinetics and pathways. *Environ. Pollut.* **2013**, *180*, 214–220.

(18) Balgooyen, S.; Alaimo, P. J.; Remucal, C. K.; Ginder-Vogel, M. Structural transformation of MnO$_2$ during the oxidation of bisphenol A. *Environ. Sci. Technol.* **2017**, *51* (11), 6053–6062.

(19) Shaikh, N.; Taujale, S.; Zhang, H.; Artyushkova, K.; Ali, A.-M. S.; Cerrato, J. M. Spectroscopic investigation of interfacial interaction of manganese oxide with triclosan, aniline, and phenol. *Environ. Sci. Technol.* **2016**, *50* (20), 10978–10987.

(20) Bisphenol A (BPA) Information & Resources http://www.bisphenol-a.org/ (accessed Sep 6, 2016).

(21) Yu, X.; Xue, J.; Yao, H.; Wu, Q.; Venkatesan, A. K.; Halden, R. U.; Kannan, K. Occurrence and estrogenic potency of eight bisphenol analogs in sewage sludge from the U.S. EPA targeted national sewage sludge survey. *J. Hazard. Mater.* **2015**, *299*, 733–739.

(22) Masoner, J. R.; Kolpin, D. W.; Furlong, E. T.; Cozzarelli, I. M.; Gray, J. L.; Schwab, E. A. Contaminants of emerging concern in fresh leachate from landfills in the conterminous United States. *Env. Sci Process. Impacts* **2014**, *16* (10), 2335–2354.

(23) Baldwin, A. K.; Corsi, S. R.; De Cicco, L. A.; Lenaker, P. L.; Lutz, M. A.; Sullivan, D. J.; Richards, K. D. Organic contaminants in Great Lakes tributaries: Prevalence and potential aquatic toxicity. *Sci. Total Environ.* **2016**, *554–555*, 42–52.

(24) Belfroid, A.; van Velzen, M.; van der Horst, B.; Vethaak, D. Occurrence of bisphenol A in surface water and uptake in fish: Evaluation of field measurements. *Chemosphere* **2002**, *49* (1), 97–103.

(25) Canesi, L.; Fabbri, E. Environmental effects of BPA: Focus on aquatic species. *Dose-Response* **2015**, *13* (3), 1–14.

(26) Gao, N.; Hong, J.; Yu, Z.; Peng, P.; Huang, W. Transformation of bisphenol A in the presence of manganese dioxide. *Soil Sci.* **2011**, *176* (6), 265–272.

(27) Lin, K.; Peng, Y.; Huang, X.; Ding, J. Transformation of bisphenol A by manganese oxide-coated sand. *Environ. Sci. Pollut. Res.* **2013**, *20* (3), 1461–1467.

(28) Laha, S.; Luthy, R. G. Oxidation of aniline and other primary aromatic amines by manganese dioxide. *Environ. Sci. Technol.* **1990**, *24* (3), 363–373.

(29) Jiang, J.; Gao, Y.; Pang, S.-Y.; Lu, X.-T.; Zhou, Y.; Ma, J.; Wang, Q. Understanding the role of manganese dioxide in the oxidation of phenolic compounds by aqueous permanganate. *Environ. Sci. Technol.* **2015**, *49* (1), 520–528.

(30) Im, J.; Prevatte, C. W.; Campagna, S. R.; Löffler, F. E. Identification of 4-hydroxycumyl alcohol as the major MnO_2-mediated bisphenol A transformation product and evaluation of its environmental fate. *Environ. Sci. Technol.* **2015**, *49* (10), 6214–6221.

(31) Rubert, Kennedy F.; Pedersen, J. A. Kinetics of oxytetracycline reaction with a hydrous manganese oxide. *Environ. Sci. Technol.* **2006**, *40* (23), 7216–7221.

(32) Klausen, J.; Haderlein, S. B.; Schwarzenbach, R. P. Oxidation of substituted anilines by aqueous MnO_2: Effect of co-solutes on initial and quasi-steady-state kinetics. *Environ. Sci. Technol.* **1997**, *31* (9), 2642–2649.

(33) Wang, Q.; Yang, P.; Zhu, M. Structural transformation of birnessite by fulvic acid under anoxic conditions. *Environ. Sci. Technol.* **2018**, *52* (4), 1844–1853.

(34) Zhang, T.; Zhang, X.; Yan, X.; Ng, J.; Wang, Y.; Sun, D. D. Removal of bisphenol A via a hybrid process combining oxidation on β-MnO_2 nanowires with microfiltration. *Colloids Surf. Physicochem. Eng. Asp.* **2011**, *392* (1), 198–204.

(35) Lafferty, B. J.; Ginder-Vogel, M.; Sparks, D. L. Arsenite oxidation by a poorly crystalline manganese-oxide 1. Stirred-flow experiments. *Environ. Sci. Technol.* **2010**, *44* (22), 8460–8466.

(36) Charbonnet, J. A.; Duan, Y.; van Genuchten, C. M.; Sedlak, D. L. Chemical regeneration of manganese oxide-coated sand for oxidation of organic stormwater contaminants. *Environ. Sci. Technol.* **2018**, *52* (18), 10728–10736.

(37) Guha, H.; Saiers, J. E.; Brooks, S.; Jardine, P.; Jayachandran, K. Chromium transport, oxidation, and adsorption in manganese-coated sand. *J. Contam. Hydrol.* **2001**, *49* (3–4), 311–334.

(38) Tong, F.; Gu, X.; Gu, C.; Xie, J.; Xie, X.; Jiang, B.; Wang, Y.; Ertunc, T.; Schäffer, A.; Ji, R. Stimulation of tetrabromobisphenol A binding to soil humic substances by birnessite and the chemical structure of the bound residues. *Environ. Sci. Technol.* **2016**, *50* (12), 6257–6266.

(39) Kang, K.-H.; Dec, J.; Park, H.; Bollag, J.-M. Effect of phenolic mediators and humic acid on cyprodinil transformation in presence of birnessite. *Water Res.* **2004**, *38* (11), 2737–2745.

(40) Li, C.; Zhang, B.; Ertunc, T.; Schaeffer, A.; Ji, R. Birnessite-induced binding of phenolic monomers to soil humic substances and nature of the bound residues. *Environ. Sci. Technol.* **2012**, *46* (16), 8843–8850.

(41) Grebel, J. E.; Charbonnet, J. A.; Sedlak, D. L. Oxidation of organic contaminants by manganese oxide geomedia for passive urban stormwater treatment systems. *Water Res.* **2016**, *88*, 481–491.

(42) Murray, J. W. The surface chemistry of hydrous manganese dioxide. *J. Colloid Interface Sci.* **1974**, *46* (3), 357–371.

(43) McConville, M. B.; Hubert, T. D.; Remucal, C. K. Direct photolysis rates and transformation pathways of the lampricides TFM and niclosamide in simulated sunlight. *Environ. Sci. Technol.* **2016**, *50* (18), 9998–10006.

(44) Ferreira, C. M. H.; Pinto, I. S. S.; Soares, E. V.; Soares, H. M. V. M. (Un)suitability of the use of pH buffers in biological, biochemical and environmental studies and their interaction with metal ions – A review. *RSC Adv.* **2015**, *5* (39), 30989–31003.

(45) Pan, Y.; Koopmans, G. F.; Bonten, L. T. C.; Song, J.; Luo, Y.; Temminghoff, E. J. M.; Comans, R. N. J. Influence of pH on the redox chemistry of metal (hydr)oxides and organic matter in paddy soils. *J. Soils Sediments* **2014**, *14* (10), 1713–1726.

(46) Ouvrard, S.; Simonnot, M.-O.; Sardin, M. Reactive behavior of natural manganese oxides toward the adsorption of phosphate and arsenate. *Ind. Eng. Chem. Res.* **2002**, *41* (11), 2785–2791.

(47) Kobe, K. A.; Toribara, T. Y. Precipitation of manganous carbonate. *Ind. Eng. Chem.* **1939**, *31* (10), 1272–1274.

(48) Manceau, A.; Marcus, M. A.; Grangeon, S. Determination of Mn valence states in mixed-valent manganates by XANES spectroscopy. *Am. Mineral.* **2012**, *97* (5–6), 816–827.

(49) Lee, Y.; Yoon, J.; von Gunten, U. Kinetics of the oxidation of phenols and phenolic endocrine disruptors during water treatment with ferrate (Fe(VI)). *Environ. Sci. Technol.* **2005**, *39* (22), 8978–8984.

(50) Stone, A. T.; Morgan, J. J. Reduction and dissolution of manganese(III) and manganese(IV) oxides by organics. 1. Reaction with hydroquinone. *Environ. Sci. Technol.* **1984**, *18* (6), 450–456.

(51) Lafferty, B. J.; Ginder-Vogel, M.; Sparks, D. L. Arsenite oxidation by a poorly-crystalline manganese oxide. 3. Arsenic and manganese desorption. *Environ. Sci. Technol.* **2011**, *45* (21), 9218–9223.

(52) Colombani, D. Chain-growth control in free radical polymerization. *Prog Polym Sci* **1997**, *22*, 1649–1720.

(53) Elzinga, E. J.; Kustka, A. B. A Mn-54 radiotracer study of Mn isotope solid–liquid exchange during reductive transformation of vernadite (δ-MnO_2) by aqueous Mn(II). *Environ. Sci. Technol.* **2015**, *49* (7), 4310–4316.

(54) Santelli, C. M.; Webb, S. M.; Dohnalkova, A. C.; Hansel, C. M. Diversity of Mn oxides produced by Mn(II)-oxidizing fungi. *Geochim. Cosmochim. Acta* **2011**, *75* (10), 2762–2776.

(55) Bargar, J. R.; Tebo, B. M.; Bergmann, U.; Webb, S. M.; Glatzel, P.; Chiu, V. Q.; Villalobos, M. Biotic and abiotic products of Mn(II) oxidation by spores of the marine *Bacillus* sp. strain SG-1. *Am. Mineral.* **2005**, *90* (1), 143–154.

(56) Feng, X. H.; Zhu, M.; Ginder-Vogel, M.; Ni, C.; Parikh, S. J.; Sparks, D. L. Formation of nano-crystalline todorokite from biogenic Mn oxides. *Geochim. Cosmochim. Acta* **2010**, *74* (11), 3232–3245.

(57) Zhu, M.; Ginder-Vogel, M.; Parikh, S. J.; Feng, X.-H.; Sparks, D. L. Cation effects on the layer structure of biogenic Mn-oxides. *Environ. Sci. Technol.* **2010**, *44* (12), 4465–4471.

(58) Zhang, H.; Chen, W.-R.; Huang, C.-H. Kinetic modeling of oxidation of antibacterial agents by manganese oxide. *Environ. Sci. Technol.* **2008**, *42* (15), 5548–5554.

Chapter 4

The effects of interlayer cations on the oxidation of phenolic contaminants by acid birnessite

4.1 Abstract

Many phenolic contaminants found in natural waters are susceptible to oxidation by manganese oxides. The variability between oxidation rates reported in laboratory studies and those from environmental reactions is investigated in this study through the introduction of metal cations. Cation cosolutes inhibited the reaction rate of four target phenols: bisphenol A, estrone, *p*-cresol, and triclosan. Reaction rates for all phenols followed the same trend, $Na^+ > K^+ > Mg^{2+} > Ca^{2+}$, which is consistent with previous studies. However, this study shows that the same trend applies to these cations when they act as interlayer cations, as well as cation cosolutes. Sorption analysis shows a difference in sorptive capacity among different cations both when they are sorbed and in the interlayer. Solid phase analysis shows that there are no notable changes to the manganese oxide mineral with variation in interlayer cation. These findings indicate that the inhibition driven by metal cosolutes is not due to competition for surface sites, as previously suggested. However, the inhibition seen in both interlayer and sorbed cations suggests that the electron transfer rate may be altered due to the variation in overall oxidation state of the mineral. This study has implications for engineered water treatment systems using manganese oxides as a reactive substrate.

4.2 Introduction

Manganese oxides are naturally occurring oxidants that drive redox reactions in a variety of environments. These minerals are found in soils and sediments, on ocean floors, in desert varnishes, and in marine and freshwater bodies.[1–5] As one of the strongest environmental oxidants, they are able to oxidize organic[6–9] and inorganic[10–13] compounds, including contaminants and other harmful species. Here we look at the oxidation of phenolic compounds by acid birnessite, a reactive phyllomanganate similar to environmental manganese oxides.[14–16]

The phenolic compounds used in this study include bisphenol A (BPA), 5-chloro-2-(2,4-dichlorophenoxy)phenol (triclosan), estrone (E1), and 4-methylphenol (*p*-cresol). Phenolic compounds such as these are found in wastewater effluents that drain into natural ecosystems.[17–26] The four target contaminants are considered harmful to the environment in various ways. They were chosen to provide a range of structures and sizes to test the oxidation mechanism by acid birnessite.[27]

Previous studies demonstrate that cations inhibit the reaction rate of phenols with manganese oxides.[6,28–36] This has been largely attributed to the cation blocking reactive sites on the oxide surface. Other suggested possibilities include aggregation stimulated by metal sorption[28,37] and competitive reaction with manganese oxide.[38] Lu et al.[28] demonstrate that oxidation rates of bisphenol F by manganese dioxide are inhibited by the addition of $CaCl_2$, $MgCl_2$, and $NaCl$ as cosolutes; pseudo-first-order rate constants are decreased by up to 85% with inhibitory effects following the trend $Ca^{2+} > Mg^{2+} > Na^+$. Lin et al.[35] show that BPA oxidation by manganese coated sand is suppressed by the same cations following the same trend. This trend is inversely related to the sorption capacity of the cation cosolutes,[39] which is likely why these effects are often attributed to cation cosolutes sorbing to and therefore blocking reactive sites.

In contrast, studies focusing on the manganese oxide mineral structure demonstrate several reasons why cation cosolutes may not affect phenol oxidation by blocking reactive sites. Several studies have investigated the localized point of zero charge (PZC) in manganese oxides, showing that the PZC is not consistent across all surface sites. In general, the PZC of birnessites is about 3. However, at the edges sites of this phyllomanganate, the PZC ranges 6-8, yielding a relatively neutral charge at pH 7, whereas above vacancy sites, which are absences of Mn atoms to retain structure, the PZC is 2-3, yielding a negative charge at pH 7.[40–42] This difference in surface charge suggests that positively charged cations and neutral phenols (or negatively charged phenolate ions) would likely sorb to different surface sites.

Furthermore, cations can change the structure of manganese oxides not only by sorbing to the surface as cosolutes, but also acting as interlayer cations. Phyllomanganate layers are negatively charged, drawing hydrated cations into the interlayer space to neutralize the overall charge. A study by Zhang et al.[43] shows that when various cations are added during MnO_2 synthesis, the resulting interlayer cations lead to slightly varying structures. First, the analysis of extended X-ray absorption fine structure spectroscopy shows that distance between corner-sharing manganese atoms increases with increasing cation radius. Second, X-ray diffraction (XRD) shows that Mg cations in the oxide interlayer leads to the formation of buserite within the sample, which is a tunnel structured manganese oxide. These findings indicate that small changes initiated by the cations present in the interlayer may contribute to the change in reactivity of birnessite in the presence of cosolutes.

This study investigates the effects of cations on the reactivity of birnessite towards phenols by investigating changes in both phenol oxidation rate and manganese oxide characteristics. Birnessites are exchanged with interlayer cations (Na^+, K^+, Mg^{2+}, and Ca^{2+}) and

analyzed for changes in solid characteristics. They are then reacted with BPA with and without corresponding cation cosolutes. This study aims to clarify the effects of sorbed cation cosolutes on reactivity and to determine if interlayer cations alone can affect the reactivity of birnessites. A thorough understanding of how cations affect this reaction is important to its environmental significance, as current laboratory studies do not represent the same matrices and conditions that are found in the environment.

4.3 Materials and Methods

4.3.1 Materials

Commercially available chemicals were used as received. Ultrapure water was supplied by a Milli-Q water purification system maintained at 18.2 MΩ·cm. Further details on the materials used are provided in Appendix C (Section **C1**).

4.3.2 Preparation and Characterization of Acid Birnessite

The mineral used in this study was prepared using the method described by McKenzie.[44] Briefly, 6 M HCl was added dropwise to a solution of boiling $KMnO_4$, which was allowed to boil for another 60 minutes. After the solution cooled, it was brought to 60°C and stirred for 20 hours. The resulting slurry was centrifuged and washed six times in Milli-Q water. The solids were then dried at room temperature. The starting material was characterized by X-ray diffraction (XRD; Rigaku Rapid II, Mo Kα source; λ = 0.7093 Å), X-ray absorption near edge structure (XANES) spectroscopy, and Brunauer-Emmett-Teller (BET) surface area measurements (Quantachrome Autosorb-1, Nitrogen Adsorbate). XRD showed that birnessite was the only crystalline phase formed (Figure **C1**). BET measurements revealed a specific

surface area of 38 m^2/g. XANES data showed that the valence state of the starting material is 3.49 valence units (v.u.), with percentages of Mn(IV), Mn(III), and Mn(II) at 59%, 32%, and 9%, respectively.

4.3.3 Interlayer Cation Pre-Exchange

The acid birnessite starting material was pre-exchanged with each of four cations: potassium (K), magnesium (Mg), sodium (Na), and calcium (Ca) to act as the interlayer cation. Solutions of 25 mM K$^+$, Mg^{2+}, Na$^+$, and Ca^{2+} were prepared and used to pre-exchange the starting material with each of the cations. Approximately 2 g of the starting material was added to 400 mL of each solution and stirred for 12 hours. The slurry was then centrifuged and the supernatant was decanted. The remaining slurry was re-suspended in another 150 mL of the 25 mM cation solution, the pH of the slurry was adjusted to pH 5 (i.e., the pH used in experimental reactions) by titrating with 1 M HCl, and the mixture was stirred for 1 hour. Adjusting the pH ensures that the surface charge of the birnessite will not change when the material is added to pH 5 buffer which could release excess cations into solution. The resulting slurry was then washed five times (centrifuged, decanted, and filled with fresh Milli-Q) to ensure all aqueous cations were removed. The concentrations of Mn, K, Mg, Na, and Ca in the solid were determined by inductively coupled plasma-optical emission spectroscopy (ICP-OES; Section **C2**) after digestion in 6 M HCl. Each of the pre-exchanged solids was characterized using XRD, XANES, and BET as described for the starting material.

4.3.4 Solution Preparation

Reactions between birnessite and organic contaminants were performed in a pH 5 solution buffered with either 10 mM sodium or potassium acetate. Acetate was selected as a buffer because it does not form complexes with Mn(II) or Mn(III)[45,46] and does not sorb to the manganese oxide surface.[47] We previously demonstrated that acetate does not impact MnO_2 reactivity with BPA over time.[48] Reactions observing interlayer cations only used a solution of acetate adjusted to pH 5 with no additional solutes. In reactions observing cation cosolutes in addition to interlayer cations, 10 mM of the cation of interest was added to the reaction media in the form of the chloride salt. In all cases, potassium acetate was used for potassium-exchanged solids, whereas sodium acetate was used to buffer all other solids. From preliminary experiments, the sodium salt present in sodium acetate proved to exchange with interlayer potassium during experimental reactions, whereas all other cations were not substituted by the sodium salt within the timescale of the reactions (20 – 40 min; Table **4.1**). BPA (80 mM), triclosan, estrone, and *p*-cresol (8 mM) stock solutions were prepared in methanol and stored at 4ºC.

4.3.5 Kinetic Reactions with Organic Contaminants

The reactivity of each of the prepared solids was quantified by calculating pseudo-first-order rate constants for the oxidation of four organic contaminants. BPA, estrone, triclosan, and *p*-cresol were reacted with each of the four solids. Reactions took place in 50 mL of the buffered media. An aliquot of the solid slurry was added to the reactor five minutes before the reaction began. At the start of the reaction, the organic contaminant was added such that <0.25% of the solution contained methanol. For BPA, the concentrations used were 0.25 g/L birnessite and 80

µM BPA; data was collected for 15 minutes of the reaction. For triclosan, estrone, and *p*-cresol, the concentrations were 0.1 g/L birnessite and 20 µM of the organic; data was collected for 40 minutes of reaction. The lower concentrations used for these phenols was due to their lower solubility.[49] Higher concentrations were used for BPA to quantify sorption to the birnessite surface. Two reaction slurry aliquots (1 mL each) were taken at pre-determined time points to quantify the concentration of the organic contaminant. One aliquot from each time point was quenched with excess ascorbic acid (40 µL of a 280 mM stock in Milli-Q stored at 4ºC) to reduce all Mn(III/IV) solids to dissolved Mn(II), while the other aliquot was filtered through a 0.2 µm polytetrafluoroethylene filter.

The samples were analyzed by high performance liquid chromatography (HPLC; Section **C2**). Each combination of the pre-exchanged solid and contaminant was conducted in triplicate. Loss rates were determined by fitting the data by assuming pseudo-first-order kinetics (Section **C3**). Error was calculated using the standard deviation of the three replicates. The pH remained constant over the reaction with a standard deviation of 0.7 pH units.

Organic sorption was determined by comparing concentrations in quenched and filtered aliquots.[48,50] Quenched samples contained total concentrations of the organic (aqueous and sorbed), whereas filtered samples contained only aqueous species. Sorbed concentration was calculated by [organic]$_{total}$ − [organic]$_{aqueous}$.

4.4 Results and Discussion

4.4.1 Impact of Cation Cosolutes on Phenol Oxidation

When each of the four phenols is added to birnessite with any of the four cation cosolutes, the phenol concentration rapidly decreases via oxidation following pseudo-first-order

kinetics. The reaction rates presented here are from samples that have been quenched in ascorbic acid, which allows us to report the reaction rate of transformation only rather than transformation and sorption combined. The pseudo-first-order rate constants for the phenols vary, ranging from $0.007 – 0.203$ min^{-1} and follow the order *p*-cresol > BPA > estrone > triclosan. The reactivity of phenols is based on a number of variables, including the type and location of functional groups, oxidative potential, and sorption capacity.[27] For example, parameters such as Hammett constants, acid dissociation constants (pK_a), energy of the highest occupied molecular orbital (E_{HOMO}), and energy required to oxidize a single electron (E_{OX}) have been used to predict reactivity of simple substituted phenols as they affect how easily a compound is oxidized.[51,52] BPA, triclosan, estrone, and *p*-cresol all react by electron transfer limited mechanism with δ-MnO_2,[27] which means sorption happens faster than electron transfer. This suggests that some amount of sorbed organic can be expected on the manganese oxide surface.

Reaction rates of all phenols are dependent on the cation cosolute added to the reactor (Figure **4.1**). For example, BPA has a reaction rate constant of 0.203 min^{-1} when Na^+ is added to solution and 0.0187 min^{-1} when Ca^{2+} is added to solution. For all phenols, the reaction rate constants follow the same trend of $Na^+ > K^+ > Mg^{2+} > Ca^{2+}$.

Previous studies observe differences in phenol oxidation rates by manganese oxide when cations are added into the reactor as cosolutes. These studies report the same trends in oxidation rate constants as seen here in which divalent cations lead to the largest suppression in the observed oxidation rate of the target phenol.[6,28–32,34–36] The effect of cation cosolutes is environmentally relevant because it simulates the reaction conditions found in natural waters. Some studies also report effects of Mn^{2+}, Fe^{3+}, Zn^{2+}, and Cr^{3+} as cosolutes, which tend to have an even greater suppression of phenol oxidation by manganese oxides. These metals were not

included in this study as their interaction with manganese oxide will be more complex due to their redox activity.

For cations that are not redox active, the variation in reaction rates of phenols is often attributed to the competitive sorption of the cation cosolute. Cations with strong sorption capacity will sorb more readily to the manganese oxide surface, occupying surface sites.[39] These studies suggest that the higher sorption of cations leads to fewer reactive sites on which the organic can sorb. However, several studies report competitive sorption may not be occurring due to the variation between the PZC at edge sites and the PZC at vacancy sites.[40–42] The variation in PZC across the Mn oxide suggests that the positively charged cations will sorb to the edge sites, while the neutral or negatively charged phenol will sorb at the vacancy sites at neutral pH. Additionally, a kinetic model of the reaction predicts that surface sites are only minimally reduced by the presence of cosolutes.[29] To test whether or not the difference in phenol oxidation is due to competitive sorption, the reactivity of birnessite with pre-exchanged interlayer cations in the absence of cosolutes are evaluated and used to compare rate constants to those found in cosolute experiments (Figure **4.1**). Minimal information has been published on the effects of interlayer cations on transformation of organics.

4.4.2 Characterization of Birnessite Interlayer Cation Stability

To determine the effects of interlayer cations, each of the four cations is pre-exchanged into the birnessite interlayer. To distinguish effects that are due to cation cosolutes rather than interlayer cations, it is necessary for the interlayer cations to remain in the interlayer to keep the mineral structure constant and avoid any effects of aqueous cations. Control experiments are conducted to ensure that the interlayer cations are not released into solution during the reaction.

Each birnessite is equilibrated in four different solutions for 20 minutes and aqueous cation concentrations are collected. The four solutions used to test cation stability are Milli-Q water, Milli-Q water adjusted to pH 5 by titration with HCl (i.e., the pH used in reactors), 10 mM pH 5 sodium acetate, and 10 mM pH 5 sodium acetate and 80 μM BPA (Table **4.1**). During the Milli-Q equilibration 0 – 2 ppm of each cation is released. During the pH 5 Milli-Q equilibration, 0.3 – 3.3 ppm of each cation is released. During both the sodium acetate equilibration and the sodium acetate equilibration with BPA added, 1 – 4 ppm of Ca^{2+} and Mg^{2+} is released. A large amount of K^+ is released during these equilibrations (23 – 25 ppm). The release of sodium cannot be determined during these last two equilibrations due to the large addition of Na^+ in the sodium acetate.

The large release of K^+ in sodium acetate-buffered solution indicates that Na^+ is able to replace K^+ as an interlayer cation for birnessite. Na^+ and K^+ provide the same charge offset to the manganese oxide layer, have similar hydrated radii (K^+ 3.31 Å and Na^+ 3.58 Å, compared to Mg^{2+} 4.28 Å and Ca^{2+} 4.12 Å), and have been shown to quickly exchange for each other using real-time XRD.[53] Drits et al.[54] described how large mono- or di-valent cations occupy different space in the interlayer than small di- or tri-valent cations. The ionic radii of Ca^{2+} and Mg^{2+} (114 pm and 86 pm, respectively) are small due to the strong pull of the nuclei; these ions would be octahedrally coordinated by layer oxygen atoms, while larger cations, such as K^+ and Na^+ (152 pm and 116 pm, respectively), are located in interlayer prisms. Transformation from one of these polytypes to another requires layer translation, which might explain why Na^+ was able to exchange with K^+ so quickly (i.e., within 20 minutes), but not with Ca^{2+} or Mg^{2+}. All reactions with K^+-interlayer birnessite in this study use pH 5 potassium acetate as a buffer in order to avoid any interlayer exchange with sodium acetate.

4.4.3 Mineralogical Effects of Interlayer Cations

Solid characterization shows that the four pre-exchanged birnessites have the same specific surface area according to BET measurements (31.4 ± 2.5 m^2/g; Table **4.2**). They also have the same bulk AMON according to XANES analysis (3.36 ± 0.9 v.u.; Table **4.3**). The cation content of each of the solids is shown in Table **4.4**. Each solid contains >2% of the desired cation by weight. Along with the desired cation, potassium is present in all of the samples, likely because it was the only cation used in the synthesis. Each of the dried samples yield the same XRD pattern showing peaks for crystalline acid birnessite (Figure **C1**).

4.4.4 Impact of Interlayer Cations on Phenol Oxidation

When the phenols are added to birnessite with varied interlayer cations, the reaction rate constant changes depending on the interlayer cation species. The variation in reaction rate follows the same trend as the cation cosolutes (Figure **4.1**). For example, BPA has a reaction rate constant of 0.094 min^{-1} when reacted with Ca^{2+}-interlayer birnessite and 0.267 min^{-1} when reacted with Na^+-interlayer birnessite. With all phenols, the reaction rate follows the same trend where Na-interlayer birnessite rate constant is the highest and Ca^{2+}-interlayer rate constant is the lowest. Overall, interlayer cations lead to the following trend in rate constants: $Na^+ > K^+ > Mg^{2+} > Ca^{2+}$.

The presence of cations can affect the solid structure of manganese oxides in a number of ways. Certain interlayer cations can promote transformation from birnessite to other oxide phases.[55–57] Additionally, cations present during oxide synthesis can influence micropmorpholoy, crystal structure, and transformation.[43] For example, Ca^{2+} and Na^+ enhance distribution of

Mn(III) within layers, while H^+ and Ni(II) promote formation of vacancy sites.[58] During interlayer exchange reactions, manganese oxide unit cell parameters are reported to undergo changes.[53] Multiple studies show that divalent intercalating cations led to lower anodic O_2 evolution, which was attributed to the stabilization of Mn(III) within the layer compared to monovalent cations.[59,60] Liu et al.[37] demonstrate that Ca^{2+} ions increase the zeta potential of MnO_2 and facilitate aggregation. However, Ca^{2+} also enhances sorption of both arsenic and humic acid due to bridging effects.[37]

The effect of these structural changes due to the presence of cations on reactivity toward organic contaminants is not clear. One study has previously investigated the reactivity of manganese oxides with different interlayer cations and found that oxidation of formaldehyde is cation-dependent, with K^+-interlayer manganese oxide being more reactive than oxides with Ca^{2+}, Mg^{2+}, or Fe^{3+} in the interlayer.[61] Aside from this study, there is no further information on the effects of interlayer cations on manganese oxide reactivity toward organic compounds. Thus, the purpose of the interlayer cation experiments in this study is to evaluate how these cations affect the reactivity with phenolic compounds and determine if the inhibition seen in previous cosolute studies is due to competition for reactive sites or due to the structural changes in the manganese oxides discussed above.

4.4.5 Comparison of Interlayer Cations and Cation Cosolutes

In this study, both the interlayer experiments and the cosolute experiments use the same solids that have been pre-exchanged with interlayer cations. Therefore, the cosolute experiments show effects of both interlayer cations and cosolute sorption. Previous studies have not compared interlayer to cosolute cations and did not use pre-exchanged solids in cosolute research. The

comparison of results from these two experiments shows that the reaction rate for each cation and phenol pair is slower than the corresponding reaction without the cation cosolute in most cases. This indicates that sorbed cations do have some effect on the reactivity of the solid toward phenolic contaminants, contrary to the PZC theory. However, the trend among cations remains the same in both the interlayer and cosolutes reactions, indicating that the same effect is likely cause the trend in both cases. As previous studies indicate,[28–30,32–36] the reactivity of birnessite with cation cosolutes both in previous studies and in this study follows the trend in cation sorption capacity ($Ca^{2+} > Mg^{2+} > Na^+ \approx K^+$).[39]

When cosolute rate constants are plotted as a function of interlayer rate constants, a relationship that is close to linear results for all four phenols (Figure **4.2**). The R-values for BPA, triclosan, estrone, and *p*-cresol are 0.99, 0.89, 0.85, and 0.92 respectively. The presence of this relationship further indicates that the cation cosolutes are affecting the reactivity by the same mechanism as interlayer cations. In this case, that would mean that the mechanism for decreased reactivity is not driven by cations blocking reactive sites. It also would mean that the transformation to buserite due to certain interlayer cations is not likely involved. One alternative is that the cations either in the interlayer or sorbed to the surface are altering the overall oxidation state and therefore slow the rate of electron transfer.

In order to test the competitive sorption theory, we examine the sorption of BPA to the manganese oxide surface during reactions with each pre-exchanged birnessite (Figure **4.3**). BPA sorption collected at three time points in triplicate reactors show that the average sorption of BPA to the birnessite surface was <10% for all solids. Looking at the interlayer only sorption, there is a trend that inversely follows the reaction rate constants (Figure **4.4a**). This indicates that the variation among interlayer cation rate constants correlates with changes in BPA sorption to

the birnessite surface. The cosolute data follows the same trend, but not to the same amplitude (Figure **4.4b**). When comparing the interlayer data to the cosolute data of each cation, there is no difference in BPA sorption. This indicates that the sorption of more cations in the cosolute experiments does not significantly affect the ability of BPA to sorb to the birnessite surface. As some previous studies suggest, sorbed cations can decrease the average oxidation state and therefore slow the rate of electron transfer. Since the cation cosolutes are not affecting the sorption rate of BPA, it is likely that is what is happening for birnessite. This would explain why the oxidation rate constants are inversely related to the sorption capacity of the cation cosolutes, but is not reflected in the BPA sorption.

4.5 Environmental Implications

The oxidation of organic contaminants by manganese oxides is an important reaction that influences contaminant fate in aqueous systems. Manganese oxides control the fate and partitioning of contaminants in natural systems.[2,6,17,62–66] Additionally, they have been proposed for passive water treatment for contaminants in urban stormwater runoff, green infrastructure, or water from contaminated sources.[7,8,17–20,23,50,67–71] Previous studies show that interlayer cations affect manganese oxide structure and behavior, yet the effect on reactivity towards organic contaminants has remained unknown. This information is important to determine if the reactivity demonstrated in laboratory studies is representative of the reactivity found in the environment or in engineered systems in which cations are often present.

Here we determine that the interlayer cation has a large effect on the manganese oxide reactivity. K^+-interlayer birnessites are much more reactive than Ca^{2+}-interlayer birnessites. However, the effect of cation cosolutes follows the same trend as interlayer cations. This, along

with sorption of organics throughout the reaction, demonstrates that cations do not compete for sorption sites with phenols. The change in reactivity is likely due to the cations lowering the oxidation state of the mineral both when they are sorbed to the surface and when they are in the interlayer. As this study and previous studies show, the interlayer cations cannot be controlled indefinitely. This study observes Na^+ exchanging with K^+ within 20 minutes. The implications of this study are that interlayer cations have a larger effect on reactivity than previous thought, and that the reaction rates reported in laboratory studies will not translate to environmental or engineered settings.

4.6 Acknowledgements

Figure 4.1. Pseudo-first-order loss rate constants for each pre-exchanged solid with (a) BPA, (b) triclosan, (c) estrone, and (d) *p*-cresol in triplicate reactors. For BPA, each reactor contained 80 μM of BPA and 0.25 g/L of the pre-exchanged birnessite. For triclosan, estrone, and *p*-cresol, each reactor contained 20 μM of the phenol and 0.1 g/L of the pre-exchanged birnessite. Cosolute reactors include 10 mM of the cation chloride salt. All reactions were conducted in a pH 5 acetate buffer. Error bars represent the standard deviation of the three reactors.
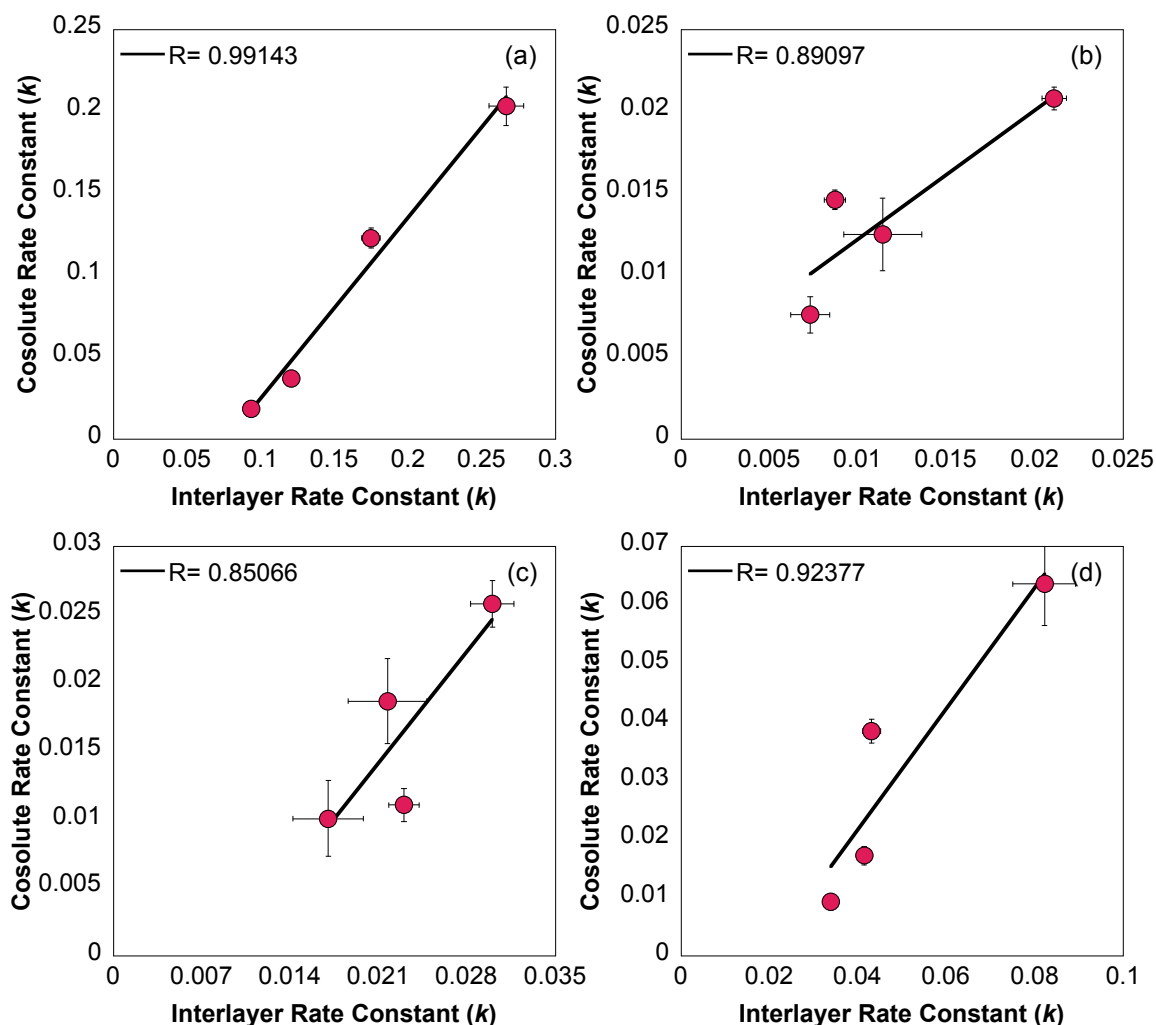
Figure 4.2. Pseudo-first-order rate constants determined in reactors with cation cosolutes compared to those with cations in the interlayer only. Relationships between the two types or reactions are shown for each pre-exchanged solid with (a) BPA, (b) triclosan, (c) estrone, and (d) *p*-cresol in triplicate reactors. For BPA, each reactor contained 80 μM of BPA and 0.25 g/L of the pre-exchanged birnessite. For triclosan, estrone, and *p*-cresol, each reactor contained 20 μM of the phenol and 0.1 g/L of the pre-exchanged birnessite. Cosolute reactors include 10 mM of the cation chloride salt. All reactions were conducted in a pH 5 acetate buffer. Error bars represent the standard deviation of the three reactors.
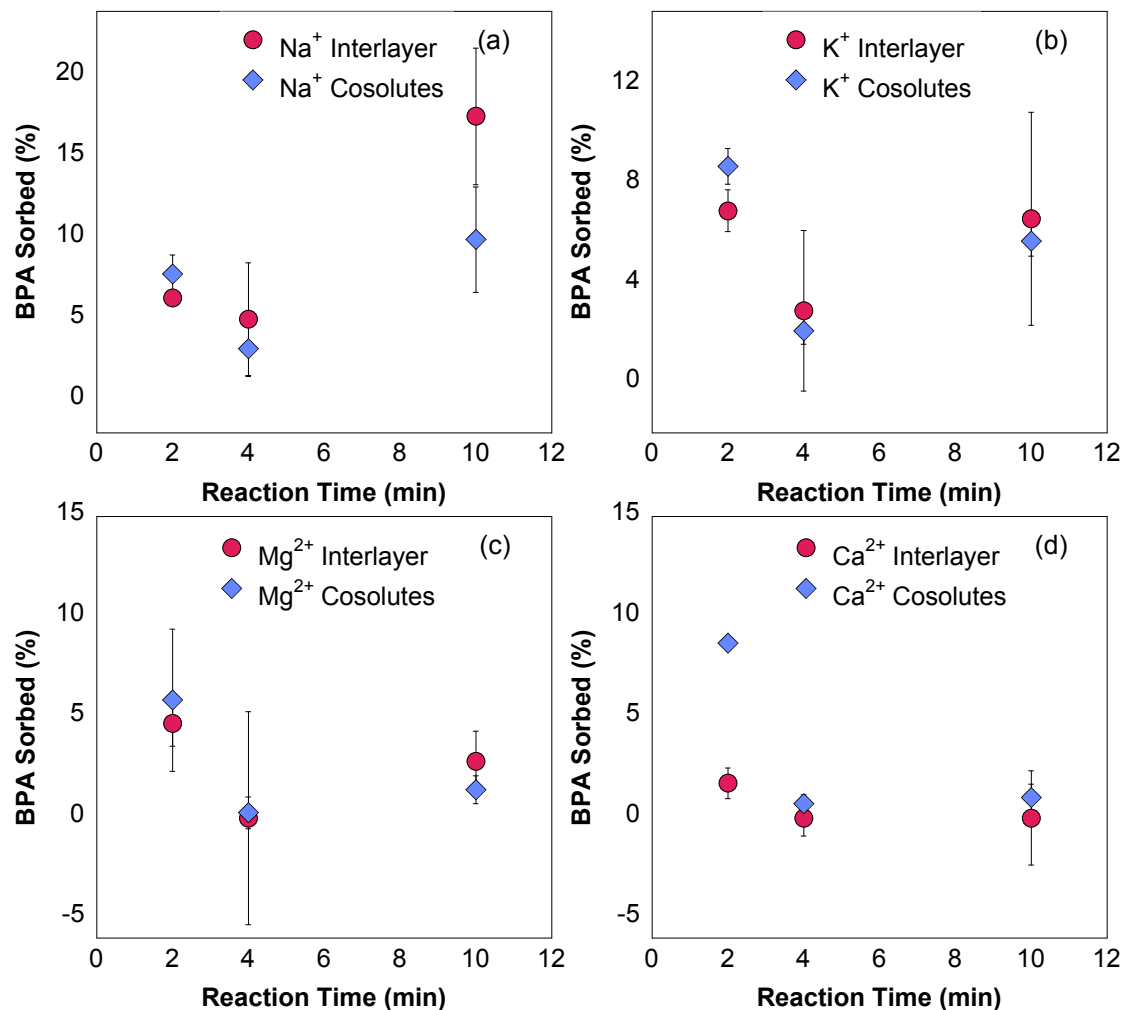
Figure 4.3. Sorbed BPA as a percentage of total remaining BPA over a 10-minute reaction of BPA with (a) Na^+, (b) K^+, (c) Mg^{2+}, and (d) Ca^{2+} pre-exchanged birnessite in triplicate reactors. Each reactor contained 80 µM of BPA and 0.25 g/L of the pre-exchanged birnessite. Cosolute reactors include 10 mM of the cation chloride salt. All reactions were conducted in a pH 5 acetate buffer. Error bars represent the standard deviation of the three reactors.
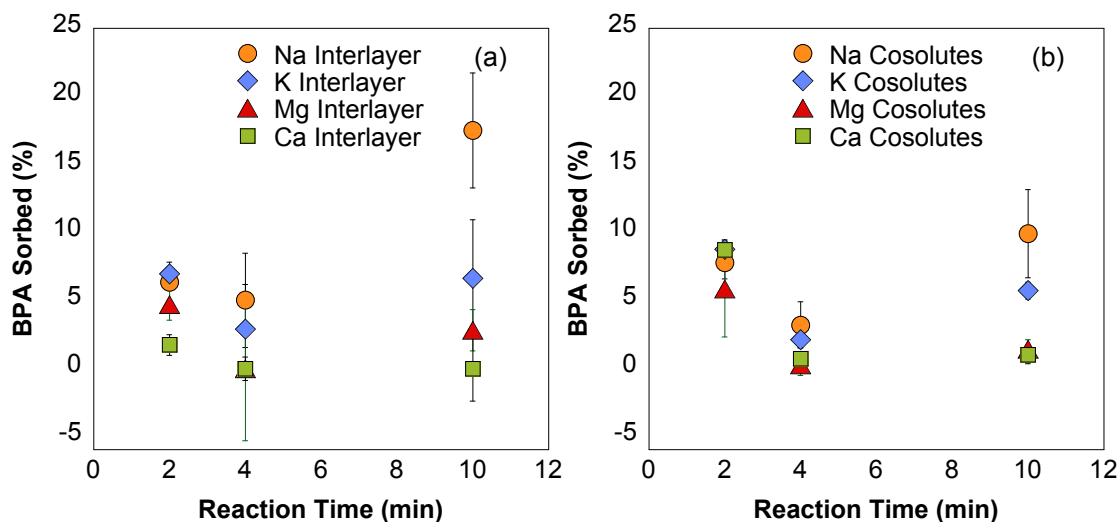
Figure 4.4. Sorbed BPA as a percentage of total remaining BPA over a 10-minute reaction of BPA with birnessite having (a) cations in the interlayer only, and (b) cations in the interlayer and as a cosolute. Each reactor contained 80 µM of BPA and 0.25 g/L of the pre-exchanged birnessite. Cosolute reactors include 10 mM of the cation chloride salt. All reactions were conducted in a pH 5 acetate buffer and were performed in triplicate. Error bars represent the standard deviation of the three reactors.

Table 4.1. Concentrations of dissolved cations after soaking pre-exchanged solids in various solutions for 20 minutes each. Concentrations were measured by ICP-OES.

Sample	Measurement	MQ Water	pH 5 MQ Water	pH 5 Sodium Acetate	pH 5 Sodium Acetate + BPA
Na^+ Interlayer	Na_{aq} (ppm)	0.78	3.33	N/A	N/A
K^+ Interlayer	K_{aq} (ppm)	1.63	3.13	22.83	24.82
Mg^{2+} Interlayer	Mg_{aq} (ppm)	0.00	0.32	1.14	2.04
Ca^{2+} Interlayer	Ca_{aq} (ppm)	0.00	0.38	1.97	4.11

Table 4.2. Surface area measurements for pre-exchanged solids determined by BET method.

Sample	Surface Area (m^2/g)
Starting Material	38.34 ± 5.3
Na^+ Interlayer	31.25 ± 5.3
K^+ Interlayer	29.74 ± 5.3
Mg^{2+} Interlayer	34.98 ± 5.3
Ca^{2+} Interlayer	29.62 ± 5.3

Table 4.3. Average manganese oxidation number (AMON) for pre-exchanged solids determined by XANES fitting.

Sample	AMON (v.u.)
Starting Material	3.49
Na^+ Interlayer	3.31
K^+ Interlayer	3.47
Mg^{2+} Interlayer	3.26
Ca^{2+} Interlayer	3.41

Table 4.4. Mole percentages of MnO_2, Na^+, K^+, Mg^{2+}, and Ca^{2+} for pre-exchanged solids measured by ICP-OES analysis of the acid dissolved solids.

Sample	% MnO_2	%Na^+	%K^+	%Mg^{2+}	%Ca^{2+}
Na^+ Interlayer	92.05	3.10	5.09	0.00	0.04
K^+ Interlayer	91.44	0.03	0.00	8.77	0.04
Mg^{2+} Interlayer	93.29	0.01	2.56	4.07	0.06
Ca^{2+} Interlayer	91.63	0.01	0.00	2.41	6.27

4.8 References

(1) Dick, G. J.; Lee, Y. E.; Tebo, B. M. Manganese(II)-oxidizing *Bacillus* spores in Guaymas Basin hydrothermal sediments and plumes. *Appl. Environ. Microbiol.* **2006**, *72* (5), 3184–3190.

(2) Post, J. E. Manganese oxide minerals: Crystal structures and economic and environmental significance. *Proc. Natl. Acad. Sci.* **1999**, *96* (7), 3447–3454.

(3) Negra, C.; Ross, D. S.; Lanzirotti, A. Oxidizing behavior of soil manganese. *Soil Sci. Soc. Am. J.* **2005**, *69* (1), 87–95.

(4) Tani, Y.; Miyata, N.; Iwahori, K.; Soma, M.; Tokuda, S.; Seyama, H.; Benny K.G Theng. Biogeochemistry of manganese oxide coatings on pebble surfaces in the Kikukawa River System, Shizuoka, Japan. *Appl. Geochem.* **2003**, *18* (10), 1541–1554.

(5) Wehrli, B.; Friedl, G.; Manceau, A. Reaction rates and products of manganese oxidation at the sediment-water interface. In *Aquatic Chemistry*; Huang, C. P., O'Melia, C. R., Morgan, J. J., Eds.; American Chemical Society: Washington, DC, 1995; Vol. 244, pp 111–134.

(6) Remucal, C. K.; Ginder-Vogel, M. A critical review of the reactivity of manganese oxides with organic contaminants. *Environ. Sci. Process. Impacts* **2014**, *16* (6), 1247–1266.

(7) Stone, A. T. Reductive dissolution of manganese(III/IV) oxides by substituted phenols. *Environ. Sci. Technol.* **1987**, *21* (10), 979–988.

(8) Stone, A. T.; Morgan, J. J. Reduction and dissolution of manganese(III) and manganese(IV) oxides by organics. 1. Reaction with hydroquinone. *Environ. Sci. Technol.* **1984**, *18* (6), 450–456.

(9) Xyla, A. G.; Sulzberger, B.; Luther III, G. W.; Hering, J. G.; Van Cappellen, P.; Stumm, W. Reductive dissolution of manganese(III,IV) (hydr)oxides by oxalate: The effect of pH and light. *Langmuir* **1992**, *8* (1), 95–103.

(10) Eary, L. E.; Rai, D. Kinetics of chromium(III) oxidation to chromium(VI) by reaction with manganese dioxide. *Environ. Sci. Technol.* **1987**, *21* (12), 1187–1193.

(11) Lafferty, B. J.; Ginder-Vogel, M.; Sparks, D. L. Arsenite oxidation by a poorly-crystalline manganese oxide. 3. Arsenic and manganese desorption. *Environ. Sci. Technol.* **2011**, *45* (21), 9218–9223.

(12) Landrot, G.; Ginder-Vogel, M.; Livi, K.; Fitts, J. P.; Sparks, D. L. Chromium(III) oxidation by three poorly crystalline manganese(IV) oxides. 2. Solid phase analyses. *Environ. Sci. Technol.* **2012**, *46* (21), 11601–11609.

(13) Tournassat, C.; Charlet, L.; Bosbach, D.; Manceau, A. Arsenic(III) oxidation by birnessite and precipitation of manganese(II) arsenate. *Environ. Sci. Technol.* **2002**, *36* (3), 493–500.

(14) Drits, V. A.; Silvester, E.; Gorshkov, A. I.; Manceau, A. Structure of synthetic monoclinic Na-rich birnessite and hexagonal birnessite: I. Results from X-ray diffraction and selected-area electron diffraction. *Am. Mineral.* **1997**, *82*, 946–961.

(15) Silvester, E.; Manceau, M.; Drits, V. A. Structure of synthetic monoclinic Na-rich birnessite and hexagonal birnessite: II. Results from chemical studies and EXAFS spectroscopy. *Am. Mineral.* **1997**, *82*, 962–978.

(16) Lafferty, B. J.; Ginder-Vogel, M.; Zhu, M.; Livi, K. J. T.; Sparks, D. L. Arsenite oxidation by a poorly crystalline manganese-oxide. 2. Results from X-ray absorption spectroscopy and X-ray diffraction. *Environ. Sci. Technol.* **2010**, *44* (22), 8467–8472.

(17) Grebel, J. E.; Charbonnet, J. A.; Sedlak, D. L. Oxidation of organic contaminants by manganese oxide geomedia for passive urban stormwater treatment systems. *Water Res.* **2016**, *88*, 481–491.

(18) Charbonnet, J. A.; Duan, Y.; van Genuchten, C. M.; Sedlak, D. L. Chemical regeneration of manganese oxide-coated sand for oxidation of organic stormwater contaminants. *Environ. Sci. Technol.* **2018**, *52* (18), 10728–10736.

(19) Grebel, J. E.; Mohanty, S. K.; Torkelson, A. A.; Boehm, A. B.; Higgins, C. P.; Maxwell, R. M.; Nelson, K. I.; Sedlak, D. L. Engineered infiltration systems for urban stormwater reclamation. *Env. Eng Sci* **2013**, *30* (8), 437–454.

(20) Luthy, R. G.; Sedlak, D. L. *Enhanced removal of nutrients and trace organic contaminants in pilot-scale stormwater treatment systems*; Annual Report; U. S. EPA: Water Research Foundation, 2017.

(21) Bina, B.; Mohammadi, F.; Amin, M. M.; Pourzamani, H. R.; Yavari, Z. Determination of 4-nonylphenol and 4-*tert*-octylphenol compounds in various types of wastewater and their removal rates in different treatment processes in nine wastewater treatment plants of Iran. *Chin. J. Chem. Eng.* **2018**, *26* (1), 183–190.

(22) Bulloch, D. N.; Nelson, E. D.; Carr, S. A.; Wissman, C. R.; Armstrong, J. L.; Schlenk, D.; Larive, C. K. Occurrence of halogenated transformation products of selected pharmaceuticals and personal care products in secondary and tertiary treated wastewaters from southern California. *Environ. Sci. Technol.* **2015**, *49* (4), 2044–2051.

(23) Huang, J.; Zhong, S.; Dai, Y.; Liu, C.-C.; Zhang, H. Effect of MnO_2 phase structure on the oxidative reactivity toward bisphenol A degradation. *Environ. Sci. Technol.* **2018**, *52* (19), 11309–11318.

(24) Lin, K.; Liu, W.; Gan, J. Reaction of tetrabromobisphenol A (TBBPA) with manganese dioxide: Kinetics, products, and pathways. *Environ. Sci. Technol.* **2009**, *43* (12), 4480–4486.

(25) Montes-Grajales, D.; Fennix-Agudelo, M.; Miranda-Castro, W. Occurrence of personal care products as emerging chemicals of concern in water resources: A review. *Sci. Total Environ.* **2017**, *595*, 601–614.

(26) Yang, Y.; Ok, Y. S.; Kim, K.-H.; Kwon, E. E.; Tsang, Y. F. Occurrences and removal of pharmaceuticals and personal care products (PPCPs) in drinking water and water/sewage treatment plants: A review. *Sci. Total Environ.* **2017**, *596–597*, 303–320.

(27) Trainer, E.; Ginder-Vogel, M.; Remucal, C. K. Organic structures and solid characteristics influence the rate limiting step of phenolic contaminant oxidation by manganese oxide. *Env. Sci Technol Rev.* **2019**.

(28) Lu, Z.; Lin, K.; Gan, J. Oxidation of bisphenol F (BPF) by manganese dioxide. *Environ. Pollut.* **2011**, *159* (10), 2546–2551.

(29) Zhang, H.; Chen, W.-R.; Huang, C.-H. Kinetic modeling of oxidation of antibacterial agents by manganese oxide. *Environ. Sci. Technol.* **2008**, *42* (15), 5548–5554.

(30) Lin, K.; Liu, W.; Gan, J. Oxidative removal of bisphenol A by manganese dioxide: Efficacy, products, and pathways. *Environ. Sci. Technol.* **2009**, *43* (10), 3860–3864.

(31) Barrett, K. A.; McBride, M. B. Oxidative degradation of glyphosate and aminomethylphosphonate by manganese oxide. *Environ. Sci. Technol.* **2005**, *39* (23), 9223–9228.

(32) Chen, W.-R.; Ding, Y.; Johnston, C. T.; Teppen, B. J.; Boyd, S. A.; Li, H. Reaction of lincosamide antibiotics with manganese oxide in aqueous solution. *Environ. Sci. Technol.* **2010**, *44* (12), 4486–4492.

(33) Zhang, H.; Huang, C.-H. Oxidative transformation of triclosan and chlorophene by manganese oxides. *Environ. Sci. Technol.* **2003**, *37* (11), 2421–2430.

(34) Zhang, T.; Zhang, X.; Yan, X.; Ng, J.; Wang, Y.; Sun, D. D. Removal of bisphenol A via a hybrid process combining oxidation on β-MnO_2 nanowires with microfiltration. *Colloids Surf. Physicochem. Eng. Asp.* **2011**, *392* (1), 198–204.

(35) Lin, K.; Peng, Y.; Huang, X.; Ding, J. Transformation of bisphenol A by manganese oxide-coated sand. *Environ. Sci. Pollut. Res.* **2013**, *20* (3), 1461–1467.

(36) Gao, N.; Hong, J.; Yu, Z.; Peng, P.; Huang, W. Transformation of bisphenol A in the presence of manganese dioxide. *Soil Sci.* **2011**, *176* (6), 265–272.

(37) Liu, R.; Liu, H.; Qiang, Z.; Qu, J.; Li, G.; Wang, D. Effects of calcium ions on surface characteristics and adsorptive properties of hydrous manganese dioxide. *J. Colloid Interface Sci.* **2009**, *331* (2), 275–280.

(38) Zhang, Y.; Yang, Y.; Zhang, Y.; Zhang, T.; Ye, M. Heterogeneous oxidation of naproxen in the presence of α-MnO_2 nanostructures with different morphologies. *Appl. Catal. B Environ.* **2012**, *127*, 182–189.

(39) Murray, J. W. The interaction of metal ions at the manganese dioxide-solution interface. *Geochim. Cosmochim. Acta* **1975**, *39* (4), 505–519.

(40) Marafatto, F. F.; Lanson, B.; Peña, J. Crystal growth and aggregation in suspensions of δ-MnO_2 nanoparticles: Implications for surface reactivity. *Environ. Sci. Nano* **2018**.

(41) Wang, Y.; Benkaddour, S.; Marafatto, F. F.; Peña, J. Diffusion- and pH-dependent reactivity of layer-type MnO_2: Reactions at particle edges versus vacancy sites. *Environ. Sci. Technol.* **2018**, *52* (6), 3476–3485.

(42) Villalobos, M. The role of surface edge sites in metal(loid) sorption to poorly-crystalline birnessites. In *Advances in the Environmental Biogeochemistry of Manganese Oxides*; ACS Symposium Series; 2015; Vol. 1197, pp 65–87.

(43) Zhang, T.; Liu, L.; Tan, W.; Suib, S. L.; Qiu, G.; Liu, F. Photochemical formation and transformation of birnessite: Effects of cations on micromorphology and crystal structure. *Environ. Sci. Technol.* **2018**, *52* (12), 6864–6871.

(44) McKenzie, R. M. The synthesis of birnessite, cryptomelane, and some other oxides and hydroxides of manganese. *Mineral. Mag.* **1971**, *38* (296), 493–502.

(45) Good, N. E.; Winget, G. D.; Winter, W.; Connolly, T. N.; Izawa, S.; Singh, R. M. Hydrogen ion buffers for biological research. *Biochemistry* **1966**, *5* (2), 467–477.

(46) Ferreira, C. M. H.; Pinto, I. S. S.; Soares, E. V.; Soares, H. M. V. M. (Un)suitability of the use of pH buffers in biological, biochemical and environmental studies and their interaction with metal ions – A review. *RSC Adv* **2015**, *5* (39), 30989–31003.

(47) Ying, S. C.; Kocar, B. D.; Fendorf, S. Oxidation and competitive retention of arsenic between iron- and manganese oxides. *Geochim. Cosmochim. Acta* **2012**, *96*, 294–303.

(48) Balgooyen, S.; Campagnola, G.; Remucal, C. K.; Ginder-Vogel, M. Impact of bisphenol A influent concentration and reaction time on MnO_2 transformation in a stirred flow reactor. *Environ. Sci. Process. Impacts* **2019**, *21* (1), 19–27.

(49) *CRC Handbook of Chemistry and Physics*, 95th ed.; CRC Press: Boca Raton, FL, 2014.

(50) Balgooyen, S.; Alaimo, P. J.; Remucal, C. K.; Ginder-Vogel, M. Structural transformation of MnO_2 during the oxidation of bisphenol A. *Environ. Sci. Technol.* **2017**, *51* (11), 6053–6062.

(51) Tratnyek, P. G.; Weber, E. J.; Schwarzenbach, R. P. Quantitative structure–activity relationships for chemical reductions of organic contaminants. *Environ. Toxicol. Chem.* **2003**, *22* (8), 1733.

(52) Arnold, W. A.; Oueis, Y.; O'Connor, M.; Rinaman, J. E.; Taggart, M. G.; McCarthy, R. E.; Foster, K. A.; Latch, D. E. QSARs for phenols and phenolates: Oxidation potential as a predictor of reaction rate constants with photochemically produced oxidants. *Environ. Sci. Process. Impacts* **2017**, *19* (3), 324–338.

(53) Lopano, C. L.; Heaney, P. J.; Post, J. E.; Hanson, J.; Komarneni, S. Time-resolved structural analysis of K- and Ba-exchange reactions with synthetic Na-birnessite using synchrotron X-ray diffraction. *Am. Mineral.* **2007**, *92* (2–3), 380–387.

(54) Drits, V. A.; Lanson, B.; Gaillot, A.-C. Birnessite polytype systematics and identification by powder X-ray diffraction. *Am. Mineral.* **2007**, *92* (5–6), 771–788.

(55) Birkner, N.; Navrotsky, A. Thermodynamics of manganese oxides: Sodium, potassium, and calcium birnessite and cryptomelane. *Proc. Natl. Acad. Sci.* **2017**, *114* (7), E1046–E1053.

(56) Golden, D. C.; Sittertz-Bhatkar, H.; Dixon, J. B. Structural changes during the transformation of birnessite to buserite and todorokite. *Sci. Geol. Memoire* **1990**, *89*, 177–183.

(57) Zhao, H.; Liang, X.; Yin, H.; Liu, F.; Tan, W.; Qiu, G.; Feng, X. Formation of todorokite from "c-disordered" H^+-birnessites: The roles of average manganese oxidation state and interlayer cations. *Geochem. Trans.* **2015**, *16* (1).

(58) Zhu, M.; Ginder-Vogel, M.; Parikh, S. J.; Feng, X.-H.; Sparks, D. L. Cation effects on the layer structure of biogenic Mn-oxides. *Environ. Sci. Technol.* **2010**, *44* (12), 4465–4471.

(59) Tao, L.; Stich, T. A.; Jaccard, H.; Britt, R. D.; Casey, W. H. Manganese-oxide solids as water-oxidation electrocatalysts: The effect of intercalating cations. In *Advances in the Environmental Biogeochemistry of Manganese Oxides*; Chapter 7; 2015; pp 135–153.

(60) Kang, Q.; Vernisse, L.; Remsing, R. C.; Thenuwara, A. C.; Shumlas, S. L.; McKendry, I. G.; Klein, M. L.; Borguet, E.; Zdilla, M. J.; Strongin, D. R. Effect of interlayer spacing on the activity of layered manganese oxide bilayer catalysts for the oxygen evolution reaction. *J. Am. Chem. Soc.* **2017**, *139* (5), 1863–1870.

(61) Wang, J.; Li, D.; Li, P.; Zhang, P.; Xu, Q.; Yu, J. Layered manganese oxides for formaldehyde-oxidation at room temperature: The effect of interlayer cations. *RSC Adv.* **2015**, *5* (122), 100434–100442.

(62) Duckworth, O. W.; Rivera, N. A.; Gardner, T. G.; Andrews, M. Y.; Santelli, C. M.; Polizzotto, M. L. Morphology, structure, and metal binding mechanisms of biogenic manganese oxides in a superfund site treatment system. *Environ. Sci. Process. Impacts* **2017**, *19* (1), 50–58.

(63) Wang, Z.; Giammar, D. E. Metal contaminant oxidation mediated by manganese redox cycling in subsurface environment. In *Advances in the Environmental Biogeochemistry of Manganese Oxides*; ACS Symposium Series; 2015; Vol. 1197, pp 29–50.

(64) Li, C.; Zhang, B.; Ertunc, T.; Schaeffer, A.; Ji, R. Birnessite-induced binding of phenolic monomers to soil humic substances and nature of the bound residues. *Environ. Sci. Technol.* **2012**, *46* (16), 8843–8850.

(65) Sim, W.-J.; Lee, S.-H.; Lee, I.-S.; Choi, S.-D.; Oh, J.-E. Distribution and formation of chlorophenols and bromophenols in marine and riverine environments. *Chemosphere* **2009**, *77* (4), 552–558.

(66) Siqueira, J. O.; Nair, M. G.; Hammerschmidt, R.; Safir, G. R.; Putnam, A. R. Significance of phenolic compounds in plant‑soil‑microbial systems. *Crit. Rev. Plant Sci.* **1991**, *10* (1), 63–121.

(67) Tebo, B. M.; Bargar, J. R.; Clement, B. G.; Dick, G. J.; Murray, K. J.; Parker, D.; Verity, R.; Webb, S. M. Biogenic manganese oxides: Properties and mechanisms of formation. *Annu. Rev. Earth Planet. Sci.* **2004**, *32* (1), 287–328.

(68) Ulrich, H. J.; Stone, A. T. The oxidation of chlorophenols adsorbed to manganese oxide surfaces. *Environ. Sci. Technol.* **1989**, *23* (4), 421–428.

(69) Klausen, J.; Haderlein, S. B.; Schwarzenbach, R. P. Oxidation of substituted anilines by aqueous MnO_2: Effect of co-solutes on initial and quasi-steady-state kinetics. *Environ. Sci. Technol.* **1997**, *31* (9), 2642–2649.

(70) Pizzigallo, M. D.; Ruggiero, P.; Crecchio, C.; Mascolo, G. Oxidation of chloroanilines at metal oxide surfaces. *J. Agric. Food Chem.* **1998**, *46* (5), 2049–2054.

(71) Shaikh, N.; Taujale, S.; Zhang, H.; Artyushkova, K.; Ali, A.-M. S.; Cerrato, J. M. Spectroscopic investigation of interfacial interaction of manganese oxide with triclosan, aniline, and phenol. *Environ. Sci. Technol.* **2016**, *50* (20), 10978–10987.

Chapter 5

Conclusions

5.1 Summary

The primary purpose of this dissertation is to elucidate details of phenolic contaminant oxidation by manganese oxides. A novel aspect of these studies is the integration of aqueous kinetic data with solid phase characterization, which provides new information about the reaction. We accomplish this by first inducing structural changes to the mineral and observing changes to the phenol mechanism and products. Second, we apply continuous introduction of the phenol to examine the effects of introduction rate on organic products and mineral transformation. Finally, we determine the influence of manganese oxide layer stacking by pre-exchanging the mineral with metal cations in the interlayer and testing their reactivity with phenols. The results from these three studies demonstrate the importance of accounting for both the organic and inorganic reactants in this complex reaction.

In Chapter 2, we employ multi-addition batch reactors to quantify bisphenol A (BPA) oxidation rates and the formation of its predominant product, 4-hydroxycumyl alcohol (HCA), in tandem with transformation of a synthetic, Mn(III)-rich δ-MnO$_2$. Twelve sequential additions of BPA are performed at neutral pH to induce structural changes to the mineral, simulating the BPA exposure that might be found in near-surface environments or water treatment systems. Over twelve additions, BPA oxidation rate decreases by three orders of magnitude and HCA yield decreases from 40% to 3%. We also determine that HCA is oxidized at a rate that is 12.6 times slower than BPA and accumulates in solution. The dramatic changes in the redox reaction over the course of twelve additions is attributed to accumulation of interlayer Mn(II/III) produced during the reaction, as observed using X-ray absorption spectroscopy.

In Chapter 3, we use stirred flow reactors to determine if higher influent BPA concentrations (i.e., introduction rates) lead to increased polymer production when oxidized by δ-MnO_2. Since HCA is formed through radical coupling, it is used as a metric for polymer production. We found that the influent BPA concentration does not affect HCA yield, suggesting that polymeric production is not strongly dependent on influent concentrations. However, changes in influent BPA concentration affect BPA oxidation rates and the rate of δ-MnO_2 reduction. Lower aqueous Mn(II) production is observed in reactors at higher BPA introduction rates, suggesting that single-electron transfer and polymer production are favored under these conditions. An examination of Mn(II) sorption during these reactions indicated that the length of the reaction, rather than BPA introduction rate, cause enhanced aqueous Mn(II) production in reactors with low introduction rates and longer reaction times due to increased opportunity for disproportionation and comproportionation.

In Chapter 4, we examine the significance of mineral structure by quantifying reactivity of birnessites toward four target phenolic compounds. Synthetic birnessite is pre-exchanged with four different cations: Na^+, K^+, Mg^{2+}, and Ca^{2+}. These cations migrate to the interlayer region of birnessite and induce changes such as d-spacing alteration and even transformation in the micromorphology. The four target phenols (i.e., BPA, triclosan, estrone, and *p*-cresol) react at different rates with the birnessites, but all follow the same trend where the birnessite with the Na^+-interlayer reacts the fastest, then K^+-interlayer, then Mg^{2+}-interlayer, and finally Ca^{2+}-interlayer. This trend is found in previous studies that examine effects of cations as cosolutes,[1–3] but here, we see that even interlayer cations drive changes in reactivity. This trend is attributed to sorbed or interlayer cations changing the overall oxidation state and altering the electron transfer rate.

Together, these chapters demonstrate that the oxidation of phenols by manganese oxide cannot be described by the initial kinetics of the organic reductant alone or by the reductive dissolution of the manganese oxide alone. Investigation of both the organic and inorganic reactants, as done in this dissertation, provides critical insights into this reaction that has not been demonstrated before. Comprehensive knowledge of this oxidation reaction is important to understand how the mechanism and products of phenolic transformation may change based on mineral characteristics. Further environmental significance of this research is the investigation of factors that affect reactions in the environment, but generally not in laboratory settings. For example, most laboratory studies typically use batch reactors to characterize the reactivity of manganese oxides.[3] These closed systems are experimentally simple and results can be readily compared to previous data. However, batch reactors retain both organic and inorganic reaction products, which can affect the reaction. In the environment, these products are continuously diluted or removed. Stirred flow reactors used in Chapter 3 simulate environmental reactions by employing slow and constant addition of an influent media and constant removal of aqueous products. Finally, the investigation of different interlayer cations represents some of the disparity that might be seen between controlled lab experiments, which generally use synthetic Na^+-interlayer birnessite, and reactivity of environmental solids, which are exposed to different cations in natural waters.

5.2 Suggestions for Future Research

There are several topics within the scope of this research that have not yet been addressed. One is that the oxidation products are not known for all phenolic contaminants. MnO_2 is shown to degrade both triclosan[4,5] and 17β-estradiol (E2),[6,7] which are both frequently detected

in the environment,[8] yet the mechanism and products of these reactions are still unknown. An understanding of the degradation process of these compounds is necessary to evaluate the effects of their presence in the environment and to determine whether or not oxidation by MnO_2 is a beneficial process.

Further, for phenols whose mechanism and products are relatively well understood (e.g., BPA), the identified products are determined in controlled laboratory settings and may not represent products formed in the environment. Radicals that are formed via single electron transfer during phenol oxidation are of concern as they can couple with dissolved organic matter or other compounds in the environment, forming unknown high molecular weight products.[9–11] The formation of these compounds need to be evaluated to determine the full impact of phenolic contaminants on the environment.

To analyze the environmental impact of a contaminant, we must take into account the toxicity of the compound itself, its transformation products, and products it might form by interacting with environmental reactants. Without an understanding of the phenol degradation process, we do not know that the products are indeed less harmful than their parent compound. A full life-cycle analysis might reveal that some of these compounds are more harmful than previously determined when based solely on the toxicity of the original contaminant.

If this oxidation process were to be used in a water treatment system to prevent environmental exposure to dangerous phenolic compounds, a couple major aspects would need to be determined. The first is the competition between phenolic compounds. Assuming many phenolic compounds would be treated at the same time from urban stormwater runoff or green infrastructure settings,[12] we would want to know how these different compounds compete to react to manganese oxide and if their products interact to form new products. One way to do this

is to predict mechanism and kinetics of a phenol, as was recently suggested.[13] Trainer et al. discuss the two mechanisms by which phenols react, electron transfer limited and sorption limited, that could determine their reactivity and competition. The second is how to regenerate the reactive manganese oxide. As we observe in this dissertation, the reactivity of manganese oxide does not last indefinitely. The reactivity decreases after one exposure to BPA (2:1000 moles BPA:moles MnO_2) in Chapter 2. One study investigates regeneration of manganese oxide-coated sand in engineered systems by addition of HOCl.[14] These techniques would need further research to prove that they are effective and safe.

5.3 References

(1) Lu, Z.; Lin, K.; Gan, J. Oxidation of bisphenol F (BPF) by manganese dioxide. *Environ. Pollut.* **2011**, *159* (10), 2546–2551.

(2) Lin, K.; Peng, Y.; Huang, X.; Ding, J. Transformation of bisphenol A by manganese oxide-coated sand. *Environ. Sci. Pollut. Res.* **2013**, *20* (3), 1461–1467.

(3) Remucal, C. K.; Ginder-Vogel, M. A critical review of the reactivity of manganese oxides with organic contaminants. *Environ. Sci. Process. Impacts* **2014**, *16* (6), 1247–1266.

(4) Zhang, H.; Huang, C.-H. Oxidative transformation of triclosan and chlorophene by manganese oxides. *Environ. Sci. Technol.* **2003**, *37* (11), 2421–2430.

(5) Shaikh, N.; Taujale, S.; Zhang, H.; Artyushkova, K.; Ali, A.-M. S.; Cerrato, J. M. Spectroscopic investigation of interfacial interaction of manganese oxide with triclosan, aniline, and phenol. *Environ. Sci. Technol.* **2016**, *50* (20), 10978–10987.

(6) Jiang, L.; Huang, C.; Chen, J.; Chen, X. Oxidative transformation of 17β-estradiol by MnO$_2$ in aqueous solution. *Arch. Environ. Contam. Toxicol.* **2009**, *57* (2), 221–229.

(7) Xu, L.; Xu, C.; Zhao, M.; Qiu, Y.; Sheng, G. Oxidative removal of aqueous steroid estrogens by manganese oxides. *Water Res.* **2008**, *42* (20), 5038–5044.

(8) Masoner, J. R.; Kolpin, D. W.; Furlong, E. T.; Cozzarelli, I. M.; Gray, J. L.; Schwab, E. A. Contaminants of emerging concern in fresh leachate from landfills in the conterminous United States. *Env. Sci Process. Impacts* **2014**, *16* (10), 2335–2354.

(9) Tong, F.; Gu, X.; Gu, C.; Xie, J.; Xie, X.; Jiang, B.; Wang, Y.; Ertunc, T.; Schäffer, A.; Ji, R. Stimulation of tetrabromobisphenol A binding to soil humic substances by birnessite and the chemical structure of the bound residues. *Environ. Sci. Technol.* **2016**, *50* (12), 6257–6266.

(10) Kang, K.-H.; Dec, J.; Park, H.; Bollag, J.-M. Effect of phenolic mediators and humic acid on cyprodinil transformation in presence of birnessite. *Water Res.* **2004**, *38* (11), 2737–2745.

(11) Li, C.; Zhang, B.; Ertunc, T.; Schaeffer, A.; Ji, R. Birnessite-induced binding of phenolic monomers to soil humic substances and nature of the bound residues. *Environ. Sci. Technol.* **2012**, *46* (16), 8843–8850.

(12) Grebel, J. E.; Charbonnet, J. A.; Sedlak, D. L. Oxidation of organic contaminants by manganese oxide geomedia for passive urban stormwater treatment systems. *Water Res.* **2016**, *88*, 481–491.

(13) Trainer, E.; Ginder-Vogel, M.; Remucal, C. K. Organic structures and solid characteristics influence the rate limiting step of phenolic contaminant oxidation by manganese oxide. *Environ. Sci. Technol.* **2019**. - In Review

(14) Charbonnet, J. A.; Duan, Y.; van Genuchten, C. M.; Sedlak, D. L. Chemical regeneration of manganese oxide-coated sand for oxidation of organic stormwater contaminants. *Environ. Sci. Technol.* **2018**, *52* (18), 10728–10736.

Appendix A

Supplementary Material for Chapter 2

Section A1: Materials

Acetonitrile (HPLC grade), methanol (HPLC grade), formic acid (ACS, 88%), calcium chloride dihydrate (ACS, 100%), and potassium permanganate (ACS), were purchased from Fisher Chemical. Bisphenol A (≥99%) and L-ascorbic acid (≥99%) were purchased from Sigma-Aldrich. Manganese(II) nitrate tetrahydrate (analytical grade), piperazine-*N,N'*-bis(2-ethanesulfonic acid) (PIPES, 99%), and sodium oxalate (98.5%) were purchased from Acros Organics. Boron nitride (99.5%, 325 mesh) was purchased from Alfa Aesar. Sodium hydroxide (98%) was purchased from Sigma Chemical Co.

A1.1 Preparation of 4-Hydroxycumyl Alcohol (HCA)

This synthesis (Figure **A1**) is a modification of the method reported by Nakamura *et al.*,[1] and provides a significantly improved yield. A 100-mL round bottom flask charged with a teflon-coated stirbar was oven-dried overnight, fitted with a rubber septum, and cooled to room temperature under a stream of nitrogen gas. The flask was charged with *p*-acetoxyacetophenone (1.04 mL; 6.6 mmol) and dry Et_2O (20 mL). The mixture was cooled to 0°C in an ice bath. A solution (3M in Et_2O) of methylmagnesium iodide (7.0 mL; 21 mmol) was added dropwise over 5 min, resulting in formation of a yellow precipitate. The ice bath was removed and the mixture was allowed to warm to room temperature with stirring overnight. The reaction was opened up to air and quenched by the slow addition of aqueous ammonium chloride (saturated, 100 mL). The mixture was extracted using EtOAc (3 x 35 mL). The combined organic layers were washed with

brine (35 mL), dried over MgSO$_4$, and filtered. The volatile materials were removed *in vacuo* to afford a pink-colored residue. The product was crystallized from hot EtOAc to give 4-hydroxycumyl alcohol (924 mg; 6.07 mmol; 92 % yield) as a white powder.
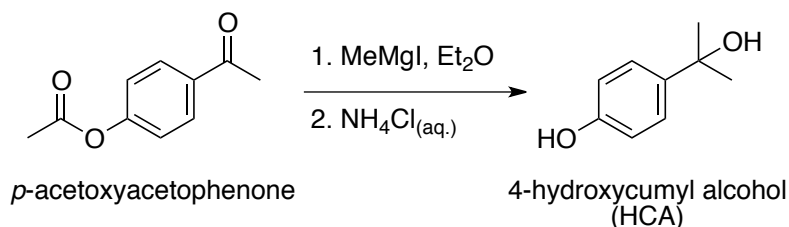
Figure A1. Synthesis reaction of HCA.

^{1}H NMR (400 MHz, CD$_3$OD): δ 7.28 (d, *J* = 8 Hz, 2H), 6.71 (d, *J* = 8 Hz, 2H), 1.48 (s, 6H) ppm. This matches the literature characterization.[1]

^{13}C NMR (100 MHz, CD$_3$OD): δ 156.8, 141.7, 127.0, 115.4, 72.7, 31.9 ppm.

IR (KBr pellet): ν 3394, 3128, 2971, 2682, 2592, 2499, 1890, 1612, 1597, 1516, 1466, 1448, 1397, 1379, 1303, 1239, 1179, 1160, 1111, 1102, 1016, 956, 935, 861 cm^{-1}.

LRMS (Agilent 6460 triple quadrupole, electrospray ionization, negative mode) calculated *m/z* for C$_9$H$_{12}$O$_2$: 152.08; found *m/z* 151.10 [M-H]$^-$, 133.10 [M-H$_3$O]$^-$ (Figure **A2**). This matches the literature characterization.[2]
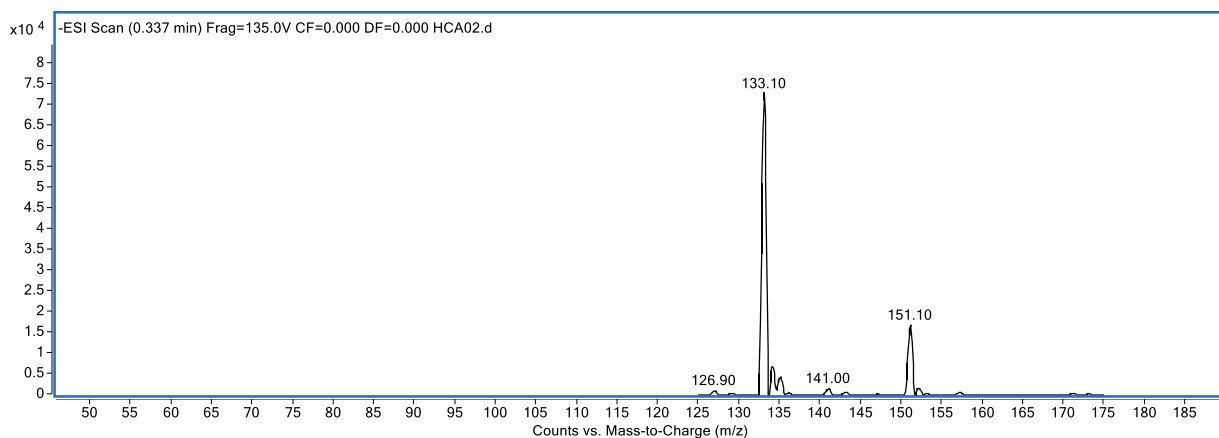
Figure A2. Mass spectrum of synthesized HCA collected using an Agilent triple quadrupole LC-MS with electrospray ionization in negative mode. Molecular ion = 151.10; base peak = 133.10.

Section A2: Analytical Methods

A2.1 High Performance Liquid Chromatography (HPLC) Analysis

HPLC analyses were performed with an Agilent 1260 instrument equipped with a fluorescence detector (Model 1260 FLD) and a UV detector (Model 1260 DAD). The peaks detected in experimental chromatograms were compared to authentic standards.

Column:	Agilent Poroshell 120 EC-C18 (4.6 x 50 mm, 2.7 µm)
Guard column:	Agilent EC-C18 (3.0 x 5 mm, 2.7 µm)
Injection volume:	5 µL
Mobile phase:	A: 0.1% Formic Acid + 10% Acetonitrile (ACN) in Milli-Q water adjusted to pH 3 (filtered through a 0.2 µm nylon filter)
	B: 100% ACN
Flowrate:	0.6 mL/min
Column temperature:	30°C
Isocratic:	% Solvent A % Solvent B
	60 40
Method duration:	6.00 min

Target Analyte	Excitation Wavelength (nm)	Emission Wavelength (nm)	Retention Time (min)
BPA	280	310	2.65
HCA	280	310	0.66
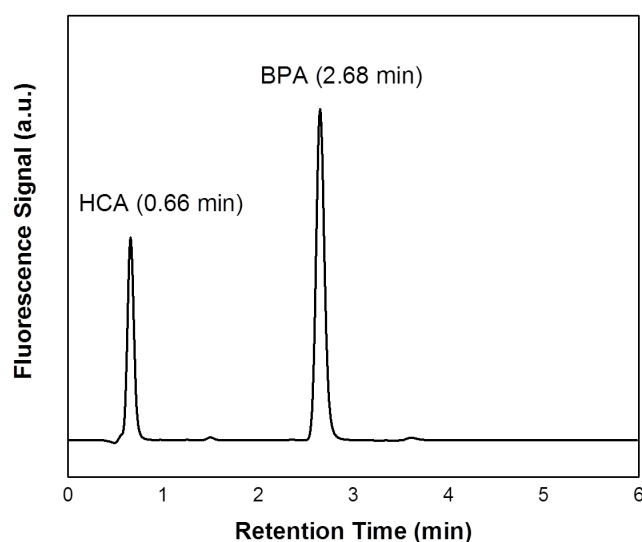
Figure A3. HPLC chromatogram of a sample from the 12-addition experiment of 80 μM BPA with 0.33 g/L Mn(III)-rich δ-MnO$_2$ in PIPES buffer (pH 7).

A2.2 Inductively Coupled Plasma-Optical Emission Spectroscopy (ICP-OES) Analysis

ICP-OES analyses were performed on a PerkinElmer Optima 4300 DV to quantify aqueous manganese in the reactors at various time intervals. All samples were filtered immediately and diluted in a solution of 2% nitric acid. Standards were made from a SPEX CertiPrep 1000 mg/L Mn stock diluted in 2% nitric acid. Error was calculated using relative standard deviations from four instrument responses.

Section A3: Rate Constant Analysis

Rate constants for the oxidation of BPA and HCA by Mn oxides were calculated assuming pseudo-first-order kinetics according to:

$$\ln[A] = -kt + \ln[A]_o \qquad \qquad \textbf{A1}$$

where A is the concentration of the organic (M), t is the time of the reaction (min), and k is the rate constant (min^{-1}). Since the reaction deviates from pseudo-first-order kinetics after long reaction durations, only data from the linear portion of these plots were used to calculate rate constants ($R^2 \geq 0.98$ for the first 4 additions, $R^2 \geq 0.90$ for additions 5-12). Reported rate constants are averages of rate constants calculated at multiple time points. For example, the data in Figure **A4a** would be used to calculate an average rate constant by using the rate constant in the first two minutes, the first three minutes, and the first four minutes. This method was used in order to provide an average and standard deviation of the rate constant throughout each reaction of BPA with MnO_2. As shown in Figure **A4b**, the data deviates from pseudo-first-order regime after a certain time point, and these later time points are not used in rate constant calculations or error determination. The error for each rate constant is the standard deviation of the rate constants collected at all useable time points. Half-lives ($t_{1/2}$) were calculated using equation **A2**:

$$t_{1/2} = \frac{\ln(2)}{k} \qquad \qquad \textbf{A2}$$

The reaction length of each addition was based on estimation to capture as much of the degradation process as possible. The first several reactions were designed to allow enough time to oxidize the entire aliquot of BPA.
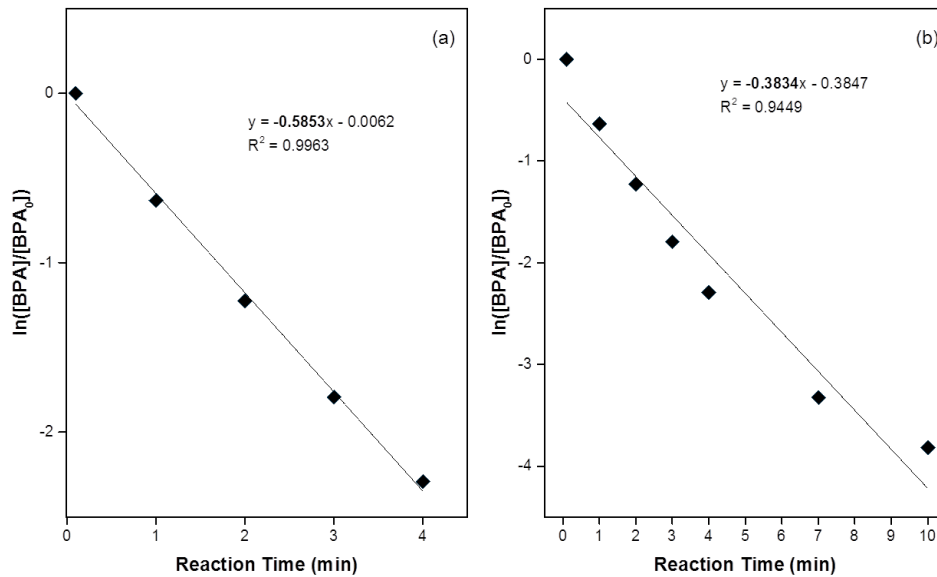
Figure A4. Pseudo-first-order rate analysis of (a) the first four minutes and (b) the first ten minutes of 80 µM BPA oxidation by 0.33 g/L Mn(III)-rich δ-MnO$_2$ in PIPES pH 7.
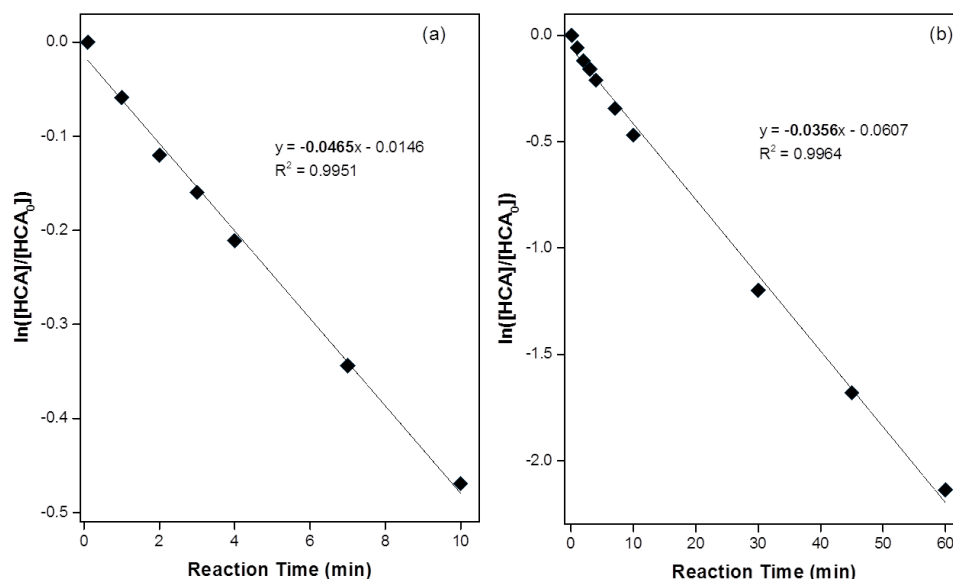
Figure A5. Pseudo-first-order rate analysis of (a) the first 10 minutes and (b) the first 60 minutes of 80 μM HCA oxidation by 0.33 g/L Mn(III)-rich δ-MnO$_2$ in PIPES pH 7.

Section A4: HCA Detection and Yield Calculation

A4.1 HCA Identification

The oxidation product in this reaction was identified as HCA by comparing its UV spectrum and HPLC retention time to pure HCA synthesized as described in Section **A1**. The UV spectra of the BPA product aligned with that of the synthesized HCA, with λ_{max} of both compounds occurring at 221 nm and 260 nm (Figure **A6**). The molar extinction coefficient of HCA at 221 nm is 7173.5 M^{-1} cm^{-1} at pH 7. The retention times of both the authentic standard and the oxidation product were at 0.657 min using the HPLC method described in Section A2 (Figure **A7**).
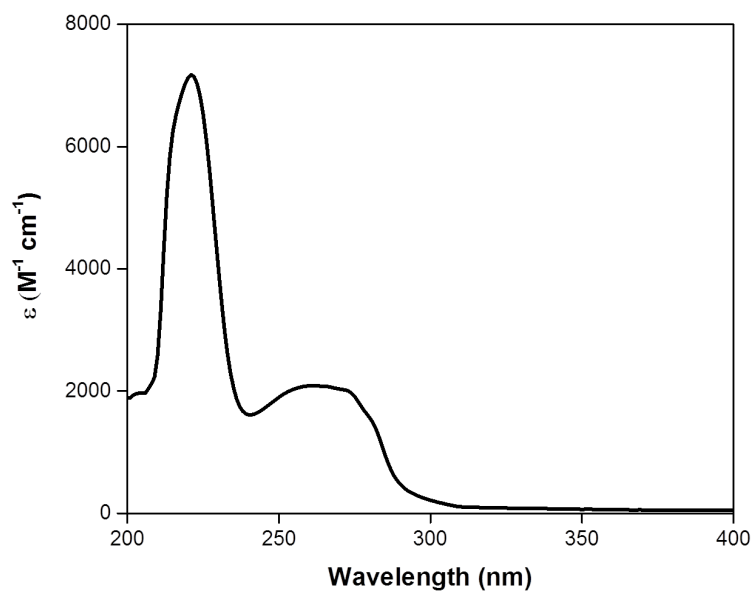
Figure A6. UV spectrum of the synthesized HCA at pH 7.
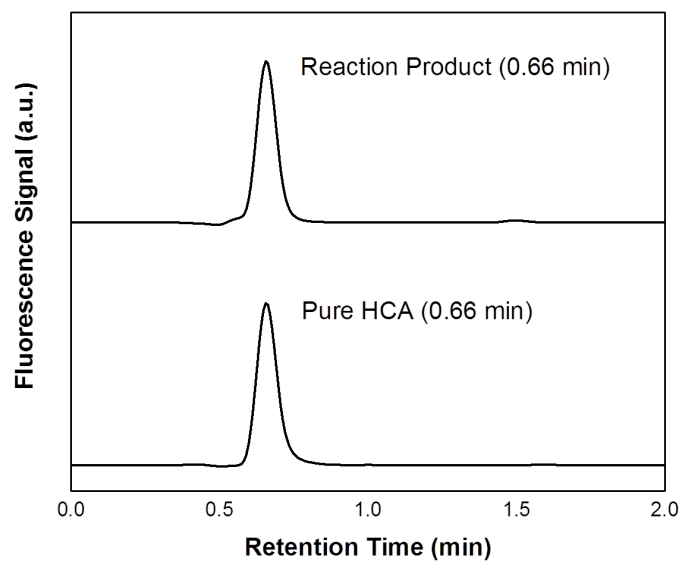
Figure A7. HPLC chromatograms of the synthesized HCA and reaction products, measured using a fluorescence detector.

A4.2 HCA Quantification

The rate of change of BPA with time was modeled by assuming pseudo-first-order kinetics according to:

$$\frac{d[BPA]}{dt} = -k_1[BPA] \qquad \textbf{A3}$$

where [BPA] is the concentration of BPA at time t and k_1 is the measured pseudo-first-order loss rate of BPA. This differential expression integrates to:

$$[BPA] = [BPA]_0 e^{-k_1 t} \qquad \textbf{A4}$$

where $[BPA]_0$ is the initial concentration of BPA.

The differential expression describing the change in HCA concentration with time is given by:

$$\frac{d[HCA]}{dt} = k_1 F_{HCA}[BPA] - k_2[HCA] \qquad \textbf{A5}$$

where [HCA] is the concentration of HCA at time t and F_{HCA} is the yield of HCA from BPA oxidation. k_2 is the pseudo-first-order loss rate of HCA, which is assumed to be 12.6 times slower than k_1 based on control experiments (Figures **A4** and **A5**). Equation **A5** can then be integrated to give an expression of the form:

$$[HCA] = \frac{k_1 F_{HCA}[BPA]_0}{k_1 - k_2} (e^{-k_1 t} - e^{-k_2 t}) \qquad \textbf{A6}$$

F_{HCA} is then determined by fitting the measured HCA concentrations according to equation **A6**, which is identical to equation 1 in the manuscript.
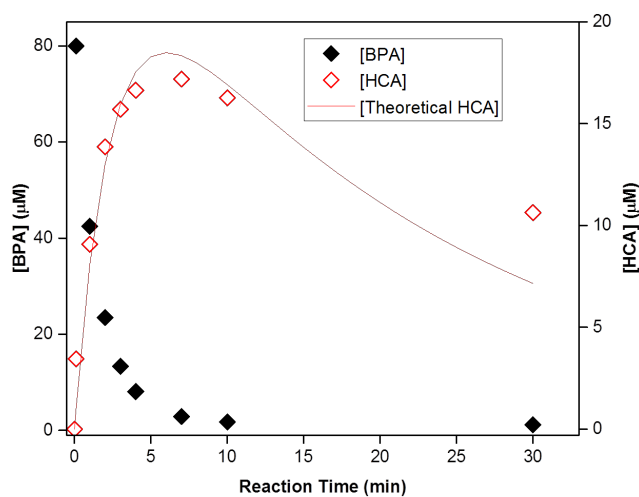
Figure A8. A sample single-addition batch reaction of 80 µM BPA with 0.33 g/L Mn(III)-rich δ-MnO$_2$ in PIPES pH 7 buffer. Theoretical HCA production is modeled using a least-squares minimization with Equation **1** in the manuscript and the measured data set.

Table A1. Percentages of BPA recovered as HCA on a molar basis during each of the twelve additions of 80 µM BPA to 0.33 g/L Mn(III)-rich δ-MnO$_2$, calculated using Equation **A1**.

Additions of BPA	HCA Yield (% of BPA)
1	39.73
2	42.31
3	35.63
4	21.33
5	17.80
6	5.63
7	2.63
8	2.98
9	2.42
10	3.58
11	1.86
12	3.54
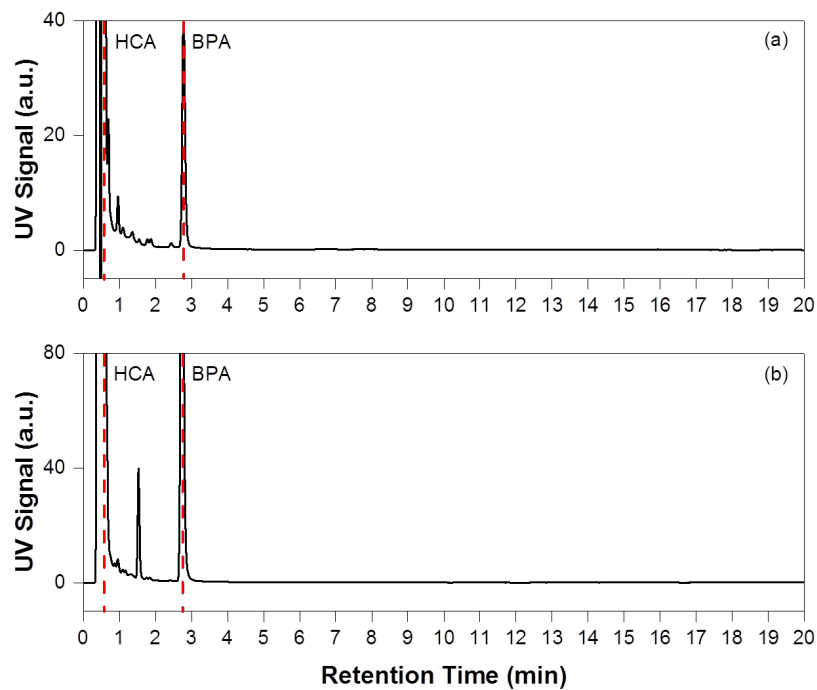
Figure A9. HPLC chromatograms using a DAD detector (230 nm) from (a) the first minute of the first addition, and (b) the last minute of the twelfth addition during twelve additions of 80 μM BPA with 0.33 g/L Mn(III)-rich δ-MnO$_2$ in PIPES pH 7 buffer.
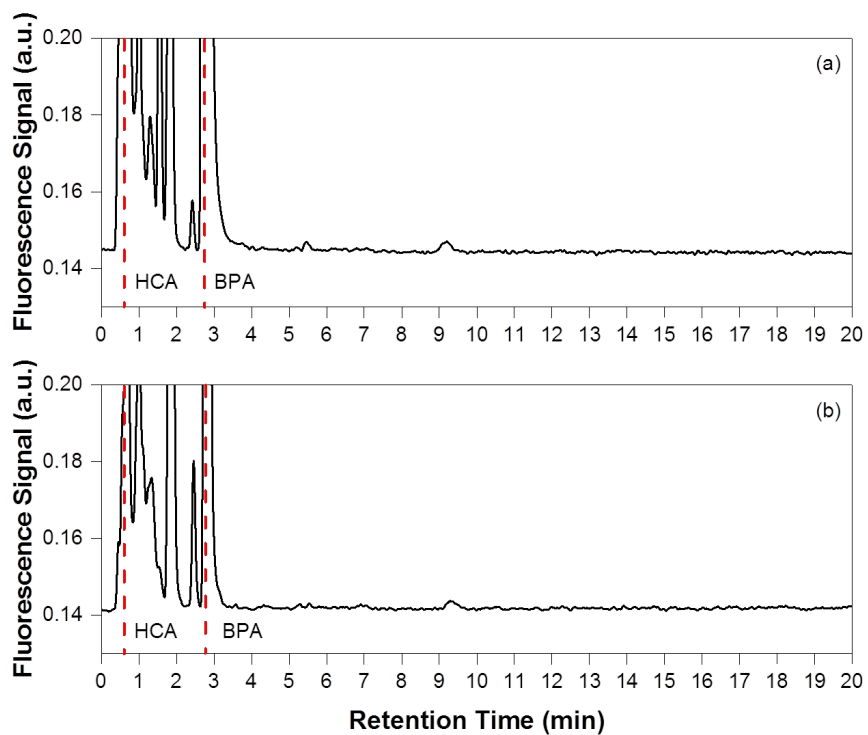
Figure A10. HPLC chromatograms using an FLD detector from (a) the first minute of the first addition, and (b) the last minute of the twelfth addition during twelve additions of 80 µM BPA with 0.33 g/L Mn(III)-rich δ-MnO$_2$ in PIPES pH 7 buffer.

Section A5: Sorption Analysis

Table A2. The percentages of BPA and HCA sorbed during three sequential additions of 80 µM BPA to 0.33 g/L Mn(III)-rich δ-MnO$_2$ in PIPES pH 7 buffer. All reactions were 60 minutes in duration.

BPA Addition		
# of BPA Additions	% BPA Sorbed	% HCA Sorbed
1	14.3 ± 7.4	0 ± 0
2	0 ± 0	0.9 ± 1.4
3	0.2 ± 0.5	1.0 ± 0.9

Section A6: Solids Analysis

Table A3. BET analysis of surface area in a subset of solids collected after each addition.

Surface Analysis	
# of BPA Additions	Surface Area (m^2/g)
0	118 ± 15
3	100 ± 15
6	106 ± 15
9	124 ± 15
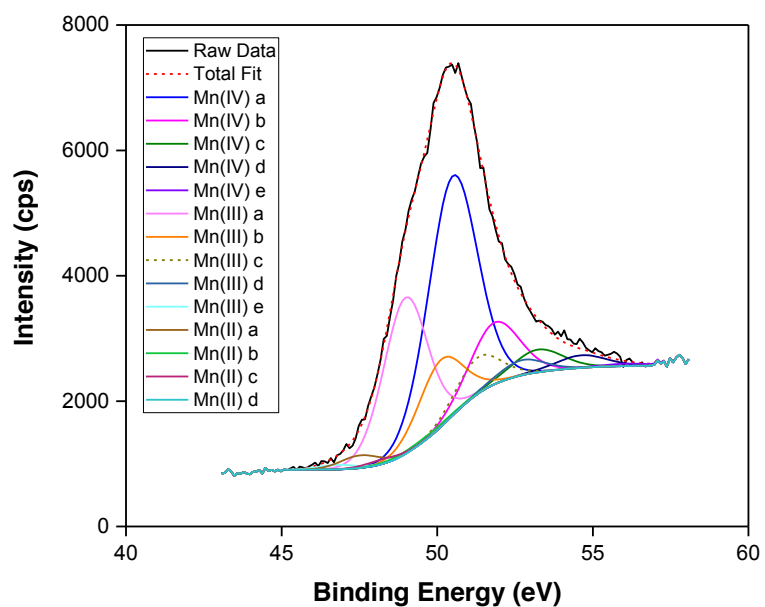
Figure A11. Fitted XPS data from the starting material using the method described in the Materials and Methods section of the manuscript. Uncertainty in the mole fraction is ±0.02 for Mn(IV) and Mn(III) and ±0.01 for Mn(II).
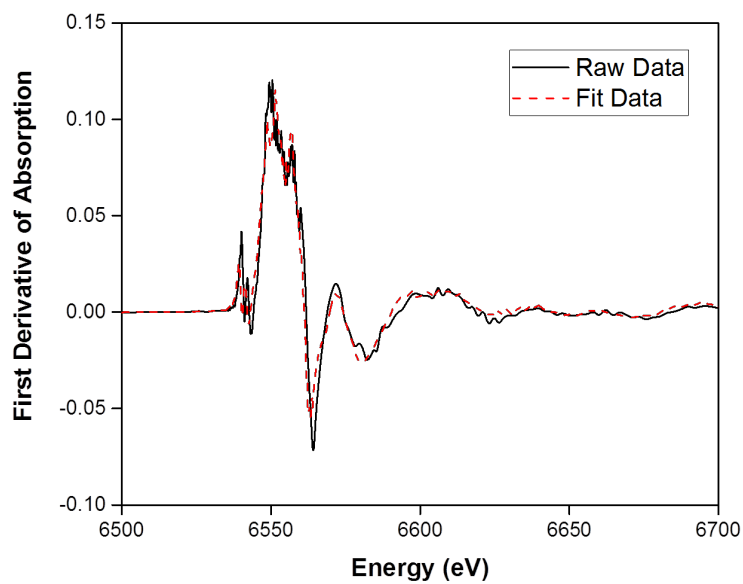
Figure A12. Fitted XANES data from the starting material using the Combo method described in the Methods and Materials section of the manuscript.
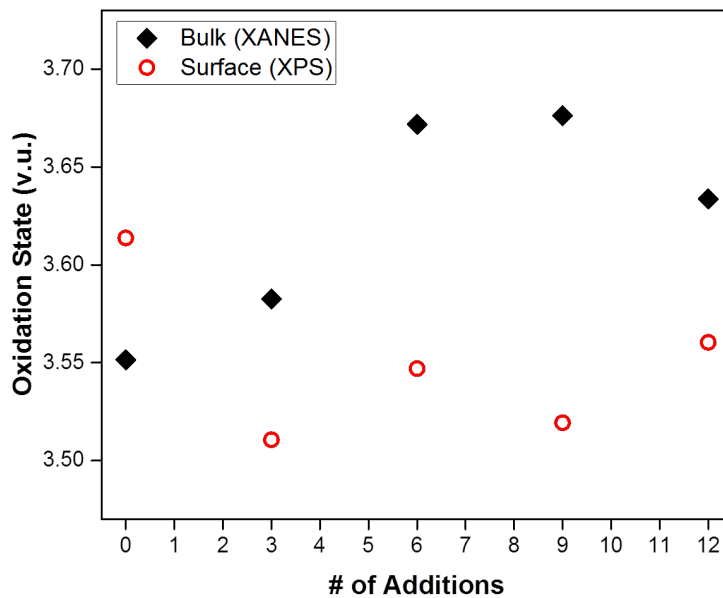
Figure A13. Oxidation state (measured by XANES and XPS) of a subset of solid samples over twelve additions of 80 μM BPA with 0.33 g/L of Mn(III)-rich δ-MnO$_2$ in a PIPES pH 7 buffer. Data is an average of two reactors.
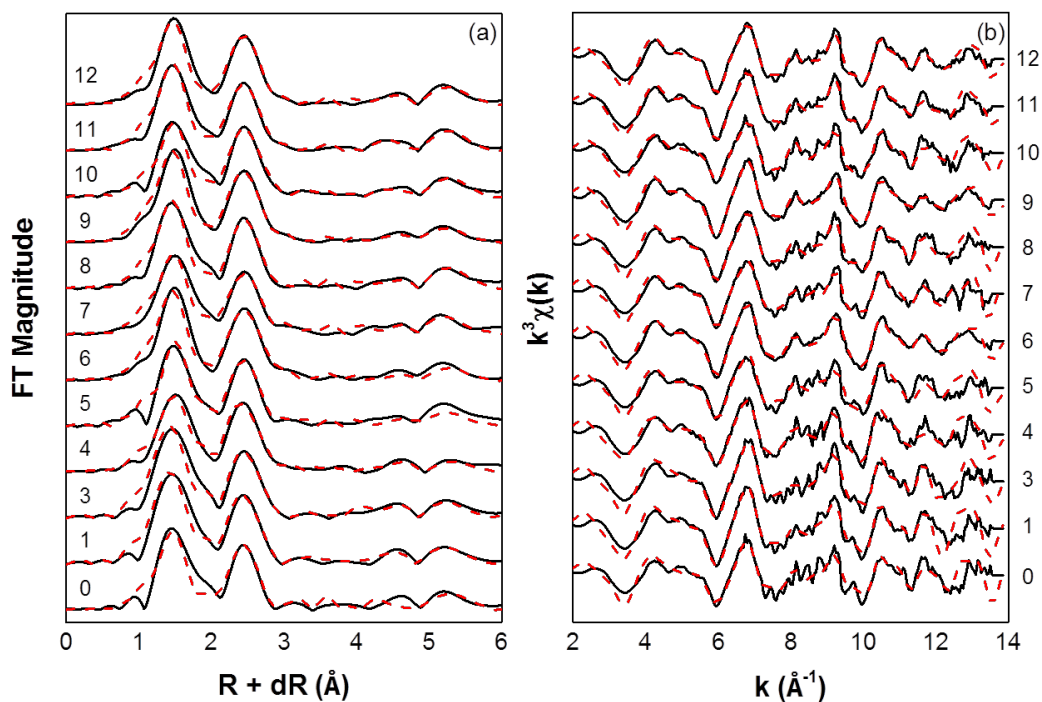
Figure A14. Raw and modeled data of (a) the chi functions and (b) relative radial distribution function from EXAFS analysis of solids over twelve additions of 80 μM BPA with 0.33 g/L of Mn(III)-rich δ-MnO$_2$ in a PIPES pH 7 buffer. The addition number is indicated by the numbers next to each data set. Samples from both reactors were combined and then analyzed.
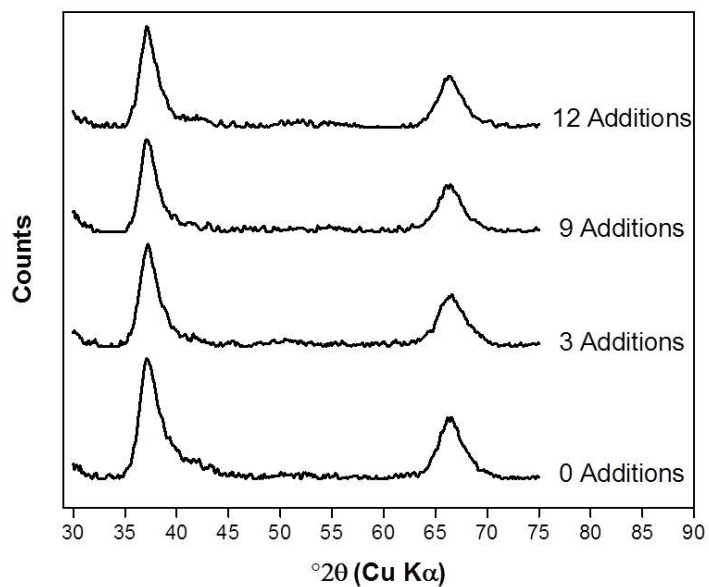
Figure A15. The crystallinity of Mn(III)-rich δ-MnO_2 during twelve additions of 80 μM BPA to 0.33 g/L Mn(III)-rich δ-MnO_2 in PIPES buffer (pH 7), as measured by XRD.
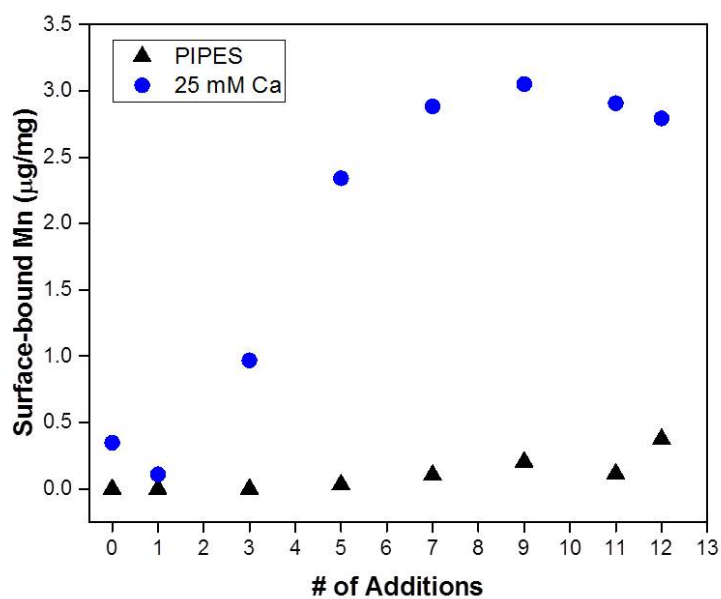
Figure A16. Surface-bound Mn extractable by a solution of 25 mM CaCl$_2$ on a Mn(III)-rich δ-MnO$_2$ during twelve additions of 80 μM BPA to 0.33 g/L Mn(III)-rich δ-MnO$_2$ in PIPES buffer (pH 7).

Table A4. EXAFS fitting results. The S_0^2 parameter was set to 0.865 for all samples.

Sample	e0	focc	S02	χ^2	Shell	CN	Dist (Å)	σ2
0 Additions	6.36	0.6(1)	0.66	621	Mn-O	4	1.89(5)	0.009(6)
					Mn-O	2	1.90(4)	0.002(4)
					Mn-Mn	2	2.71(4)	0.006(4)
					Mn-Mn	4	2.85(1)	0.002(2)
					Mn-O	4	3.30(4)	0.001(4)
					Mn-O	2	3.48(9)	0.001(4)
					Mn-Na inter	2(4)	4.2(2)	0.005
					Mn-O	4	4.5(1)	0.001(7)
					Mn-O	8	4.69(8)	0.001(7)
					Mn-Mn	4	4.92(8)	0.003(2)
					Mn-Mn	2	5.0(1)	0.003(2)
					Mn-Mn	2	5.59(9)	0.002(3)
					Mn-Mn	4	5.83(5)	0.002(3)
1 Additions	5.39	0.9(1)	0.66	779	Mn-O	4	1.87(6)	0.005(7)
					Mn-O	2	1.9(1)	0.002(1)
					Mn-Mn	2	2.71(2)	0.005(1)
					Mn-Mn	4	2.86 (1)	0.002(1)
					Mn-O	4	3.35(4)	0.004(5)
					Mn-O	2	3.6(1)	0.004(5)
					Mn-Na inter	2(3)	4.1(2)	0.005
					Mn-O	4	4.4(1)	0.002(7)
					Mn-O	8	4.65(5)	0.002(7)
					Mn-Mn	4	4.89(4)	0.001(2)
					Mn-Mn	2	5.03(7)	0.001(2)
					Mn-Mn	2	5.72(8)	0.002
					Mn-Mn	4	5.82(4)	0.002
3 Additions	5.23	0.9(1)	0.66	423	Mn-O	4	1.87(6)	0.005(6)
					Mn-O	2	1.9(1)	0.002(1)
					Mn-Mn	2	2.69(1)	0.005(2)
					Mn-Mn	4	2.85(1)	0.003(1)
					Mn-O	4	3.33(5)	0.006(6)
					Mn-O	2	3.6(1)	0.006(6)
					Mn-Na inter	0(2)	4.0(6)	0.005
					Mn-O	4	4.5(1)	0.005(1)
					Mn-O	8	4.68(9)	0.005(1)
					Mn-Mn	4	4.89(2)	0.002(2)
					Mn-Mn	2	5.00(4)	0.002(2)
					Mn-Mn	2	5.70(8)	0.002
					Mn-Mn	4	5.83(5)	0.002
4 Additions	4.08	0.7(1)	0.71	316	Mn-O	4	1.87(4)	0.009(6)
					Mn-O	2	1.91(6)	0.003(1)
					Mn-Mn	2	2.72(2)	0.005(2)
					Mn-Mn	4	2.85(1)	0.002(1)

Sample	e0	focc	S02	χ2	Shell	CN	Dist (Å)	σ2
					Mn-O	4	3.35(6)	0.006(2)
					Mn-O	2	3.6(1)	0.006(2)
					Mn-Na inter	1(2)	4.1(1)	0.005
					Mn-Mn corn	0.2(2)	3.48	0.003
					Mn-O	4	4.4(1)	0.006(2)
					Mn-O	8	4.6(1)	0.006(2)
					Mn-Mn	4	4.91(6)	0.006(3)
					Mn-Mn	2	5.3(2)	0.006(3)
					Mn-Mn	2	5.6(1)	0.002
					Mn-Mn	4	5.83(3)	0.002
Sample	**e0**	**focc**	**S02**	**χ2**	**Shell**	**CN**	**Dist (Å)**	**σ2**
5 Additions	5.83	0.7(1)	0.66	841	Mn-O	4	1.87(3)	0.011(4)
					Mn-O	2	1.91(2)	0.001(1)
					Mn-Mn	2	2.71(2)	0.006(3)
					Mn-Mn	4	2.86(1)	0.003(1)
					Mn-O	4	3.41(6)	0.007(4)
					Mn-O	2	3.73(9)	0.007(4)
					Mn-Na inter	2(3)	4.0(1)	0.005
					Mn-Mn corn	0.6(3)	3.31(5)	0.003
					Mn-O	4	4.5(1)	0.004(3)
					Mn-O	8	4.69(9)	0.004(3)
					Mn-Mn	4	4.91(9)	0.005(2)
					Mn-Mn	2	5.2(2)	0.005(2)
					Mn-Mn	2	5.8(2)	0.002
					Mn-Mn	4	5.8(1)	0.002
Sample	**e0**	**focc**	**S02**	**χ2**	**Shell**	**CN**	**Dist (Å)**	**σ2**
6 Additions	6.13	0.7(1)	0.66	695	Mn-O	4	1.87(2)	0.007(2)
					Mn-O	2	1.91(3)	0.002
					Mn-Mn	2	2.75(2)	0.008(2)
					Mn-Mn	4	2.86(1)	0.003(1)
					Mn-O	4	3.23(4)	0.009(3)
					Mn-O	2	3.4(1)	0.009(3)
					Mn-Na inter	1(3)	4.1(1)	0.005
					Mn-Mn corn	0.6(2)	3.45(3)	0.003
					Mn-O	4	4.46(5)	0.005(3)
					Mn-O	8	4.67(3)	0.005(3)
					Mn-Mn	4	4.91(3)	0.005(3)
					Mn-Mn	2	5.44(5)	0.005(3)
					Mn-Mn	2	5.76(4)	0.001(1)
					Mn-Mn	4	5.86(2)	0.001(1)
Sample	**e0**	**focc**	**S02**	**χ2**	**Shell**	**CN**	**Dist (Å)**	**σ2**
7 Additions	6.42	0.9(1)	0.60	337	Mn-O	4	1.86(2)	0.006(4)
					Mn-O	2	1.93(4)	0.002
					Mn-Mn	2	2.72(2)	0.008(2)
					Mn-Mn	4	2.86(1)	0.004(1)
					Mn-O	4	3.38(3)	0.007(2)
					Mn-O	2	3.68(9)	0.007(2)
					Mn-Na inter	0(2)	4.0(2)	0.005
					Mn-Mn corn	0.4(3)	3.49(4)	0.003
					Mn-O	4	4.49(5)	0.001(1)
					Mn-O	8	4.71(3)	0.001(1)
					Mn-Mn	4	4.94(2)	0.004(1)
					Mn-Mn	2	5.19(5)	0.004(1)
					Mn-Mn	2	5.76(4)	0.002(1)

					Shell	CN	Dist (Å)	σ2
					Mn-Mn	4	5.85(2)	0.002(1)

Sample	**e0**	**focc**	**S02**	**χ2**	**Shell**	**CN**	**Dist (Å)**	**σ2**
8 Additions	6.20	0.7(1)	0.66	299	Mn-O	4	1.86(1)	0.005(2)
					Mn-O	2	1.94(3)	0.002
					Mn-Mn	2	2.70(3)	0.007(2)
					Mn-Mn	4	2.85(1)	0.002(1)
					Mn-O	4	3.30(4)	0.003(3)
					Mn-O	2	3.57(4)	0.003(3)
					Mn-Na inter	0(2)	4.10	0.005
					Mn-Mn corn	0.7(3)	3.49(7)	0.003
					Mn-O	4	4.50(7)	0.002(4)
					Mn-O	8	4.70(5)	0.002(4)
					Mn-Mn	4	4.92(5)	0.004(2)
					Mn-Mn	2	5.26(9)	0.004(2)
					Mn-Mn	2	5.81(7)	0.002(2)
					Mn-Mn	4	5.85(4)	0.002(2)

Sample	**e0**	**focc**	**S02**	**χ2**	**Shell**	**CN**	**Dist (Å)**	**σ2**
9 Additions	5.35	0.9(1)	0.66	449	Mn-O	4	1.86(2)	0.006(4)
					Mn-O	2	1.91(4)	0.002
					Mn-Mn	2	2.73(3)	0.010(3)
					Mn-Mn	4	2.85(1)	0.004(1)
					Mn-O	4	3.22(6)	0.014(8)
					Mn-O	2	3.5(1)	0.014(8)
					Mn-Na inter	1(2)	4.1(1)	0.005
					Mn-Mn corn	0.6(2)	3.43(4)	0.003
					Mn-O	4	4.42(9)	0.009(6)
					Mn-O	8	4.64(6)	0.009(6)
					Mn-Mn	4	4.91(5)	0.010(3)
					Mn-Mn	2	5.3(1)	0.010(3)
					Mn-Mn	2	5.76(4)	0.003(2)
					Mn-Mn	4	5.85(3)	0.003(2)

Sample	**e0**	**focc**	**S02**	**χ2**	**Shell**	**CN**	**Dist (Å)**	**σ2**
10 Additions	6.08	0.7(1)	0.66	421	Mn-O	4	1.86(3)	0.009(4)
					Mn-O	2	1.92(3)	0.002
					Mn-Mn	2	2.71(2)	0.006(3)
					Mn-Mn	4	2.85(1)	0.002(1)
					Mn-O	4	3.31(6)	0.005(3)
					Mn-O	2	3.60(7)	0.005(3)
					Mn-Na inter	1(3)	4.1(1)	0.005
					Mn-Mn corn	0.9(3)	3.53(7)	0.003
					Mn-O	4	4.46(9)	0.007(7)
					Mn-O	8	4.68(8)	0.007(7)
					Mn-Mn	4	4.92(6)	0.008(4)
					Mn-Mn	2	5.29(9)	0.008(4)
					Mn-Mn	2	5.75(4)	0.006(2)
					Mn-Mn	4	5.84(2)	0.006(2)

Sample	**e0**	**focc**	**S02**	**χ2**	**Shell**	**CN**	**Dist (Å)**	**σ2**
11 Additions	6.23	0.8(1)	0.66	514	Mn-O	4	1.86(1)	0.005(2)
					Mn-O	2	1.93(2)	0.002
					Mn-Mn	2	2.72(1)	0.007(2)
					Mn-Mn	4	2.86(1)	0.003(1)
					Mn-O	4	3.33(3)	0.004(2)
					Mn-O	2	3.64(4)	0.004(2)

Sample	e0	focc	S02	χ2	Shell	CN	Dist (Å)	σ2
					Mn-Na inter	0.37 ± 1.11	4.1(1)	0.005
					Mn-Mn corn	1.1(3)	3.52(2)	0.003
					Mn-O	4	4.23(3)	0.013(6)
					Mn-O	8	4.56(5)	0.013(6)
					Mn-Mn	4	4.88(4)	0.008(3)
					Mn-Mn	2	5.29(9)	0.008(3)
					Mn-Mn	2	5.82(3)	0.003(1)
					Mn-Mn	4	5.83(9)	0.003(1)
12 Additions	5.76	0.7(1)	0.66	379	Mn-O	4	1.87(2)	0.008(3)
					Mn-O	2	1.91(3)	0.002
					Mn-Mn	2	2.72(2)	0.008(2)
					Mn-Mn	4	2.85(1)	0.003(1)
					Mn-O	4	3.29(7)	0.003(2)
					Mn-O	2	3.62(3)	0.003(2)
					Mn-Na inter	1(2)	4.1(1)	0.005
					Mn-Mn corn	1.3(2)	3.49(2)	0.003
					Mn-O	4	4.48(8)	0.004(5)
					Mn-O	8	4.70(4)	0.004(5)
					Mn-Mn	4	4.94(4)	0.004(2)
					Mn-Mn	2	5.22(6)	0.004(2)
					Mn-Mn	2	5.79(5)	0.002(1)
					Mn-Mn	4	5.85(3)	0.002(1)

Section A7: References

(1) Nakamura, S.; Tezuka, Y.; Ushiyama, A.; Kawashima, C.; Kitagawara, Y.; Takahashi, K.; Ohta, S.; Mashino, T. Ipso substitution of bisphenol A catalyzed by microsomal cytochrome P450 and enhancement of estrogenic activity. *Toxicol. Lett.* **2011**, *203* (1), 92–95.

(2) Im, J.; Prevatte, C. W.; Campagna, S. R.; Löffler, F. E. Identification of 4-hydroxycumyl alcohol as the major MnO$_2$-mediated bisphenol A transformation product and evaluation of its environmental fate. *Environ. Sci. Technol.* **2015**, *49* (10), 6214–6221.

Appendix B

Supplementary Material for Chapter 3

Section B1: Materials

B1.1 Purchased Chemicals

Acetonitrile (HPLC grade), methanol (HPLC grade), formic acid (ACS, 88%), calcium chloride dihydrate (ACS, 100%), sodium acetate trihydrate (ACS, 100%), sodium chloride (ACS, 100%), polyvinylpyrrolidone (Molecular Biology Grade), and potassium permanganate (ACS) were purchased from Fisher Chemical. Boric acid (ACS) was purchased from Amresco, Inc. Bisphenol A (≥99%) and L-ascorbic acid (≥99%) were purchased from Sigma Aldrich. Manganese(II) nitrate tetrahydate (analytical grade) and piperazine-*N,N'*-bis(2-ethanesulfonic acid) (PIPES, 99%) were purchased from Acros Organics. Sodium hydroxide (98%) was purchased from Sigma Chemical Co.

B1.2 Preparation and Characterization of δ-MnO$_2$

δ-MnO$_2$ was prepared by dissolving 11.29 g Mn(NO$_3$)$_2$·4H$_2$O in 100 mL of ultrapure water, followed by dropwise addition to a 100 mL solution containing 2.4 g NaOH and 4.74 g KMnO$_4$ and stirring for at least twelve hours. The resulting slurry was centrifuged and washed five times in ultrapure water. The solids were then suspended in ultrapure water, stored at 4°C, and used within 10 days of synthesis. The slurry concentration was determined by gravimetric analysis. The starting material was characterized by X-ray diffraction (XRD; Rigaku Rapid II, Mo Kα source; λ = 0.7093 Å), showing that δ-MnO$_2$ was the only crystalline phase produced.

This synthesis yielded a mineral with an average valence state of 3.94 ± 0.11 v.u. determined by oxalate titration,[1] indicating that the mineral is predominantly Mn(IV).

Section B2: Buffer Selection
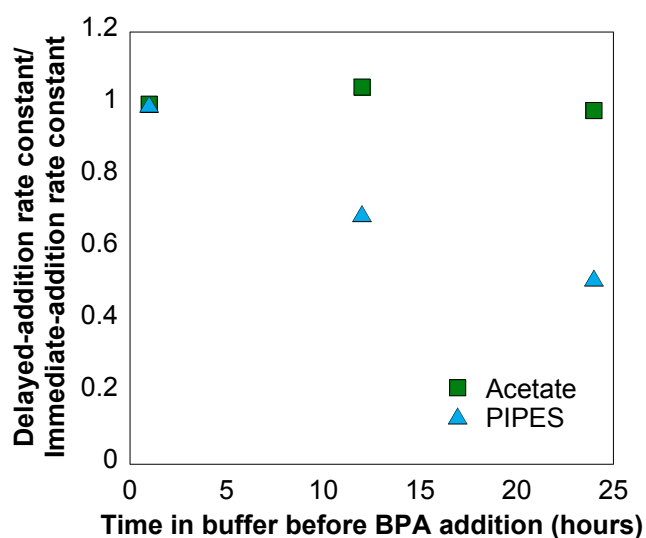
Figure B1: BPA oxidation rate constants with δ-MnO$_2$, where the reaction begins after δ-MnO$_2$ is stirred with the buffer for a designated time. These delayed-addition rate constants are plotted as a fraction of the initial rate constant. Buffers used are PIPES (10 mM; pH 7) and acetate (10 mM; pH 5).

Section B3: Stirred Flow Reactors
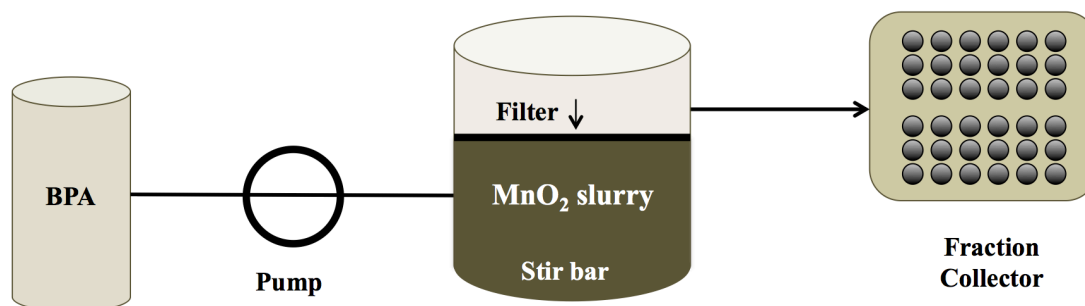
Figure B2: Schematic of stirred flow reactors.
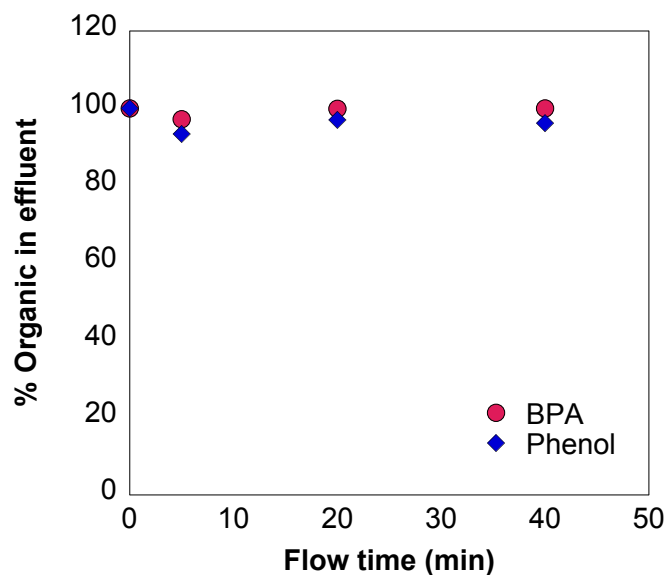
Figure B3: Percentages of initial BPA and phenol concentrations (initial concentration = 20 μM) in effluent when pumped through a line of Pt-cured silicone tubing.

Section B4: XANES Analysis

XANES data was collected at beamline 10-BM at the Advanced Photon Source at Argonne National Laboratory. This beamline has a bending magnet source equipped with a Si(111) double crystal monochromator, which was detuned by 40%. Data was collected at room

temperature in transmission mode. Successive XANES scans were identical, indicating no change in Mn oxidation state during data collection. XANES data was processed using SIXPack[2] and was fit using the multi-standard Combo method[3] by fitting the first derivative of the spectra with restriction to a non-negative fit.

Section B5: HCA Yield Calculations

The steady-state approximation is used in stirred flow reactors that have reached a plateau in BPA and HCA concentrations. These reactors are not truly at steady-state since manganese oxide is still oxidizing both BPA and HCA, but the reaction has reached a point where the oxidation rate is changing very little from one data point to the next. The steady-state approximation assumes that the concentration of any intermediates remain the same throughout the duration of the reaction, which is what is observed when the plateau is reached (i.e., BPA and HCA concentrations are generally constant throughout the reaction). When steady-state is assumed, the following mass balance equation can be used:

$$\frac{d[HCA]}{dt}V = -Q[HCA] + F_{HCA}k_1[BPA]V - k_2[HCA]V = 0 \qquad \textbf{(B1)}$$

where Q is the flow rate of the reactor (1 mL/min), V is the volume of the reactor (12.7 mL), [BPA] and [HCA] are the concentrations of BPA and HCA, respectively, and k_1 and k_2 are the oxidation rate constants of BPA and HCA, respectively. F_{HCA} is the fraction of BPA converted to HCA. This equation can be rearranged to form equation **2** in the manuscript. The BPA oxidation rate constant, k_1, is calculated using the following mass balance equation:

$$\frac{d[BPA]}{dt}V = Q[BPA]_0 - Q[BPA] - k_1[BPA]_0V = 0 \qquad \textbf{(B2)}$$

where $[BPA]_0$ is the initial BPA concentration. This equation can be rearranged to form equation **3** in the manuscript. Separate batch reactors comparing BPA and HCA oxidation rate constants at

each condition are used to determine k_2, the HCA oxidation rate constant in each stirred flow reactor.

Section B6: HCA Identification and Acid Dissociation Constant (pK$_a$) Determination
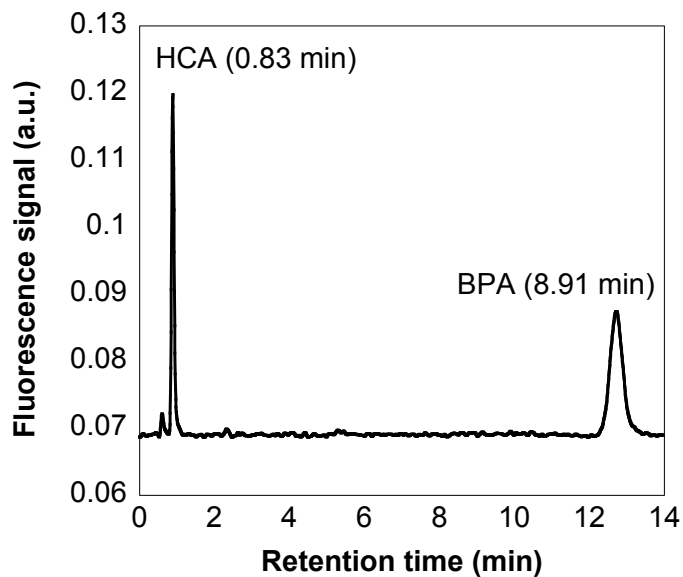

Figure B4: Example HPLC chromatogram from a batch reactor with 0.1 g/L δ-MnO$_2$ and 40 μM BPA in a 10 mM sodium acetate buffer. Both BPA and HCA peaks are identified and their retention times were confirmed using authentic standards.
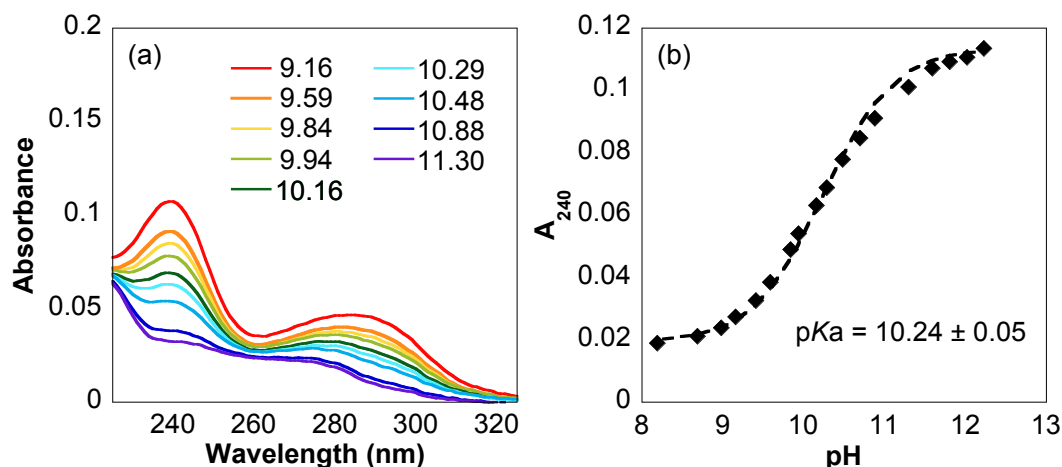
Figure B5: HCA (a) absorbance spectra at the pH values indicated in the legend and (b) absorbance at 240 nm versus pH. The dashed line represents the fit of the data using least squares minimization to determine the pKa.

Section B7: Batch Reactor Experiments

Sorption was determined by quantifying BPA and HCA concentrations in a quenched sample (10.8 mM ascorbic acid) and in a filtered sample (0.2 μm polytetrafluoroethylene). The difference between these concentrations was used to quantify the HCA or BPA associated with the solid.

Table B1: BPA and HCA oxidation rate constants and percent sorption in identical batch reactors containing 0.1 g/L δ-MnO$_2$ and 40 μM of the added phenol. Solutions contained 10 mM acetate buffer at pH 5 and were brought to an ionic strength of 25 mM using NaCl.

	Rate Constant (min^{-1})	Sorption (%)
BPA	0.228 ± 0.005	13.57 ± 18.45
HCA	0.029 ± 0.000	-0.72 ± 3.61
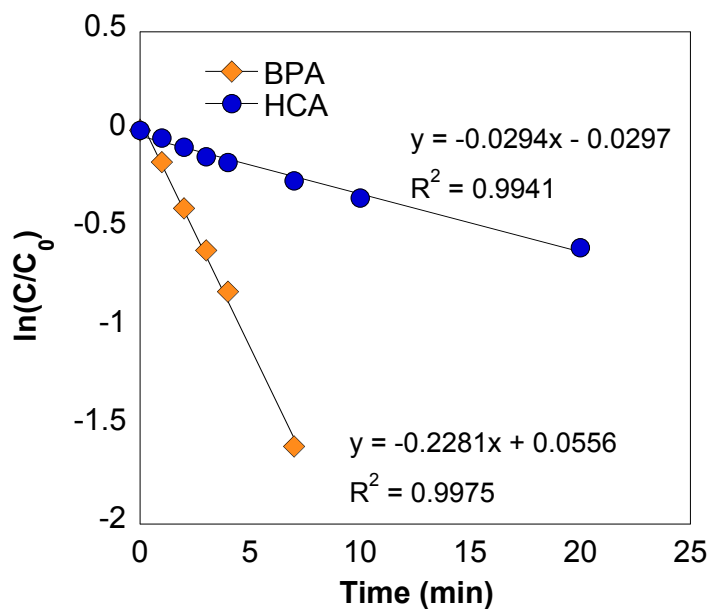
Figure B6: Pseudo-first-order rate analysis for BPA and HCA in identical batch reactors containing 0.1 g/L δ-MnO$_2$ and 40 µM of the added phenol at pH 5. All solutions contained 10 mM acetate and were brought to an ionic strength of 25 mM using NaCl.

Section B8: Stirred Flow Experiments
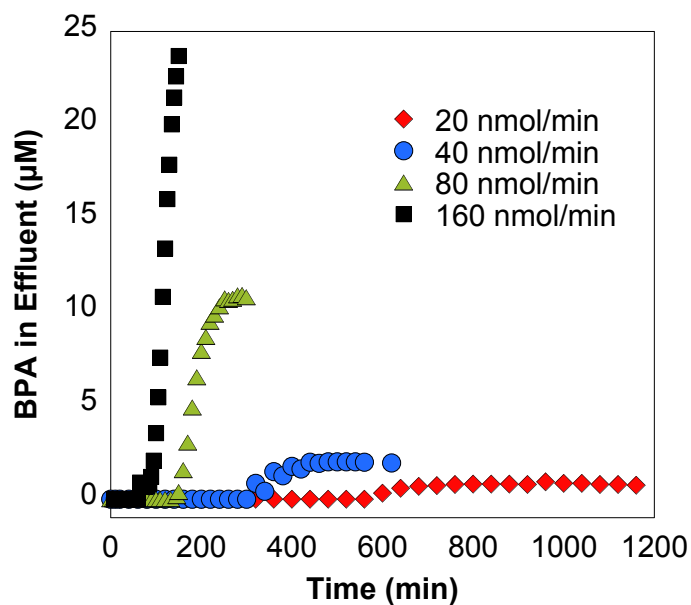
Figure B7: BPA present in the effluent as a function of time in stirred flow reactors containing 1.58 g/L δ-MnO$_2$ (10 mM acetate; pH 5) containing variable initial BPA concentrations.
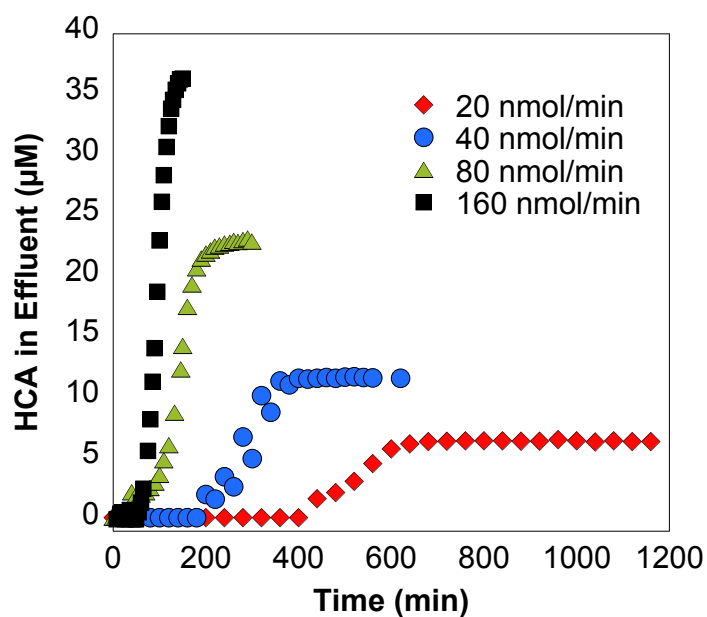
Figure B8: HCA present in the effluent as a function of time in stirred flow reactors containing 1.58 g/L δ-MnO$_2$ (10 mM acetate; pH 5) containing variable initial BPA concentrations.
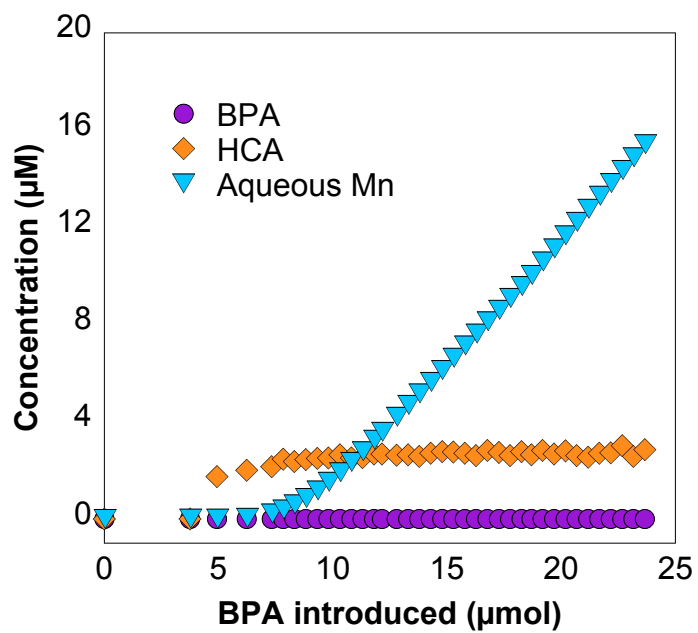
Figure B9: Concentrations of BPA, HCA, and aqueous Mn in the effluent of a stirred flow reactor containing 1.58 g/L δ-MnO$_2$ containing 5 μM BPA and 10 mM acetate (pH 5) over 83 hours.
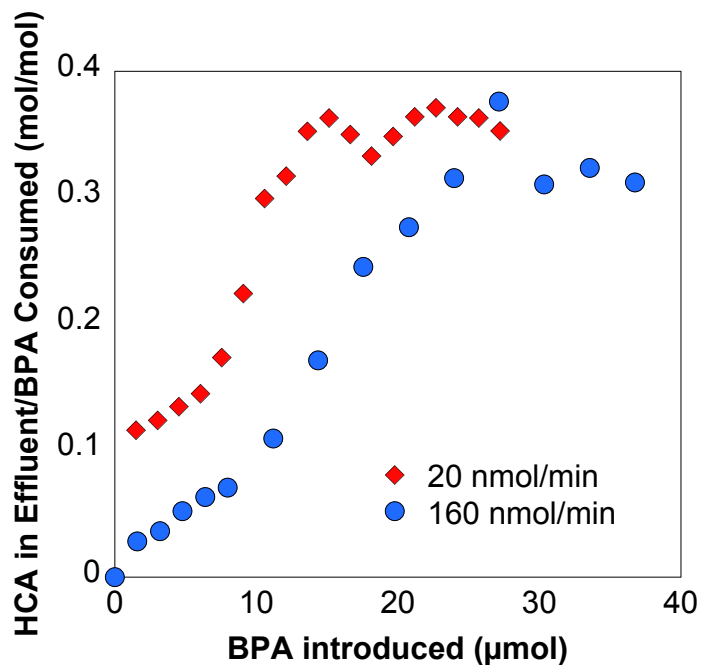
Figure B10: Ratios of HCA produced to BPA consumed in stirred flow reactors containing 1.58

g/L δ-MnO$_2$ in 10 mM acetate (pH 5).

Section B9: Solids Characterization

Table B2: Average manganese oxidation numbers and speciation of solids recovered from

stirred flow reactors containing 1.58 g/L δ-MnO$_2$ (10 mM acetate; pH 5) containing variable

initial BPA concentrations, as determined by XANES spectroscopy.

Sample	AMON (v.u.)	% Mn(IV)	%Mn(III)	%Mn(II)
Starting Material	3.85	90	5	5
20 nmol/min	3.66	77	12	11
40 nmol/min	3.67	78	12	10
80 nmol/min	3.68	78	12	10
160 nmol/min	3.67	78	12	10

Table B3: Estimated net electron transfer from organic compounds to δ-MnO$_2$ calculated for each reactor using the method described in Wang et al.[4]

Sample	Net Electron Transfer (μmol)
20 nmol/min	79.7
40 nmol/min	72.0
80 nmol/min	64.9
160 nmol/min	50.7

Section B10: References

(1) Murray, J. W. The surface chemistry of hydrous manganese dioxide. *J. Colloid Interface Sci.* **1974**, *46* (3), 357–371.
(2) Webb, S. M. SIXpack: A graphical user interface for XAS analysis using IFEFFIT. *Phys. Scr.* **2005**, *2005* (T115), 1011–1014.
(3) Manceau, A.; Marcus, M. A.; Grangeon, S. Determination of Mn valence states in mixed-valent manganates by XANES spectroscopy. *Am. Mineral.* **2012**, *97* (5–6), 816–827.
(4) Wang, Q.; Yang, P.; Zhu, M. Structural transformation of birnessite by fulvic acid under anoxic conditions. *Environ. Sci. Technol.* **2018**, *52* (4), 1844–1853.

Appendix C

Supplementary Material for Chapter 4

Section C1: Materials

C1.1 Purchased Chemicals

Acetonitrile (HPLC grade), methanol (HPLC grade), formic acid (ACS, 88%), calcium chloride dihydrate (ACS, 100%), sodium acetate trihydrate (ACS, 100%), sodium chloride (ACS, 100%), polyvinylpyrrolidone (Molecular Biology Grade), potassium acetate (ACS crystalline) and potassium permanganate (ACS) were purchased from Fisher Chemical. Bisphenol A (≥99%), potassium chloride (ACS reagent, ≥99%), *p*-cresol (99%), and L-ascorbic acid (≥99%) were purchased from Sigma Aldrich. Manganese(II) nitrate tetrahydate (analytical grade) and estrone (≥99%) were purchased from Acros Organics. Sodium hydroxide (98%) was purchased from Sigma Chemical Co. Magnesium chloride hexahydate (≥99%) was purchased from DOT Scientific Inc. Triclosan (99.5%) was purchased from Crescent Chemical Co., Inc.

Section C2: Analytical Methods

C2.1 High Performance Liquid Chromatography (HPLC) Analysis

HPLC analyses were performed with an Agilent 1260 instrument equipped with a fluorescence detector (Model 1260 FLD) and a UV detector (Model 1260 DAD). The peaks detected in experimental chromatograms were compared to authentic standards.

Column: Agilent Poroshell 120 EC-C18 (4.6 x 50 mm, 2.7 μm)
Guard column: Agilent EC-C18 (3.0 x 5 mm, 2.7 μm)
Injection volume: 5 μL
Mobile phase: A: 0.1% Formic Acid + 10% Acetonitrile (ACN) in Milli-Q water
                                        adjusted to pH 3 (filtered through a 0.2 μm nylon filter)
                                        B: 100% ACN
Column temperature: 30°C

Target Analyte	Flow Rate (mL/min)	% Mobile Phase A	UV Detector Wavelength (nm)	Excitation Wavelength (nm)	Emission Wavelength (nm)	Retention Time (min)
BPA	0.6	60	-	280	310	2.6
Estrone	0.6	65	280	-	-	2.4
Triclosan	1	40	280	-	-	1.2
p-cresol	0.6	75	210	305	290	1.6

C2.2 Inductively Coupled Plasma-Optical Emission Spectroscopy (ICP-OES) Analysis

ICP-OES analyses were performed on a PerkinElmer Optima 4300 DV to quantify aqueous manganese in the reactors at various time intervals. All samples were filtered immediately and diluted in a solution of 2% nitric acid. Standards were made from a SPEX CertiPrep 1000 mg/L Mn stock diluted in 2% nitric acid. Error was calculated using relative standard deviations from four instrument responses.

Section C3: Rate Constant Analysis

Rate constants for the oxidation of organic contaminants by birnessite were calculated assuming pseudo-first-order kinetics according to:

$$\ln[A] = -kt + \ln[A]_o \qquad\qquad\qquad \textbf{C1}$$

where A is the concentration of the organic (M), t is the time of the reaction (min), and k is the rate constant (min^{-1}). The error for each rate constant is the standard deviation of the rate

constants collected each of three replicate reactors. Half-lives ($t_{1/2}$) were calculated using equation **C2**:

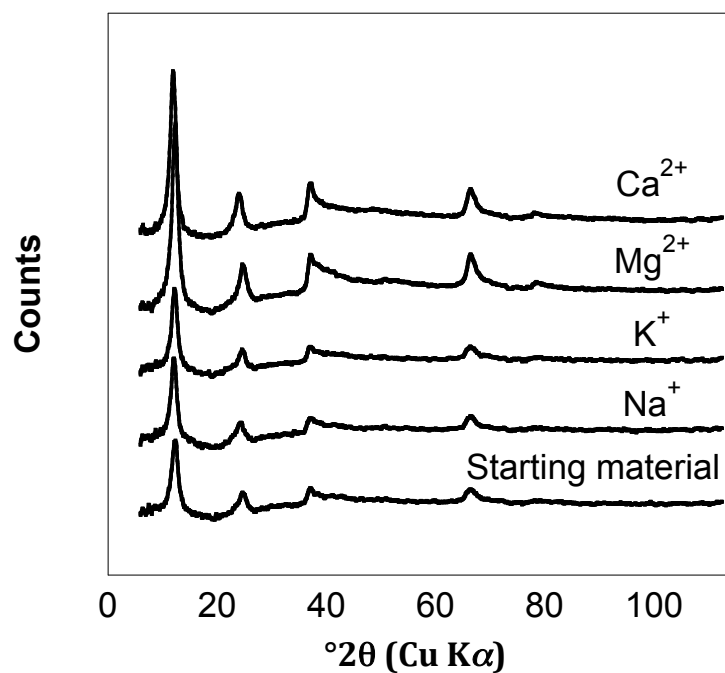$$t_{1/2} = \frac{\ln(2)}{k}$$ **C2**

Figure C1. XRD patterns of each pre-exchanged birnessite.

Appendix D

Investigation of Solution Conditions

Section D1: Introduction

Solution conditions such as pH and presence of oxygen can affect redox reaction kinetics. Solution pH affects the rate of BPA oxidation, with increasing pH generally leading to decreased reaction rates.[1,2] Presence of oxygen has no observed effect on manganese oxide dissolution rates when reacted with hydroquinone;[3] however, re-oxidation of the mineral is observed in the presence of oxygen above pH 8.[4] In this section, the effects of pH and presence of oxygen on the oxidation of bisphenol A (BPA) by δ-MnO$_2$ are investigated. The formation of 4-hydroxycumyl alcohol (HCA), a major oxidation product of BPA, is observed to detect changes in mechanism or product formation. HCA is synthesized as described Section **A1.1** and used to determine its oxidation rates with δ-MnO$_2$ under the same conditions.

Section D2: Methods

Batch reactors were used to determine initial rates of BPA and HCA oxidation by δ-MnO$_2$, the effect of pH, and the effect of presence of oxygen. Prepared δ-MnO$_2$ slurry (stock concentrations: 30-50 g/L) was equilibrated in buffered solution for 30 minutes before the addition of BPA or HCA (initial concentration: 40 or 80 μM). Batch reactors testing the effect of presence of oxygen were performed at pH 7 in 10 mM PIPES since these reactors were the same length and therefore exhibited the same amount of δ-MnO$_2$ reduction by the buffer. Batch reactors testing the effect of pH used sodium acetate at pH 5, PIPES at pH 6 and 7, and borate at pH 8 with a concentration of 10 mM and ionic strength adjusted to 25 mM using NaCl. None of

these buffers affected the δ-MnO$_2$ reactivity over the length of these short reactions (Table **D1**). BPA and HCA concentrations were determined by high-performance liquid chromatography (HPLC). HCA yield was calculated as described in Section **A4.2**. Sorption was determined by quantifying BPA and HCA concentrations in a quenched sample (10.8 mM ascorbic acid) and in a filtered sample (0.2 μm polytetrafluoroethylene). The difference between these concentrations was used to quantify the HCA or BPA associated with the solid. Experiments with varied pH were conducted in triplicate.

To determine the impact of oxygen on BPA oxidation, multi-addition batch experiments were performed under ambient conditions or in an anaerobic chamber. In these experiments, duplicate 6 L reactors were prepared with 0.33 g/L δ-MnO$_2$ (pH 7, 10 mM PIPES). BPA was added to these reactors 12 times sequentially. Aqueous samples were collected as described above. Aqueous manganese was quantified by inductively coupled plasma-optical emission spectroscopy (ICP-OES) analysis of filtered samples diluted in 2% nitric acid. Solid samples were collected by removing 150 mL from the reactor and filtering to isolate the solid phase. This material was washed in methanol to remove organics, dried at room temperature, and ground before analysis. Average oxidation state of manganese oxide was determined using X-ray absorption near edge structure (XANES) spectra collected at beamline 10-BM at the Advanced Photon Source at Argonne National Laboratory (Section **B4**). Samples were prepared by diluting 3 mg of manganese oxide into 8 mg of polyvinylpyrrolidone, grinding until homogenous, and pressing into a 7 mm pellet.

Section D3: Results

D3.1 Effect of pH on Oxidation Rate and Product Formation

The oxidation rate of BPA by δ-MnO$_2$ is pH dependent. BPA concentration quickly decreases upon reaction with δ-MnO$_2$, resulting in generation of its major oxidation product, HCA (Figure **3.1**). Observed BPA oxidation rates consistently decrease with increasing pH (Figure **D1**), with rate constants of 0.228 min^{-1} at pH 5 and 2.76 x 10^{-2} min^{-1} at pH 8. The rate constant decreases by a smaller margin between pH 6 and 7, which may be attributable to partial reduction of the manganese oxide by PIPES over the 20-minute reaction (Figure **B1**).

HCA, the major product of BPA oxidation, is also susceptible to oxidation by δ-MnO$_2$, which is consistent with previous literature.[5,6] In order to calculate HCA yield from BPA oxidation, it is necessary to quantify the oxidation rate of HCA by δ-MnO$_2$ in a separate reactor. As observed with BPA, HCA oxidation rate constants generally decrease with increasing pH values (Figure **D1**). BPA is oxidized by δ-MnO$_2$ much more quickly than HCA and the ratio of BPA:HCA oxidation rate constants is dependent on pH (Figure **D2**). For example, BPA is oxidized 22 times faster than HCA at pH 6 and 8 times faster at pH 5. These ratios are used to calculate HCA yields using equations **A5** and **A6**.

The HCA yield from BPA oxidation increases steadily as a function of pH (Figure **D2**). At pH 5, 32% of BPA is converted to HCA, while 53% of BPA is converted to HCA at pH 8. This implies that BPA preferentially undergoes two sequential single-electron transfers before desorbing from the surface at lower pH, while at higher pH, BPA favors desorption from the surface before a second single-electron transfer can occur.

The pH dependence of BPA and HCA oxidation confirms previous observations of faster BPA oxidation rates by manganese oxides under acidic conditions.[1,2] Similar trends have been

observed during the oxidation of other organic pollutants by manganese oxides,[7–15] which is commonly attributed to the decrease in redox potential (E_H) of MnO_2 as a function of pH.[15] Additionally, the negative charge density on the mineral increases with increasing pH, resulting in increased adsorption of Mn(II) produced during the reaction that can block potential reaction sites for phenols.[1,2,16–18] However, the observed pH dependence is not explained by changes in sorption of BPA and HCA to the mineral surface. BPA sorbs at an average rate of 13.6 ± 1.1% across the pH range, with no observed pH dependence, and HCA sorption is negligible (Figure **D3**). This result is consistent with the high pK_a's of both phenols; BPA has pK_a's of 9.6 and 10.2,[19] while HCA was determined to have a pK_a of 10.24 ± 0.05 in Chapter 3 (Figure **B5**). This data indicates that the surface charge is not changing enough to affect sorption.

D3.2 Effects of Oxygen on BPA Oxidation

The presence of oxygen can potentially alter the reactivity of manganese oxide with organic compounds. Since BPA oxidation forms carbon-centered radicals,[2,20] the presence of oxygen may alter the types of products formed. Products formed from the first single-electron transfer may react very quickly with oxygen, preventing a second single-electron transfer with δ-MnO_2. Additionally, Mn(II) can regenerate to form Mn(III/IV) above pH 8 when in the presence of oxygen and a mineral surface, potentially preserving and/or increasing mineral reactivity.[4]

To investigate the impact of oxygen on manganese oxide reactivity, BPA oxidation by δ-MnO_2 is observed under aerobic and anaerobic conditions. The reaction is performed using 12 sequential additions of BPA to the same batch reactor containing δ-MnO_2. This method induces changes to the mineral surface, amplifies Mn(II) production, and enables comparison with a previous study using Mn(III)-rich δ-MnO_2 at pH 7.[5] In both this study and previous work, the

BPA oxidation rate decreases over 12 sequential additions of BPA (Figure **D4a**). However, there is no difference in oxidation rate between aerobic and anaerobic conditions over the 12 additions (Figure **D4a**), indicating that oxygen has no effect on the rate of BPA oxidation by manganese oxide. This result is consistent with a previous observation of no difference in reaction rate of hydroquinone oxidation by manganese oxide with or without oxygen.[3]

Calculated HCA yields remain the same in both aerobic and anaerobic reactors (Figure **D4b**), showing that the presence of oxygen does not affect the favored mechanisms and product distribution in this reaction. Additionally, there is minimal variation in HCA yield, indicating that the BPA oxidation mechanism remains constant even as the oxidation rate decreases during mineral transformation. Due to the slow kinetics during the final six BPA additions, the yield calculations are not reliable and are not included here.

In contrast, the presence of oxygen does impact the reductive dissolution of the δ-MnO_2. The concentration of aqueous manganese in each reactor increases across 12 sequential additions of BPA (Figure **D4c**). All aqueous manganese is considered to be Mn(II) since there are no strong ligands to solubilize Mn(III) present in the reactors.[21,22] More Mn(II) is produced in the anaerobic reactors than in the aerobic reactors, with the difference between aerobic and anaerobic reactors increasing as the reaction proceeds. This indicates that some Mn(II) may be oxidized by O_2 in the aerobic reactors, while Mn(II) preferentially desorbs and remains in the aqueous phase in the anaerobic reactors. Previous work shows that oxidation of Mn(II) is possible in the presence of rhodochrosite ($MnCO_{3(s)}$) at a rate of approximately 4 μmol over 5 days at pH 8.8, indicating the use of rhodochrosite as a surface catalyst in the reaction.[4] Here the rate of oxidation is 39 μmol over 12 hours, indicating the increased efficiency of δ-MnO_2 as a surface catalyst compared to rhodochrosite. These results agree with analysis of reactor solids by

XANES, which demonstrates that the average oxidation state of the solids decreases with each addition of BPA (Figure **D4d**). Oxidation state decreases more rapidly in the anaerobic reactor, suggesting that some regeneration of Mn(III/IV) solids occurs in the presence of oxygen. A Student's T-test performed using pooled error variance demonstrates that the two regression lines are significantly different (p-value = 0.033; Table **D2**).

Table D1: Observed pseudo-first order BPA oxidation rate constants in each of the three buffers in this study where the reaction begins either immediately after addition of δ-MnO$_2$ to the buffer or one hour after δ-MnO$_2$ has equilibrated with the buffer.

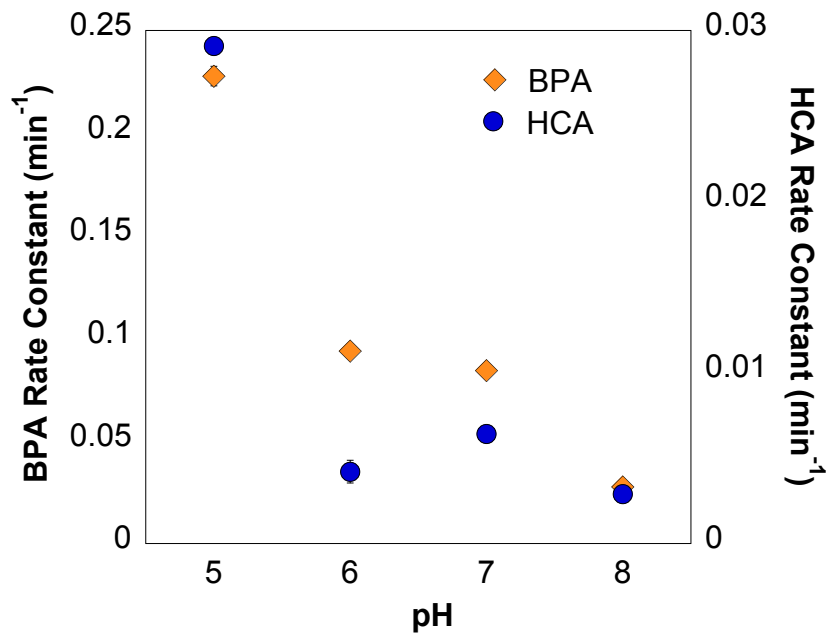| k_{BPA} *(min^{-1})*	Acetate pH 5	PIPES pH 7	Borate pH 8
0 hours after δ-MnO$_2$ addition	0.790 ± 0.037	0.268 ± 0.016	0.329 ± 0.010
1 hour after δ-MnO$_2$ addition	0.815 ± 0.073	0.220 ± 0.010	0.372 ± 0.004

Figure D1: Observed BPA and HCA oxidation rate constants in identical batch reactors containing 0.1 g/L δ-MnO$_2$ and 40 µM of the added phenol at varying pH. All solutions contained 10 mM buffer (acetate at pH 5, PIPES at pH 6 and 7, and borate at pH 8) and were brought to an ionic strength of 25 mM using NaCl. Error bars are standard deviation values from triplicate reactors.

Figure D2: Ratios of BPA and HCA oxidation rate constants in identical reactors and HCA yield from BPA oxidation in batch reactors containing 0.1 g/L δ-MnO$_2$ and 40 µM of the added phenol at varying pH values. All solutions contained 10 mM buffer (acetate at pH 5, PIPES at pH 6 and 7, and borate at pH 8) and were brought to an ionic strength of 25 mM using NaCl. Error bars are standard deviation values from triplicate reactors.
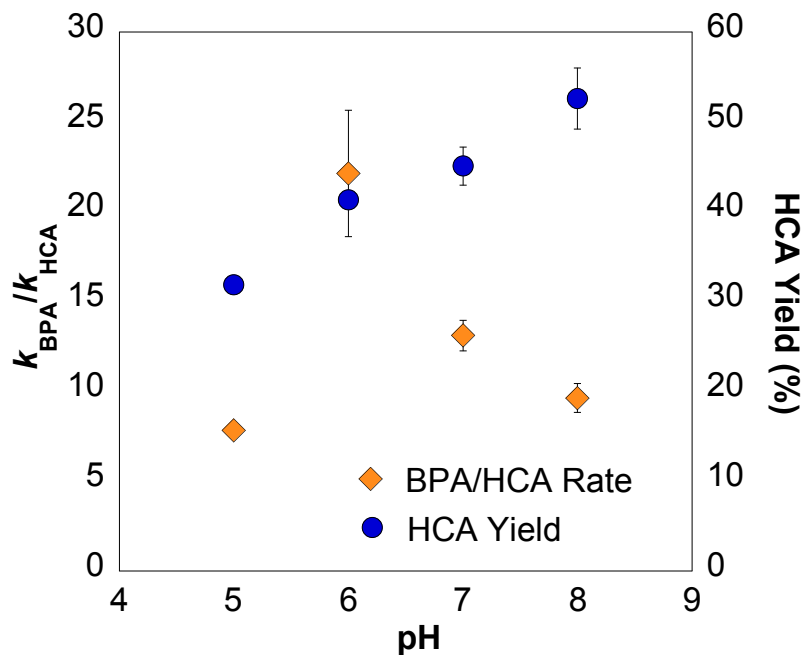
Figure D3: BPA and HCA sorption in identical batch reactors containing 0.1 g/L δ-MnO$_2$ and 40 μM of the added phenol at varying pH. All solutions contained 10 mM buffer (acetate at pH 5, PIPES at pH 6 and 7, and borate at pH 8) and were brought to an ionic strength of 25 mM using NaCl. Error bars are standard deviation values from triplicate reactors.
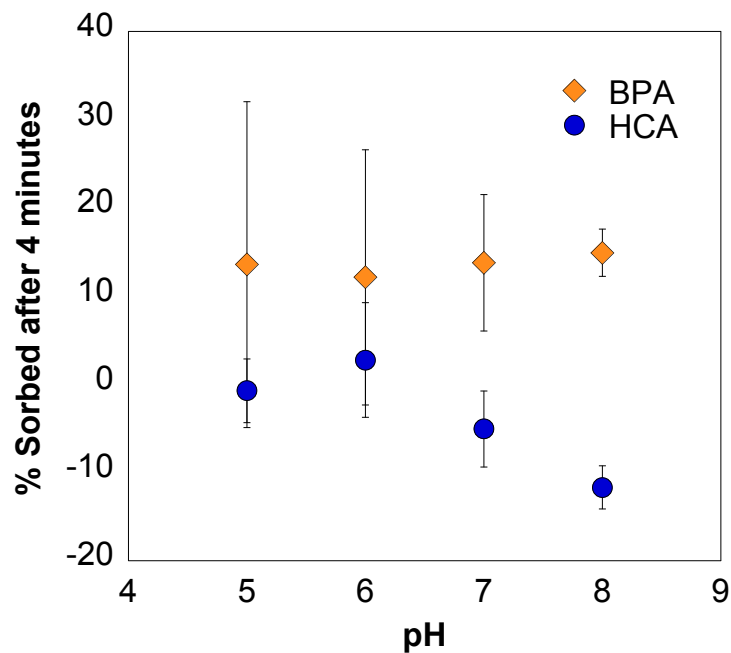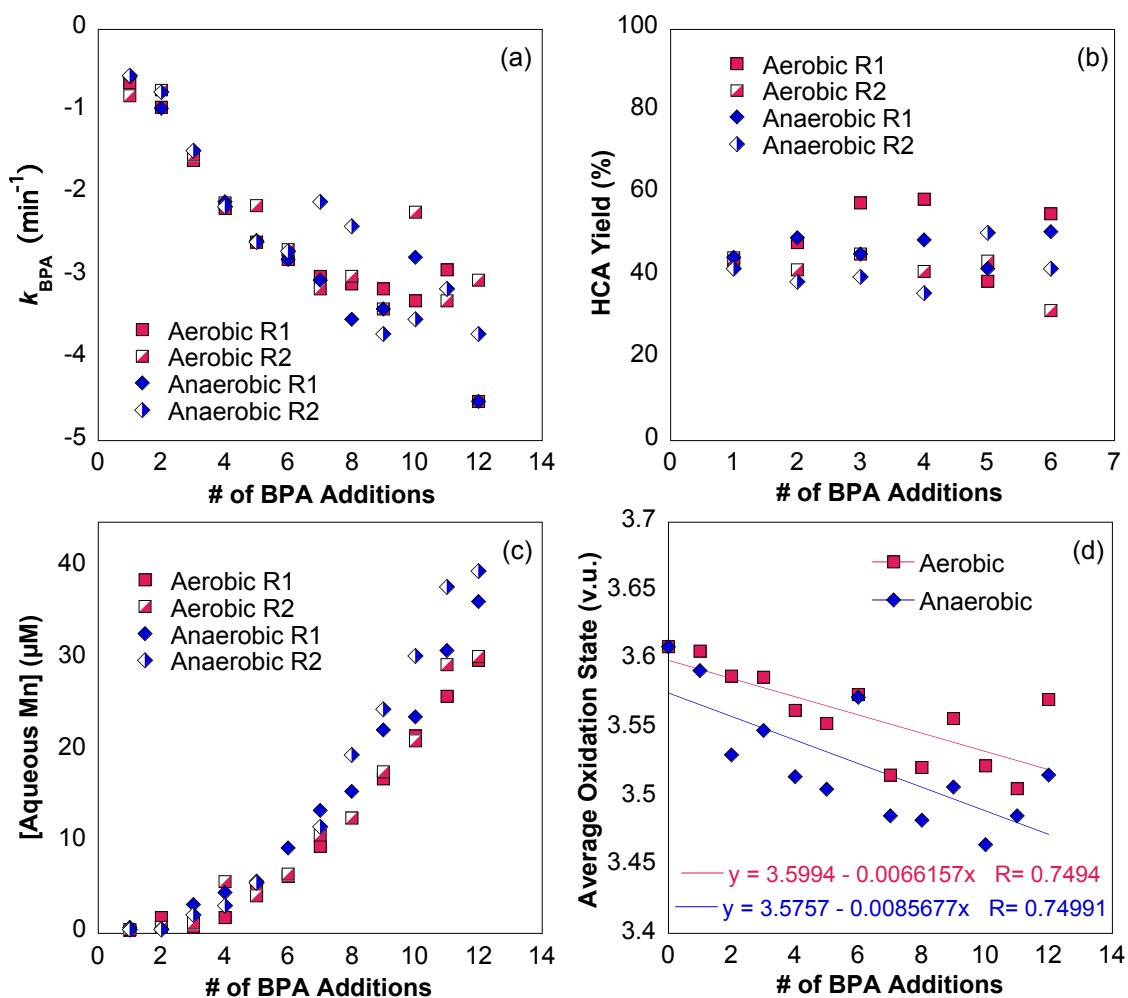
Figure D4: (a) Observed initial BPA oxidation rate constants, (b) calculated HCA yields, (c) aqueous Mn(II) concentrations, and (d) average manganese oxidation number of solids in aerobic and anaerobic batch reactors containing 0.33 g/L δ-MnO$_2$ in 10 mM PIPES buffer (pH 7) over 12 sequential additions of 80 μM BPA.

Table D2: Student's T-test comparing average oxidation states of manganese oxide solids in aerobic and anaerobic batch reactors containing 0.33 g/L δ-MnO$_2$ in 10 mM PIPES buffer (pH 7) over 12 sequential additions of 80 μM BPA.

	Anaerobic	Aerobic
Mean	3.5243292	3.559710432
Variance	0.00197969	0.001182025
Observations	13	13
Pooled Variance	0.00158086	
Hypothesized Mean Difference	0	
df	24	
t Stat	-2.2687338	
p-value (two-tail)	0.03256063	
t Critical (two-tail)	2.06389856	

Section D4: References

(1)   Gao, N.; Hong, J.; Yu, Z.; Peng, P.; Huang, W. Transformation of bisphenol A in the presence of manganese dioxide. *Soil Sci.* **2011**, *176* (6), 265–272.

(2)   Lin, K.; Liu, W.; Gan, J. Oxidative removal of bisphenol A by manganese dioxide: Efficacy, products, and pathways. *Environ. Sci. Technol.* **2009**, *43* (10), 3860–3864.

(3)   Stone, A. T.; Morgan, J. J. Reduction and dissolution of manganese(III) and manganese(IV) oxides by organics. 1. Reaction with hydroquinone. *Environ. Sci. Technol.* **1984**, *18* (6), 450–456.

(4)   Diem, D.; Stumm, W. Is dissolved Mn^{2+} being oxidized by O_2 in absence of Mn-bacteria or surface catalysts? *Geochim. Cosmochim. Acta* **1984**, *48*, 1571–1573.

(5)   Balgooyen, S.; Alaimo, P. J.; Remucal, C. K.; Ginder-Vogel, M. Structural transformation of MnO_2 during the oxidation of bisphenol A. *Environ. Sci. Technol.* **2017**, *51* (11), 6053–6062.

(6)   Im, J.; Prevatte, C. W.; Campagna, S. R.; Löffler, F. E. Identification of 4-hydroxycumyl alcohol as the major MnO_2-mediated bisphenol A transformation product and evaluation of its environmental fate. *Environ. Sci. Technol.* **2015**, *49* (10), 6214–6221.

(7)   Zhang, H.; Huang, C.-H. Oxidative transformation of fluoroquinolone antibacterial agents and structurally related amines by manganese oxide. *Environ. Sci. Technol.* **2005**, *39* (12), 4474–4483.

(8)   Zhang, H.; Huang, C.-H. Oxidative transformation of triclosan and chlorophene by manganese oxides. *Environ. Sci. Technol.* **2003**, *37* (11), 2421–2430.

(9)   Zhang, H.; Chen, W.-R.; Huang, C.-H. Kinetic modeling of oxidation of antibacterial agents by manganese oxide. *Environ. Sci. Technol.* **2008**, *42* (15), 5548–5554.

(10)   Zhao, L.; Yu, Z.; Peng, P.; Huang, W.; Dong, Y. Oxidative transformation of tetrachlorophenols and trichlorophenols by manganese dioxide. *Env. Toxicol Chem* **2009**, *28* (6), 1120–1129.

(11)   Zhao, L.; Yu, Z.; Peng, P.; Huang, W.; Feng, S.; Zhou, H. Oxidation kinetics of pentachlorophenol by manganese dioxide. *Environ. Toxicol. Chem.* **2006**, *25* (11), 2912–2919.

(12)   Laha, S.; Luthy, R. G. Oxidation of aniline and other primary aromatic amines by manganese dioxide. *Environ. Sci. Technol.* **1990**, *24* (3), 363–373.

(13)   Stone, A. T. Reductive dissolution of manganese(III/IV) oxides by substituted phenols. *Environ. Sci. Technol.* **1987**, *21* (10), 979–988.

(14)   Rubert, K. F.; Pedersen, J. A. Kinetics of oxytetracycline reaction with a hydrous manganese oxide. *Environ. Sci. Technol.* **2006**, *40* (23), 7216–7221.

(15)   Klausen, J.; Haderlein, S. B.; Schwarzenbach, R. P. Oxidation of substituted anilines by aqueous MnO_2: Effect of co-solutes on initial and quasi-steady-state kinetics. *Environ. Sci. Technol.* **1997**, *31* (9), 2642–2649.

(16)   Lu, Z.; Lin, K.; Gan, J. Oxidation of bisphenol F (BPF) by manganese dioxide. *Environ. Pollut.* **2011**, *159* (10), 2546–2551.

(17)   Lin, K.; Peng, Y.; Huang, X.; Ding, J. Transformation of bisphenol A by manganese oxide-coated sand. *Environ. Sci. Pollut. Res.* **2013**, *20* (3), 1461–1467.

(18)   Zhang, T.; Zhang, X.; Yan, X.; Ng, J.; Wang, Y.; Sun, D. D. Removal of bisphenol A via a hybrid process combining oxidation on β-MnO_2 nanowires with microfiltration. *Colloids Surf. Physicochem. Eng. Asp.* **2011**, *392* (1), 198–204.

(19) Lee, Y.; Yoon, J.; von Gunten, U. Kinetics of the oxidation of phenols and phenolic endocrine disruptors during water treatment with ferrate (Fe(VI)). *Environ. Sci. Technol.* **2005**, *39* (22), 8978–8984.

(20) Remucal, C. K.; Ginder-Vogel, M. A critical review of the reactivity of manganese oxides with organic contaminants. *Environ. Sci. Process. Impacts* **2014**, *16* (6), 1247–1266.

(21) Klewicki, J. K.; Morgan, J. J. Kinetic behavior of Mn(III) complexes of pyrophosphate, EDTA, and citrate. *Environ. Sci. Technol.* **1998**, *32* (19), 2916–2922.

(22) Wang, Y.; Stone, A. T. Phosphonate- and carboxylate-based chelating agents that solubilize (hydr)oxide-bound Mn^{III}. *Environ. Sci. Technol.* **2008**, *42* (12), 4397–4403.